Springer Theses
Recognizing Outstanding Ph.D. Research

Jason M. Spruell

The Power of Click Chemistry for Molecular Machines and Surface Patterning

Springer

Springer Theses

Recognizing Outstanding Ph.D. Research

For further volumes:
http://www.springer.com/series/8790

Aims and Scope

The series "Springer Theses" brings together a selection of the very best Ph.D. theses from around the world and across the physical sciences. Nominated and endorsed by two recognized specialists, each published volume has been selected for its scientific excellence and the high impact of its contents for the pertinent field of research. For greater accessibility to non-specialists, the published versions include an extended introduction, as well as a foreword by the student's supervisor explaining the special relevance of the work for the field. As a whole, the series will provide a valuable resource both for newcomers to the research fields described, and for other scientists seeking detailed background information on special questions. Finally, it provides an accredited documentation of the valuable contributions made by today's younger generation of scientists.

Theses are accepted into the series by invited nomination only and must fulfill all of the following criteria

- They must be written in good English.
- The topic of should fall within the confines of Chemistry, Physics and related interdisciplinary fields such as Materials, Nanoscience, Chemical Engineering, Complex Systems and Biophysics.
- The work reported in the thesis must represent a significant scientific advance.
- If the thesis includes previously published material, permission to reproduce this must be gained from the respective copyright holder.
- They must have been examined and passed during the 12 months prior to nomination.
- Each thesis should include a foreword by the supervisor outlining the significance of its content.
- The theses should have a clearly defined structure including an introduction accessible to scientists not expert in that particular field.

Jason M. Spruell

The Power of Click Chemistry for Molecular Machines and Surface Patterning

Doctoral Thesis accepted by
Northwestern University for Chemistry,
Evanston, IL, USA

Springer

Author
Dr. Jason M. Spruell
California NanoSystems Institute and
Materials Research Laboratory
University of California
Santa Barbara
CA 93106
USA
e-mail: jspruell@mrl.ucsb.edu

Supervisor
Dr. J. Fraser Stoddart
Board of Trustees Professor of Chemistry
Department of Chemistry
Northwestern University
Evanston
IL 60208
USA

ISSN 2190-5053 e-ISSN 2190-5061

ISBN 978-1-4419-9646-6 e-ISBN 978-1-4419-9647-3

DOI 10.1007/978-1-4419-9647-3

Springer New York Dordrecht Heidelberg London

Cover design: eStudio Calamar, Berlin/Figueres

Printed on acid-free paper

Springer is part of Springer Science+Business Media (www.springer.com)

For Joy

Supervisor's Foreword

Chemical synthesis is being redefined on a daily basis by the present generation of graduate students in chemistry departments the world over. The doctoral thesis accepted by Northwestern University from Jason Spruell is an outstanding case in point: it bears witness to this evolutionary process in our time.

Gone are the days when the synthesis of organic compounds is a narrowly defined pursuit synonymous with natural product chemistry. Unnatural products have not only claimed their rightful place as a worthwhile intellectual pursuit in chemical synthesis, they are also a modern-day expression of Marcellin Berthelot's doctrine that chemistry can be distinguished alongside the other natural sciences and philosophies by the fact that "chemistry creates its own object."

Gone are the days when most of chemical synthesis is achieved under kinetic control, often under quite extreme reaction conditions. With the advent of supramolecular chemistry, we have witnessed the rapid development of dynamic covalent chemistry. The carrying out of reactions under thermodynamic control has made it possible to reach complex unnatural products in one step from relatively simple starting materials. That's not to say that this contemporary approach to chemical synthesis can provide quick and efficient routes to all the unnatural products we might wish to create. One of the current weaknesses of the thermodynamic approach to chemical synthesis is the relatively small number of reactions that can be performed under equilibrium conditions, even in the presence of a catalyst. This deficiency is being addressed rather convincingly by "click chemistry," a concept which was introduced into the chemical lexicon a decade or so ago by Barry Sharpless, with his observation that Cu(I) catalyzes the azide-alkyne cycloaddition much studied in former times by Rolf Huisgen. The CuAAC reaction is a great example of a kinetically controlled reaction which goes more or less to completion (100%) in double quick time. Reactions under kinetic control which are high yielding are certainly competitively placed alongside thermodynamic control in the synthesis of unnatural products.

Generally speaking, "click chemistry" under kinetic control is more functional group tolerant when it comes to the choice of starting materials and conditions. It was exactly for these reasons that, as a graduate student, Jason Spruell went out

in search of fast and efficient ways of making mechanically interlocked molecules (MIMs). His early work in solution demonstrates just how easy it is to synthesize donor–acceptor [2]-, [3]- and [4]rotaxanes using CuAAC "click chemistry." His penchant for going that extra mile was satisfied by his crafting of a one-pot synthesis of constitutionally unsymmetrical donor–acceptor rotaxanes using "click chemistry" in the CuAAC mode. Their amphiphilic bistable cousins have already found application in the field of molecular electronics when fabricating crossbar memory circuits.

Two words express the common theme which runs through the Spruell PhD thesis. They are "copper catalysis."

Jason describes the template-directed synthesis of a switchable [2]catenane through a Cu(II)-mediated Eglinton coupling of a [2]pseudorotaxane formed between cyclobis(paraquat-*p*-phenylene) ($CBPQT^{4+}$) and a bispropargyl-functionalized tetrathiafulvalene (TTF) derivative which, as a consequence of containing a single switchable recognition unit, exists as one translational isomer in its ground state that may be switched entirely to another translational isomer in the excited oxidized state and exhibits very fast and reversible switching between the two forms. In the parlance of electrical engineers, this single-pole, single-throw (SPST) molecular switch operates between two distinct states in the face of electrochemical stimuli. Call it a push-button molecular switch!

When Dr Spruell applied the same synthetic approach in the presence of the expanded cyclobis(paraquat-4,4′-biphenylene) instead of $CBPQT^{4+}$ as the templating electron-poor cyclophane, he obtained a five-state [3]catenane which can house highly stable TTF radical dimers. As a result of this creative leap in unnatural product synthesis, it became possible for Jason to investigate both the mixed valence and radical cation dimers of tetrathiafulvalene within a "molecular flask." In this way, chemical synthesis entered a radical phase in solution in more ways than one: it was the crowning glory of the Spruell PhD thesis.

Gone are the days when chemical synthesis begins and ends with reactions carried out in solution. Indeed, the fabrication of a molecular memory device based on a crossbar architecture is no more and no less than chemical synthesis at its best. In this spirit, Dr Spruell records in his PhD thesis the various routes he explored to effect the CuAAC protocol in different environments *beyond solution*. A heterogeneous reaction where dissolved alkyne and catalyst react with a surface-bound azide, constitutes a *solution surface* approach to chemical synthesis. On the other hand, a heterogeneous reaction, where the alkyne and catalyst are brought together into contact with a surface-bound azide in a condensed phase, constitutes a *reagent-stamping* approach to chemical synthesis. Finally, there is the so-called *StampCat* method where immobilized copper catalyzes the reaction of an alkyne in the condensed phase. Using this methodology, direct-write "click chemistry" was carried out with sub-100 nm spatial resolution using a copper-coated atomic force microscope (AFM) tip at writing speeds as high as 64 μm/s—a considerable advance over the speeds obtained when patterning with conventional dip-pen nanolithography (DPN). All that is needed is (1) an azide surface, (2) a solution of a terminal alkyne and (3) a copper-coated AFM tip!

The Spruell thesis is a testament to the power of chemical synthesis in contemporary chemistry.

Evanston, May 2011 Fraser Stoddart

Preface

Great strides in the synthetic accessibility of donor–acceptor mechanically interlocked molecules have been made by the application of highly efficient and ultramild chemical transformations during their template-directed synthesis. These new departures in synthesis have indeed played a transformative role in that more complex, higher-order, and functional architectures—once only a dream—are now comfortably within reach. Specifically, the formation of mechanical bonds in [2]-, [3]-, and [4]-rotaxanes and in [2]- and [3]-catenanes has become ever easier through the use of the Cu^{+}-catalyzed azide-alkyne cycloaddition and the Cu^{2+}-catalyzed Eglinton oxidative acetylenic homocoupling. The unique features of donor–acceptor mechanically interlocked molecules—including dynamic mechanical bonds which lend great structural and translational freedom, as well as the ability to stimulate structural rearrangements through redox events—predisposes them towards working as molecular machinery in functional materials and devices. Their increased accessibility, combined with the application of such mild and efficient processes for use in surface patterning techniques, bodes well for strategies seeking to interface molecular machines and surfaces in the shape of working devices. The development of such synthetic methods for high yielding rotaxane and catenane syntheses, as well as finely resolved surface patterning techniques is featured. Additionally, the unique workings of two electrochemically switchable catenanes borne out of these synthetic protocols are presented.

Santa Barbara, March 2011 Jason M. Spruell

Acknowledgments

I must begin by expressing my gratitude to Professor Fraser Stoddart for providing me with the opportunity to work under his direction amongst a group of truly special individuals, in not one but two excellent academic institutions. His supportive and patient mentoring style will remain for me a constant source of inspiration.

The mentorship, advice, and friendship that grew out of a relationship with the very skilled post-doctoral scholar William Dichtel started me down the right path at the beginning of this journey. Additionally, in a similar capacity, Ognjen Miljanić and Diego Benítez have lent crucial support over the years, for which I am also most grateful.

I gratefully acknowledge the financial assistance from the National Science Foundation in the form of a Graduate Student Research Fellowship that has allowed additional dimensions of research and intellectual freedom. Additional support from Northwestern University through the Presidential Fellowship, along with my recent involvement with the Northwestern Society of Fellows, has become a wellspring of new friends, contacts, and ideas.

I am grateful for two unique opportunities to work outside of Fraser's laboratories collaboratively. Professor Jim Heath and the California Institute of Technology shared warm hospitality and the use of facilities, along with helpful guidance and support in a relationship that has continued to flourish. I must also acknowledge Alshakim Nelson and the IBM Almaden Research Center for the opportunity to spend a summer of research out of which has grown my interests in polymer nanotechnology.

None of the research reported here would have been possible without the excellent support of analytical services and the support staff therein. Jane Strouse deserves special attention for nearly single-handedly running the analytical services at UCLA. Jennifer Seymour also played a special role in my research at Northwestern through her skilled use of mass spectrometry. I am also grateful to Professor Alexandra Slawin of the University of St Andrews for her exceptional crystallographic abilities.

I must also thank and acknowledge my thesis committee composed of, in addition to Fraser, Professors SonBinh Nguyen and Emily Weiss. Although our association at Northwestern has been far too short, they have provided me with lasting and valuable advice and input. An additional note of thanks must be directed towards the entire Chemistry Department at Northwestern University for the hearty reception and support they provided following our move across the country.

The Stoddart group is a dynamic group of people that have made my daily experiences both stimulating and always entertaining. While there are far too many to mention here—Travis Gasa, Wenyu Zhang, J.C. Olsen, Matthew Belowich, Ross Forgan, and Wally Paxton—have helped to create, throughout the years, a particularly amiable work environment. My apologies to those I have forgotten in this listing.

Finally, none of this work could have taken place without the constant and patient support of my loving wife Joy. Her gentle guidance provided the needed perspective to always press forward. She has not only provided for me, but has always given of herself for our two wonderful sons, Nathan and London. What has been achieved, we did together.

Contents

Chapter 1
Kinetic and Thermodynamic Approaches for the Efficient Formation of Mechanical Bonds

1.1 Introduction

The mechanical bonds and noncovalent forces that hold together the separate components in mechanically interlocked molecules give rise to relative motions, such as circumrotation and shuttling, which can be used in solid-state devices, e.g., ultradense molecular memory circuits [1]. Bistable [2]rotaxanes and [2]catenanes, which incorporate cyclobis(paraquat-*p*-phenylene) ($CBPQT^{4+}$) as a π-electron-accepting ring component, are particularly well suited to these applications, on account of the fact that their switching actions can be controlled by the reversible oxidation of their π-electron-donating primary recognition sites, e.g., tetrathiafulvalene (TTF). This feature allows these bistable molecules to be switched across a range of different environments, without the addition of chemical reagents. Since their emergence [2] almost two decades ago, virtually every member of these classes of compounds have been synthesized using kinetically-controlled "clipping" approaches (Fig. 1.1) in which a partially formed $CBPQT^{4+}$ ring recognizes a dumbbell or macrocycle containing complementary π-electron-rich recognition units. This recognition process templates the final bond-forming step, which results in closure of the ring. Moderate yields, long reaction times, operationally challenging reaction conditions (12 kbar pressure), and the incompatibility of the $CBPQT^{4+}$ ring to most subsequent chemical transformations limit the practical utility of this approach to the preparation of bistable [2] rotaxanes and [2] catenanes.

This Chapter is reproduced in part with permission from: Dichtel WR, Miljanić OŠ, Zhang W, Spruell JM, Patel K, Aprahamian I, Heath JR, Stoddart JF. *Acc. Chem. Res.* **2008** *41*, 1750–1761. *Author Contributions*: W.R. Dichtel, O.Š. Miljanić, W. Zhang, J.M. Spruell, K. Patel, and I. Aprahamian prepared the original manuscript in part, with relation to each of their reviewed contributions (J.M. Spruell prepared Sect. 1.4). J.R. Heath and J.F. Stoddart supervised the original research and the preparation of the manuscript.

J. M. Spruell, *The Power of Click Chemistry for Molecular Machines and Surface Patterning*, Springer Theses, DOI: 10.1007/978-1-4419-9647-3_1,

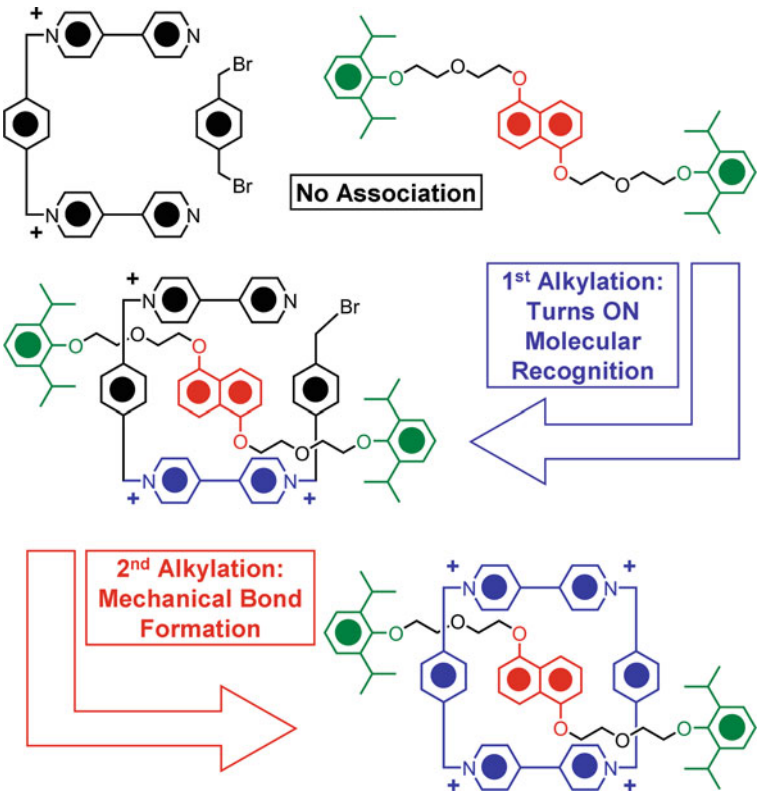

Fig. 1.1 The template-directed clipping reaction used historically for the formation of $CBPQT^{4+}$ rings and mechanical bonds in donor–acceptor rotaxanes (and catenanes)

These shortcomings represent serious challenges to the further development of increasingly sophisticated donor–acceptor mechanically interlocked compounds.

A key realization in the establishment of improved synthetic protocols for these compounds (Fig. 1.2) is that the noncovalent bonding interactions which template their synthesis live on in the final structures, and indeed, are crucial for their subsequent function. Thus, kinetically controlled reactions, where these stabilizing forces are retained in the transition state, can be expected to give mechanically interlocked compounds in high yields. Furthermore, these compounds are lower in free energy than their non-mechanically interlocked components, suggesting that their synthesis under thermodynamic control should also be highly efficient. This approach employs reversible reactions to ultimately provide the most thermodynamically stable products, even if less stable side products are formed during the course of the reaction. Donor–acceptor mechanically interlocked compounds had not been synthesized previously under these conditions, which offer unique advantages relative to kinetically controlled approaches, such as the dynamic exchange of less stable mechanical bonds for more stable ones.

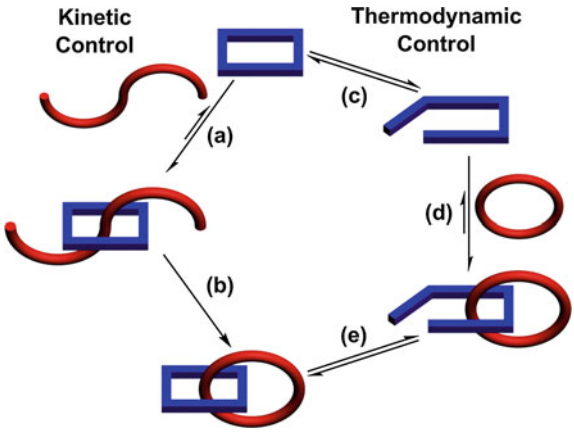

Fig. 1.2 Both kinetic (*left*) and thermodynamic (*right*) control can be exercised in the catenanes synthesis. Kinetically controlled reactions proceed through (**a**) pseudorotaxane formation, followed by (**b**) an irreversible ring closure. Thermodynamically controlled methods rely on (**c**) reversible ring opening of $CBPQT^{4+}$, followed by the (**d**) coordination to a crown ether, and finally (**e**) reversible ring closure

Our recent success in developing both types of synthetic methodologies is a direct result of our investigations of mild chemical transformations compatible with the $CBPQT^{4+}$ ring and its host–guest complexes. This chapter describes the development of new kinetically and thermodynamically controlled protocols for the preparation of donor–acceptor rotaxanes and catenanes and the use of these new protocols for the incorporation of mechanical bonds into increasingly complex molecules.

1.2 Highly Efficient Kinetically Controlled Syntheses of [2]Rotaxanes

The $CBPQT^{4+}$ cyclophane binds π-electron rich aromatic systems, such as 1,5-dioxynaphthalene (DNP) and TTF with high association constants ($K_a \approx 10^5\ M^{-1}$ for oligoethyleneglycol-bearing derivatives) [3]. Consequently, the 1:1 complexes are the dominant species in DMF or MeCN solutions containing the cyclophane and a DNP or TTF derivative at concentrations (1–200 mM) used typically in preparative procedures. Hence, synthetic transformations which are sufficiently mild, so as to be compatible with the complex formation can, in principle, be used either (i) to attach bulky stoppers, affording rotaxanes, or (ii) to effect macrocyclizations, affording catenanes, both in high yield. Until recently, few such transformations were known, largely because of the sensitivity of the $CBPQT^{4+}$ ring towards nucleophiles and bases. We have found, however, that the mild conditions, excellent functional group tolerance, complete regioselectivity, and the high efficiency of the Cu(I)-catalyzed azide-alkyne cycloaddition [4, 5] (CuAAC) make it an ideal reaction for the formation of mechanical bonds under kinetic control [6]. The protocol is exemplified (Scheme 1.1) by the synthesis of the [2]rotaxane **3**·$4PF_6$. The cyclophane CBPQT·$4PF_6$ is threaded by the DNP derivative **1**, bearing two triethyleneglycol chains terminated by azide groups, forming the

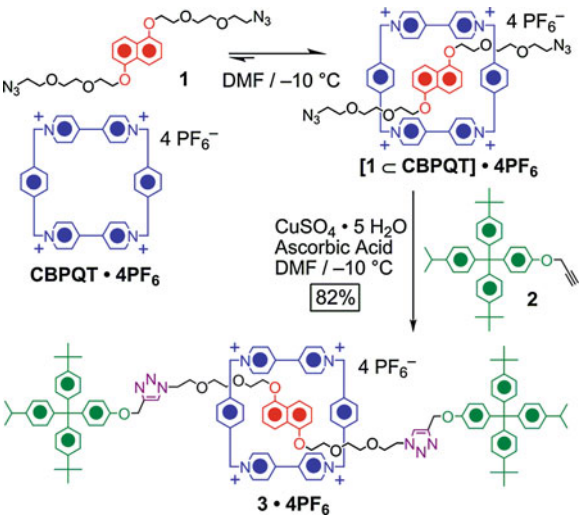

Scheme 1.1 Template-directed synthesis of the [2]rotaxane **3**·4PF$_6$ using the CuAAC methodology

pseudorotaxane [**1** ⊂ CBPQT]·4PF$_6$. The addition of the bulky propargyl ether **2** with its tetraarylmethane core, along with catalytic amounts of $CuSO_4 \cdot 5H_2O$ and ascorbic acid, resulted in the efficient formation of the [2]rotaxane **3**·4PF$_6$. Notably, the formation of the corresponding dumbbell—the CuAAC product without the encircling CBPQT^{4+} ring—was not observed, even when only a slight excess of CBPQT^{4+} (1.05 eq. relative to **1**) was employed in the reaction. No doubt inspired by the increasing use of the CuAAC reaction in materials science [7] and biochemistry [8], several researchers have used this approach successfully to prepare [2]rotaxanes of other kinds [9]. A particularly elegant example is the one described by Leigh and coworkers [10] in which the Cu(I) ion serves both as a catalyst and as a templating element in the formation of the rotaxane.

1.3 Syntheses of [*n*]Catenanes Under Kinetic and Thermodynamic Control

A similar kind of "click chemistry" strategy (Fig. 1.2a and b) was employed in the synthesis (Scheme 1.2) of [2]catenanes [11], simply by performing a macrocyclization of a DNP derivative, whose oligoethylene glycol chains are terminated at one end by an alkyne and at the other by an azide in the presence of CBPQT^{4+}. The efficiency of the macrocyclization was investigated [12] as a function of ring size by subjecting the [2]pseudorotaxanes [**4a–c** ⊂ CBPQT]·4PF$_6$ to either the conditions employed for the synthesis of **3**·4PF$_6$ or to CuI in MeCN. These conditions gave the corresponding [2]catenanes **5b**·4PF$_6$ and **5c**·4PF$_6$ in 41 and 23% isolated yields, respectively. The [2]pseudorotaxane [**4a** ⊂ CBPQT]·4PF$_6$, however, failed

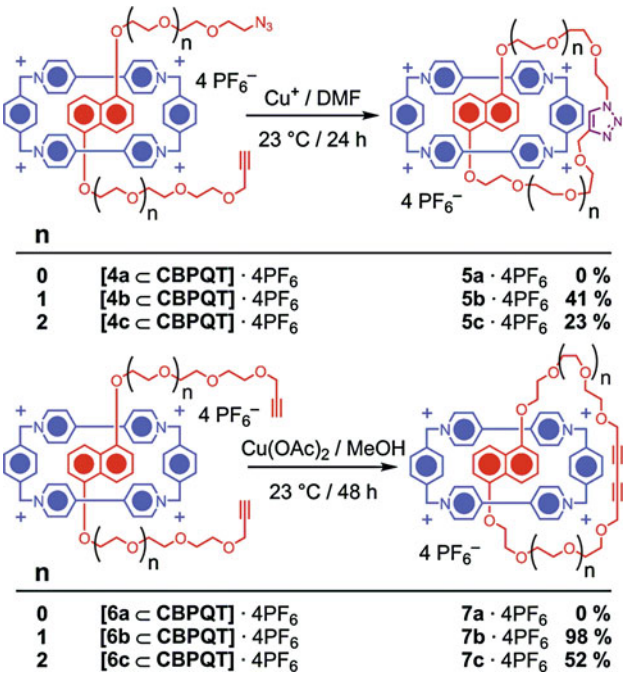

Scheme 1.2 Template-directed synthesis of donor–acceptor [2]catenanes **5a–c**·4PF$_6$ and **7a–c**·4PF$_6$ with varying sizes of the DNP-containing macrocycles using either the CuAAC or Eglington oxidative alkyne homocoupling

to react and only **4a** and CBPQT·4PF$_6$ were recovered, possibly because the glycol chains of **4a** are too short to form a macrocycle free of significant ring strain.

The successful syntheses of the [2]rotaxane **3**·4PF$_6$ and the catenanes **5b**·4PF$_6$ and **5c**·4PF$_6$ demonstrate that the copper acetylides, that most likely serve as intermediates in the CuAAC reaction, are compatible with the chemically sensitive CBPQT^{4+} and its pseudorotaxane-like host–guest complexes. We have also investigated the likelihood of [2]catenane formation employing other reactions, such as the Eglington oxidative alkyne homocoupling [13], which also proceed through Cu-acetylide intermediates. In addition to the more symmetrical nature of the starting materials and products, we found the same trends in yields relative to the oligoethylene glycol chain lengths during the formation of the catenanes **7a–c**·4PF$_6$, as was observed for those using the CuAAC approach. The dialkyne-containing catenanes, however, were formed in significantly improved yields, as exemplified most notably in the synthesis of **7b**·4PF$_6$, which was isolated in 97% yield, reflecting a remarkably efficient macrocyclization process. As observed in the case of [**4a**·CBPQT]·4PF$_6$, no catenane was obtained during the attempted cyclization of the pseudorotaxane [**6a**·CBPQT]·4PF$_6$: a single-crystal X-ray structural analysis of this pseudorotaxane also suggested that the oligoethylene glycol chains of **6a** are far too short to form a strain-free macrocycle.

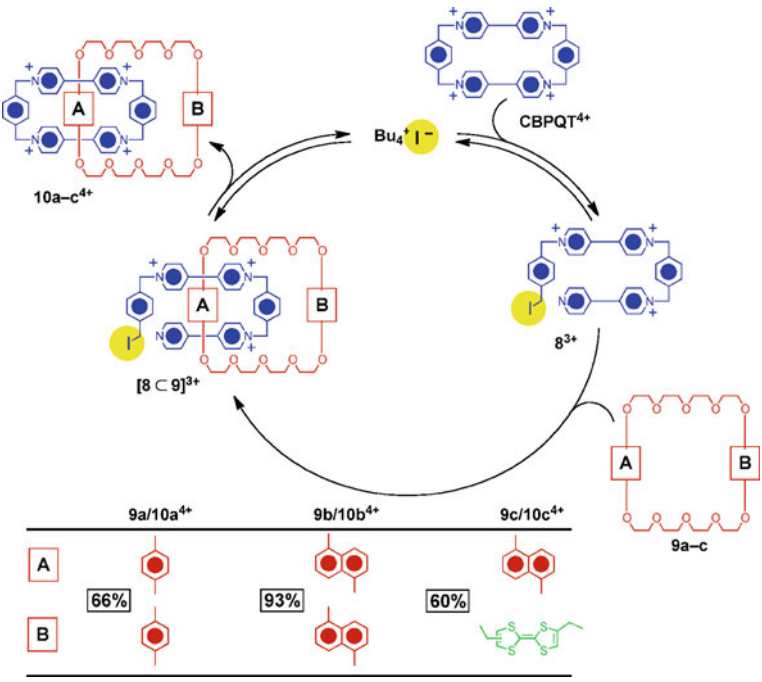

Scheme 1.3 Mechanism for the template-directed synthesis of various donor–acceptor [2]catenanes (**10a–c**$^{4+}$) under thermodynamic control

The noncovalent bonding interactions between the components of catenanes and rotaxanes stabilize these molecules significantly relative to the sum of their individual components lacking mechanical bonds. This pronounced energetic bias renders dynamic covalent chemistry (DCC) [14, 15] appealing for the synthesis (Fig. 1.2c–e) of mechanically interlocked compounds. DCC depends on thermodynamically controlled reactions that recycle the starting materials and the side-products until equilibria favoring the mechanically interlocked compounds as the most stable ones are established. We have shown [16] recently that a thermodynamically controlled nucleophilic substitution can provide an efficient route to donor–acceptor catenanes incorporating the CBPQT^{4+} ring. In this research, tetrabutylammonium iodide (TBAI) was employed as the catalyst in a "magic ring" experiment, in which the CBPQT^{4+} ring was first of all opened and then reversibly closed around a crown ether ring to form a donor–acceptor catenane. Mechanistically, this transformation commences (Scheme 1.3) with a rate-limiting nucleophilic attack of TBAI onto the CBPQT^{4+} ring to generate the trication **8**$^{3+}$. TBAI was chosen as the catalyst because it is a good nucleophile, a good leaving group, a poor reducing agent, and soluble in MeCN. The tricationic π-acceptor **8**$^{3+}$ complexes readily [17] with crown ethers, such as **9a–c**, to give pseudorotaxanes [**8** π**9**]$^{3+}$. Nucleophilic attack then occurs, closing the CBPQT^{4+} ring around the crown ethers to give catenanes **10a–c**$^{4+}$, regenerating the iodide ion.

The reversibility of the overall reaction was confirmed by an exchange experiment. The preformed [2]catenane **10a**$^{4+}$ was treated with an excess of the crown ether **9b**, which has been shown to associate more strongly with CBPQT^{4+}, and presumably with the trication **8**$^{3+}$. After equilibrium was reached over the course of 11 days, the more stable [2]catenane **10b**$^{4+}$ constituted about ∼90% of the final reaction mixture.

Since the reaction proceeds only at elevated temperatures (∼80 °C), the equilibration can be arrested on cooling to room temperature, a property which allows the convenient isolation of the catenated products. The approach is general in scope, easy to execute—since protecting atmospheres and dry solvents are not required—and proceeds in yields as high as 93%. In the context of molecular devices, the bistable catenane **10c**$^{4+}$ was prepared in a straightforward manner by dynamic nucleophilic substitution in 60% yield—that is, almost three times more efficiently than by using [18] the traditional kinetically controlled approach. We have, however, failed thus far to extend this method to the synthesis of rotaxanes. Our rationalization for this failure is that—at the elevated temperatures required for reaction to occur—the association of the π-electron accepting **8**$^{3+}$ with an acyclic π-donating dumbbell is less favorable compared to the association of **8**$^{3+}$ with a much more constrained π-donating macrocycle. However, on going from the CBPQT^{4+} ring to cyclobis(paraquat-4,4′-biphenylene)—a larger π-accepting ring which associates [19] with crown ethers with 1:2 stoichiometry—we were able to prepare [20] the respective [3]catenanes, derived from **9a** and **9b**, in yields greater than 84 and 91%, respectively. This virtually undiminished efficiency of conversion suggests that even larger mechanically interlocked systems—including perhaps the elusive donor–acceptor polycatenanes—could be targeted by the protocol involving dynamic nucleophilic substitution.

1.4 Formation of Higher Order Rotaxanes Using CuAAC

One of the most significant challenges towards realizing the long-standing objective to incorporate multiple CBPQT^{4+} rings into higher order rotaxane architectures and ultimately into a wide variety of materials, is the modest efficiency of the clipping reaction and the low convergence that characterized the strategy associated with its synthesis. For example, the simultaneous clipping of two CBPQT^{4+} rings onto a bistable dumbbell afforded [21] only 9% of the desired [3]rotaxane, which represents one of the most complex compounds of this kind that can be prepared practically using this synthetic approach. No longer constrained by the requirement of performing the clipping reaction on a fully formed dumbbell template in the final step of the synthesis, retrosynthetic analysis of a palindromic [3]rotaxane structure suggested a disconnection in the middle of the molecule, with the simultaneous formation of the final structure and incorporation of the CBPQT^{4+} rings using the CuAAC reaction. Indeed, a similar—albeit simplified—palindromic [3]rotaxane **13**·8PF_6 was synthesized [6] (Scheme 1.4) from

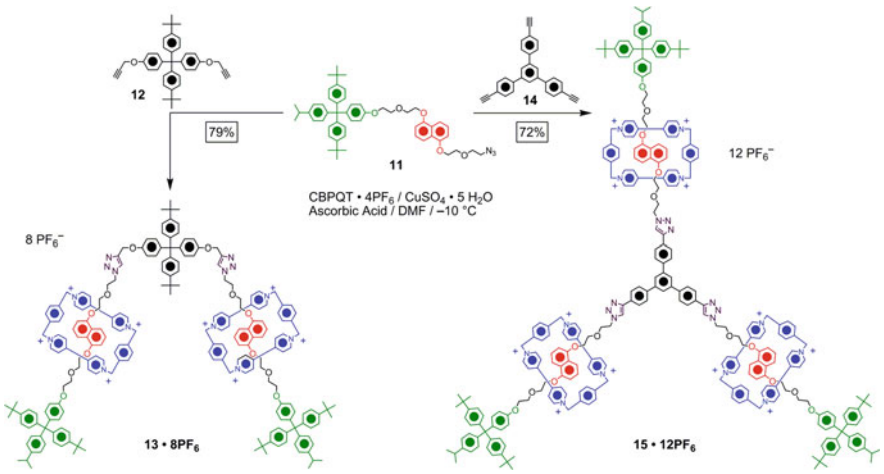

Scheme 1.4 Template-directed synthesis of the [3]- and [4]rotaxanes **13**·8PF_6 and **15**·12PF_6 through CuAAC of a stoppered DNP-derivative with bi- and trifunctional alkynes

the stoppered DNP azide **11**, the bis(propargyl ether) **12**, and CBPQT·4PF_6 in a significantly improved 79% isolated yield. Furthermore, by substituting tris-1,3,5(4′-ethynylphenyl)benzene **14** for **12**, the branched [4]rotaxane **15**·12PF_6 was obtained in 72% isolated yield, and represents the first example of a donor–acceptor [4]rotaxane prepared in our laboratory. The good yields obtained during the synthesis of these higher order rotaxanes point to a significant advantage of the CuAAC stoppering approach, since there is essentially no penalty in the yields of the compounds when incorporating multiple cyclophanes into the molecules.

We have subsequently elaborated this methodology to enable the one-pot synthesis of rotaxanes with two different stoppers, employing sequential CuAAC reactions [22]. The order of the two cycloadditions is controlled by protecting the alkyne functions with trimethylsilyl (TMS) groups, which are then removed after the first CuAAC reaction is complete. Though methods commonly employed for alkyne desilylation occur under more strongly nucleophilic conditions and are thus not compatible with the presence of the $CBPQT^{4+}$ ring, we confirmed that Ag(I)-catalyzed hydrolysis of the TMS groups [23] is compatible both with the presence of the $CBPQT^{4+}$ ring and the carrying out of the subsequent CuAAC reactions in the same pot. In order to highlight the efficiency of this methodology, the three-fold symmetric amphiphilic [4]rotaxane **21**·12PF_6 was synthesized [24] (Scheme 1.5) in one-pot, first by (a) performing the CuAAC reaction between the monofunctional DNP derivative **17** and the triazide **16**, (b) the removal of the silyl protecting groups, and (c) the second stoppering reaction with the hydrophilic azide **20** in the presence of the $CBPQT^{4+}$ ring. The complexity of the final products available from comparatively simple starting materials using this strategy is noteworthy, and—as a consequence of identifying mild and efficient desilylation conditions—the introduction of the $CBPQT^{4+}$ ring need not occur in the final step of the synthesis of the

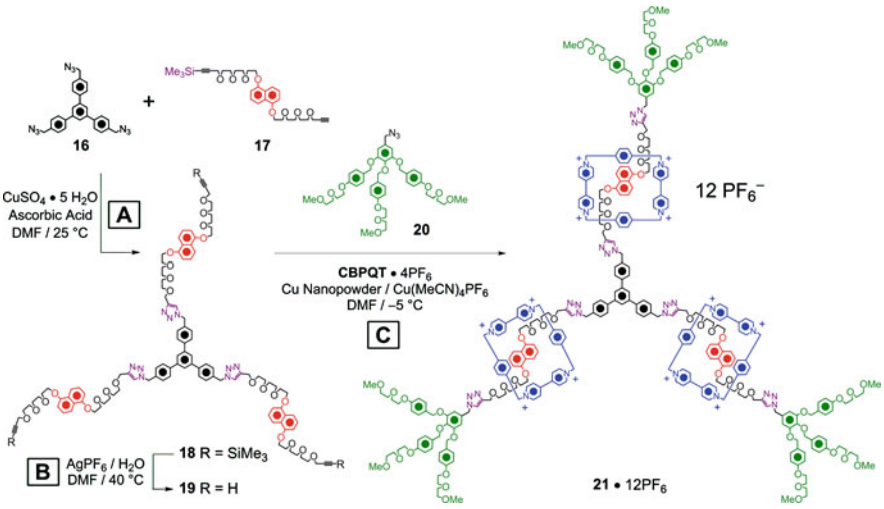

Scheme 1.5 Sequential template-directed CuAAC synthesis in one pot of an amphiphilic [4]rotaxane **21**·12PF_6

rotaxane. We are currently taking advantage of these features to design and synthesize previously unavailable topologies of mechanically interlocked donor–acceptor compounds.

1.5 Shuttling and Switching Within Triazole-Containing [2]Rotaxanes

An important aspect of the development of the CuAAC threading-followed-by-stoppering synthetic approach involved an investigation of whether the incorporation of disubstituted 1,2,3-triazole units into the dumbbell components of [2]rotaxanes would impact significantly either (i) the thermally activated or (ii) electrochemically controlled motions of the $CBPQT^{4+}$ ring. The former situation was investigated [25] by measuring (Fig. 1.3) the rate of shuttling of the cyclophane between two degenerate DNP recognition sites separated by a bis(triazole)-containing central spacer unit in the molecular shuttle **21**·4PF_6. When the motion of the $CBPQT^{4+}$ ring is slow on the NMR time scale, the resonances of protons on opposite sides of the dumbbell separate into two signals of equal intensity. See, for example, the resonances for the *t*-Bu (H_a, H_a') and *i*-Pr (H_b, H_b') protons in the partial spectrum recorded at 261 K in Fig. 1.3. The frequency of the shuttling increases with temperature, resulting eventually in the coalescence of the two pairs of signals at 309 K, corresponding to an energy barrier of 15.5 ± 0.1 kcal mol^{-1}. This value is similar to those measured previously [26] for degenerate molecular shuttles containing triphenylene and tetraethylene glycol spacers (15.0 ± 0.2 and 15.5 ± 0.1 kcal mol^{-1},

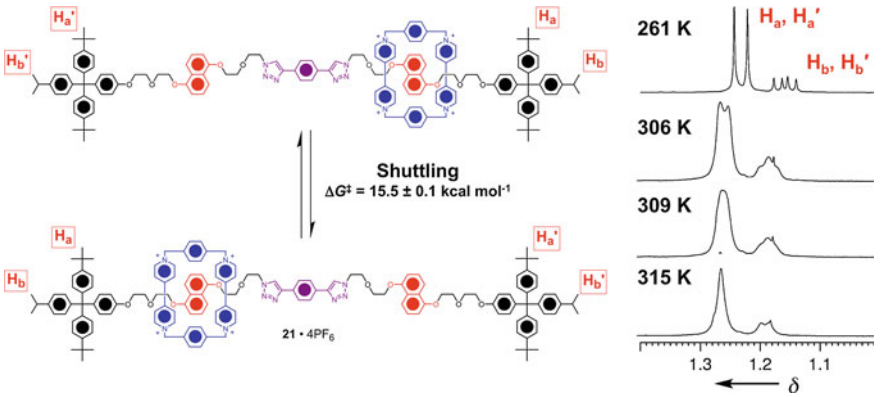

Fig. 1.3 The two degenerate co-conformations of the **21**·4PF_6 shuttle (*left*) and portions of the variable-temperature ^{1}H NMR spectra (500 MHz, CD_3COCD_3) obtained at different temperatures containing the *t*-Bu (H_a/H_a') and *i*-Pr (H_b/H_b') resonances

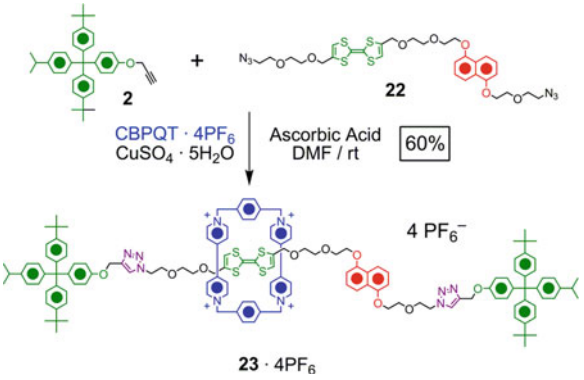

Scheme 1.6 Template-directed CuAAC-mediated synthesis of an electrochemically switchable bistable [2]rotaxane **23**·4PF_6

respectively). These findings suggest that the disubstituted 1,2,3-triazole rings may be incorporated into rotaxanes and may even be located between the recognition sites without significant concern that they will interfere with the movement of the $CBPQT^{4+}$ ring.

Satisfied that the disubstituted 1,2,3-triazole units do not disrupt the thermally activated shuttling of the $CBPQT^{4+}$ ring, we went on to assess their compatibility with the electrochemical switching processes of bistable [2]rotaxanes. The prototypical bistable [2]rotaxane **23**·4PF_6 was prepared (Scheme 1.6) through CuAAC-mediated stoppering of the diazide **22** containing both a TTF and a DNP moiety [27]. The ^{1}H NMR spectrum of **23**·4PF_6 in CD_3COCD_3, in common with those of other bistable [2]rotaxanes of this type, indicated the dominant presence (>95%) of the TTF-encircled translational isomer at equilibrium. The reversibility of the electromechanical switching process of **23**·4PF_6 is evident (Fig. 1.4) from spectroelectrochemical (SEC) measurements. Before the switching process is initiated ($E = 0$ vs. Ag wire), the absorbance centered at 840 nm corresponds to

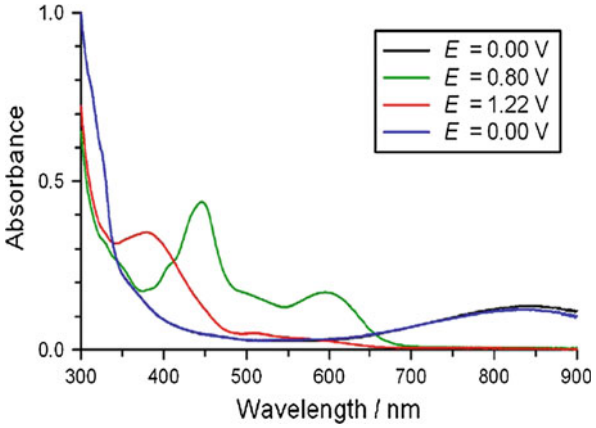

Fig. 1.4 UV–Visible spectra obtained during the SEC measurements (MeCN, 0.25 mV s^{-1} scan rate) of the CuAAC-derived bistable [2]rotaxane **23**·4PF_6. The applied potential was changed from $E = 0$ to 1.22 V and then back to $E = 0$ V

the charge transfer (CT) interaction typically observed when a TTF unit is encircled by a $CBPQT^{4+}$ ring. Between +0.50 and +0.80 V, new bands appear with maxima at 445 and 595 nm, corresponding to the absorbance of the TTF radical cation (TTF^{+}). These changes are accompanied by the bleaching of the TTF-$CBPQT^{4+}$ CT band. When the applied potential was increased further, the absorption band of the TTF^{+} was replaced by a new peak with a λ_{max} at 380 nm, which can be assigned to the TTF dication (TTF^{2+}). In contrast to the TTF^{+}, the TTF^{2+} does not absorb significantly between 500 and 600 nm, and so permits the observation of the weak DNP–$CBPQT^{4+}$ CT peak at ca. 530 nm. Finally, when the applied potential is returned to zero, the spectrum gradually makes its way back to its original state containing the TTF–$CBPQT^{4+}$ CT band, verifying the full reversibility of the redox process. These observations, along with other supporting ^{1}H NMR spectroscopic data and the full electrochemical characterization of **23**·4PF_6, confirmed that the triazole rings do not interfere with the unique switching mechanisms of these compounds, paving the way for their incorporation into range of new material and device architectures.

1.6 Incorporating Mechanical Bonds into Materials and New Environments

The mechanical force and changes associated with the generation of translational isomers during the electrochemical switching process of these bistable rotaxanes and catenanes form the *raison d'etre* for their incorporation into molecular electronic devices, nanoelectromechanical systems, and nanoparticle-based controlled release vehicles. These technological applications motivated an investigation of the fundamental thermodynamic and kinetic parameters of the switching processes in a range of condensed environments, such as within polymer gels [28], self-assembled monolayers (SAMs) on gold surfaces [29], and molecular switch tunnel

junctions (MSTJs) [3]. The correlation of these parameters across each of these environments for several bistable rotaxanes and catenanes provides compelling evidence for (i) a universal switching mechanism and for (ii) attributing this mechanism to the hysteretic response of molecular memory circuits.

The subsequent development of the CuAAC methodology has greatly enhanced our efforts to prepare new bistable [2]rotaxanes which can operate in different environments, e.g., the recent development of a derivative which forms liquid crystalline (LC) phases [30]. The ordering of liquid crystals is a cooperative phenomenon that is highly sensitive to weak perturbations, including the photoisomerization of small quantities of added molecular rotors [31]. Hence, we set out to align electrochemically switchable bistable [2]rotaxanes within LC phases, as a possible means of amplifying the effect of molecular switching and so influence the bulk LC ordering. The bistable [2]rotaxane **24**·4PF_6 (Fig. 1.5) with dendritic mesogens as stoppers was synthesized by subjecting the diazide **22** and mesogens functionalized with propargyl ester groups to the same CuAAC conditions employed for the synthesis of **23**·4PF_6. The convergence of the CuAAC approach is particularly noteworthy in this case: it allows **22** to be employed as a general precursor to nearly all symmetrically stoppered bistable rotaxanes. The high efficiency of the reaction was also critical, as our efforts to attach these mesogens to threads containing TTF and DNP units under esterification conditions had been unsuccessful, precluding even an attempt at synthesizing the mesogenic bistable [2]rotaxane using the clipping protocol. As expected, **24**·4PF_6 exhibits an LC smectic A (S_A) phase from 10 to 150 °C, above which it undergoes thermal decomposition. Peaks with d spacings of 83.0 (100), 41.5 (200), and 27.3 Å (300) were observed in its small angle X-ray scattering (SAXS) pattern obtained at 40 °C. This layer spacing of $\sim$8 nm observed for the S_A phase corresponds to the extended molecular length of **24**·4PF_6. The electrochemical switching of **24**·4PF_6, which was characterized in solution by CV and SEC, was qualitatively similar to that shown in Fig. 1.4 for **22**·4PF_6. Our current efforts focus on switching LC assemblies of **24**·4PF_6 while monitoring its effect on the LC properties of the system as a whole.

In moving beyond using the CuAAC reaction to facilitate the synthesis of well-defined [2]-, [3]-, or [4]rotaxanes, we have recently achieved a long-standing goal of synthesizing donor–acceptor polyrotaxanes which incorporate a considerable number of $CBPQT^{4+}$ rings [32]. We are particularly interested in studying the effect of electromechanical switching on the bulk properties of the associated polymer. Relatively few examples of polyrotaxanes have been reported, with the exception of those which incorporate more chemically robust cyclodextrin [33] or cucurbituril [34] derivatives as the macrocyclic component. Donor–acceptor polyrotaxanes have remained synthetically elusive, mostly because the clipping reaction is unlikely to provide a high coverage of $CBPQT^{4+}$ rings onto a stoppered polymer template, i.e., dumbbell. We employed a CuAAC step-growth polymerization to prepare [32] (Scheme 1.7) azide-terminated polymers **27** ranging in M_n from 32 to 180 kDa by adjusting the feed ratio of the monomers—bis(triethyleneglycol propargyl ether) DNP derivative **25** and the DNP diazide **26**. Following purification of the polymers,

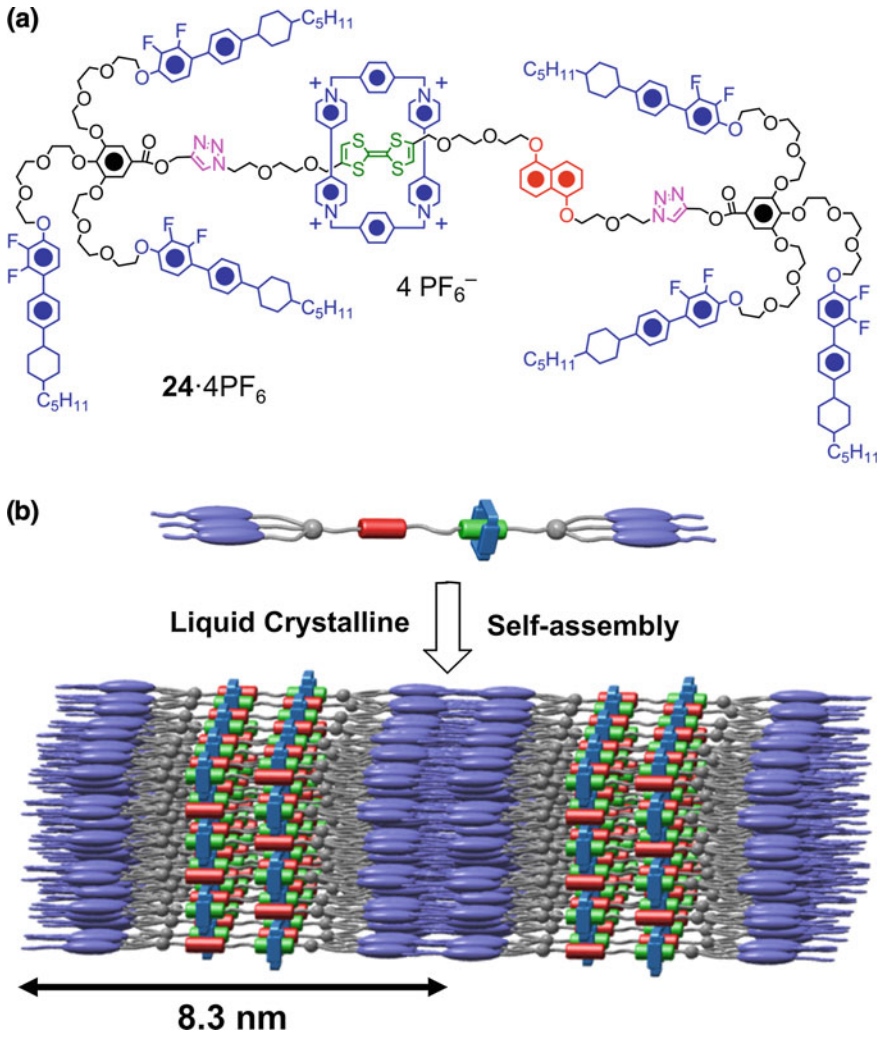

Fig. 1.5 **a** Structural formula of a mesogenic electrochemically switchable bistable [2]rotaxane **24**·4PF_6. **b** Illustration of the hypothetical organization of **24**·4PF_6 into a smectic A phase, as suggested by small angle X-ray scattering data

$CBPQT^{4+}$ rings were threaded onto the chains, and alkyne-bearing stoppers were finally attached, once again using the CuAAC reaction, providing the polyrotaxane **29**·4nPF_6. The use of 0.6 equivalents of $CBPQT^{4+}$·4PF_6 relative to the total number of DNP units resulted in polyrotaxanes with an average coverages ranging from 90 to 58% of the repeat units encircled by $CBPQT^{4+}$ rings, as measured by integration of the appropriate ^{1}H NMR resonances.

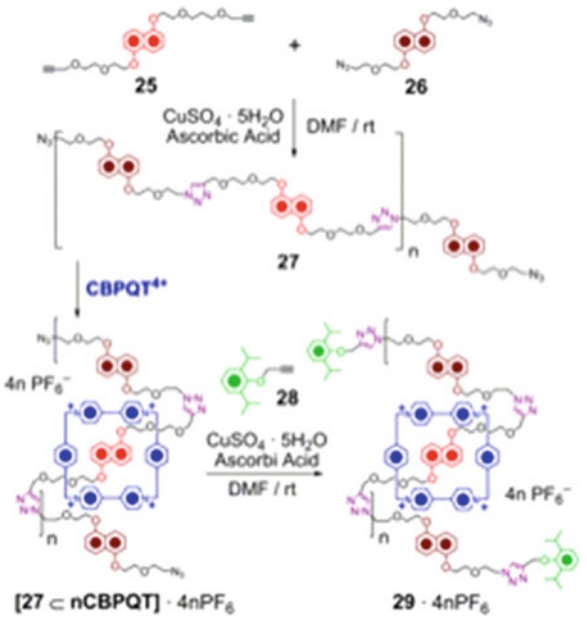

Scheme 1.7 CuAAC-mediated polymerization and subsequent template-directed threading and stoppering processes for the preparation of the polyrotaxane **29**·4nPF$_6$

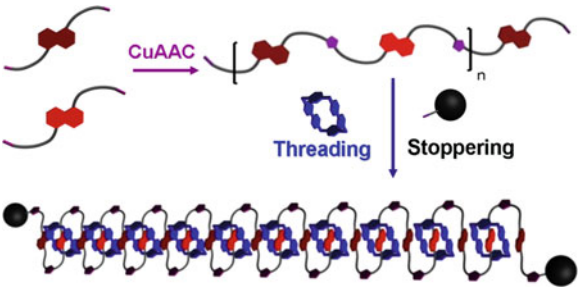

Fig. 1.6 Graphical representation of the synthetic approach towards the synthesis of CBPQT^{4+}-containing polyrotaxanes and an idealized representation of the folding observed in these materials as a consequence of stacking of the alongside DNP units against the outside of the CBPQT^{4+} rings

One of the first unique properties observed in the polyrotaxanes is that they fold into a compact structure as a consequence of secondary intramolecular interactions. By limiting the CBPQT^{4+} incorporation to less than 50% of the available DNP units and using alternating DNP-containing monomers with differing binding affinities, a majority of the rings encircle the more favorable DNP units, while the secondary DNP recognition sites stack on the outside of the rings. In this manner, the polymer adopts a folded conformation (Fig. 1.6), an effect observed previously [35] in aqueous solutions of polymers containing alternating π-electron donors and acceptors and in more rigid polymers and oligomers of certain polyamide [36] and *m*-phenylene ethylene [37] "foldamers". The folding behavior was characterized

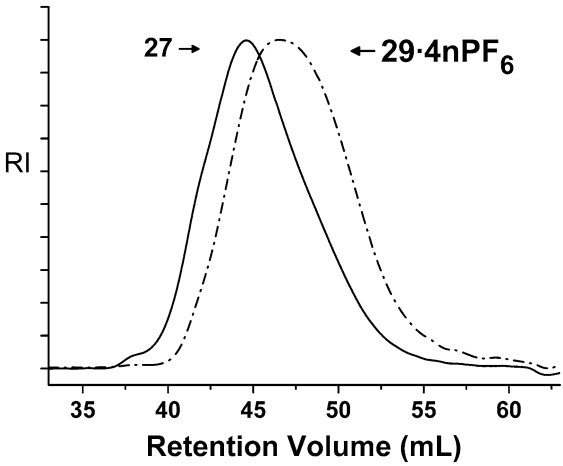

Fig. 1.7 Gel permeation chromatographs of the polymer thread **27** (M_n = 32 kDa) and its corresponding polyrotaxane **29**·4nPF$_6$, in which an average of 90% of the repeat units contain a CBPQT^{4+} ring. Although the molecular weight of **29**·4nPF$_6$ is nearly twice that of **27**, the retention volume of the polyrotaxane increases, a phenomenon which can be attributed to its folded structure

(Fig. 1.7) by several techniques, such as gel permeation chromatography (GPC), in which the apparent molecular weight of each polyrotaxane sample was smaller than that measured for its polymer thread precursor, a phenomenon which is suggestive of a more compact structure. The noncovalent interactions responsible for the folding process were further characterized by variable-temperature ^{1}H NMR spectroscopy of the polyrotaxanes and an oligomeric model compound. Finally, the lengths of the polyrotaxanes were found to be significantly shorter than the precursor polymeric threads, as measured by atomic force microscopy performed on the polymers drop-cast onto highly ordered pyrolytic graphite. Our current work on these polyrotaxanes focuses on incorporating TTF monomers into the polymer backbone, a modification which will allow study of the electromechanical switching process of the CBPQT^{4+} rings along the polymer backbone, both in solution and in the bulk.

Finally, inspired by the increasing use of the CuAAC for surface functionalization [38–40], we have successfully attached stoppering groups to surface-bound pseudorotaxanes—a simple and direct route to simultaneously synthesizing [2]rotaxanes and interfacing them with nanostructured materials. We have used this approach for the preparation (Fig. 1.8) of snap-top covered silica nanocontainers (SCSNs) [41]. An SCSN consists of a [2]rotaxane tethered to the surface of a silica particle (400 nm in diameter) containing hexagonally arranged 2 nm diameter pores. The [2]rotaxanes on the surface incorporate α-cyclodextrin (α-CD) rings, each encircling an oligoethylene glycol thread and fixed in place by a CuAAC reaction with a cleavable stopper. When intact, these rotaxanes efficiently trap guest molecules, such as the fluorescent probe rhodamine B, within the pores of the silica. However, hydrolysis of the adamantyl ester-containing stopper, catalyzed by porcine liver esterase, results in dethreading of the α-CD rings and diffusion of the guest molecules out of the pores, while non-cleavable control stoppers or denatured samples of the enzymes showed no such evidence of guest

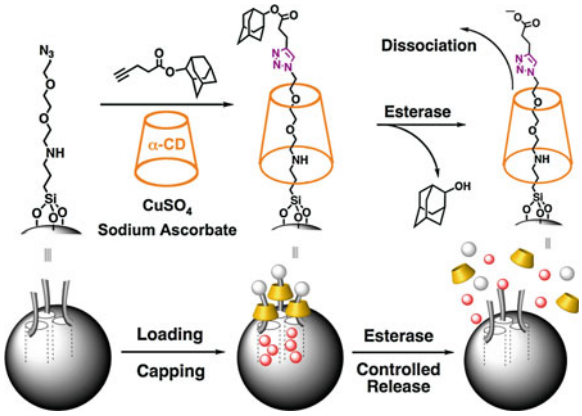

Fig. 1.8 The preparation and opening of adamantyl ester stoppered snap-top covered silica nanocontainers. The empty pores of the silica nanoparticles are loaded with the desired payload, such as fluorescent marker Rhodamine B (*small spheres*). The openings to the pores are blocked by α-cyclodextrin (α-CD) based rotaxanes containing enzyme-cleavable stoppers. Cleavage of the stoppers by the appropriate enzyme releases the α-CD macrocycles and allows the payload to diffuse from the pores

molecule release. Because of the wide range of stoppering units that can be attached to the SCSN precursor, a multitude of snap-top systems with differentiated modes of activation can be prepared with relative ease. In addition to further developing the SCSN systems, we anticipate using the CuAAC reaction—carried out either in solution or through recently-developed microcontact printing techniques [42]—to incorporate new classes of electrochemically active mechanically interlocked compounds into molecular electronic devices.

1.7 Conclusions

As a result of investigating mild chemical transformations compatible with the $CBPQT^{4+}$ cyclophane which operate under either kinetic or thermodynamic control, we have developed template-directed synthetic protocols to provide well-defined donor–acceptor mechanically interlocked compounds with increased convergence and reaction efficiency. These complementary advances serve to make bistable [2]rotaxanes and bistable [2]catenanes of this type more compatible with a variety of new device architectures and aid and abet the efficient preparation of previously inaccessible compounds, including large well-defined mechanically interlocked compounds and polymers. These synthetic tools are indispensible as we seek to create complex systems with emergent properties [43] and increasingly sophisticated functions, especially within device settings.

References

1. Green JE, Choi JW, Boukai A, Bunimovich Y, Johnston-Halpering E, DeIonno E, Luo Y, Sheriff BA, Xu K, Shin YS, Tseng H-R, Stoddart JF, Heath JR (2007) Nature 445:414–417
2. Ashton PR, Goodnow TT, Kaifer AE, Reddington MV, Slawin AMZ, Spencer N, Stoddart JF, Vicent C, Williams DJ (1989) Angew Chem Int Ed Engl 28:1396–1399
3. Choi JW, Flood AH, Steuerman DW, Nygaard S, Braunschweig AB, Moonen NNP, Laursen BW, Luo Y, DeIonno E, Peters AJ, Jeppesen JO, Xu K, Stoddart JF, Heath JR (2006) Chem Eur J 12:261–279
4. Rostovtsev VV, Green LG, Fokin VV, Sharpless KB (2002) Angew Chem Int Ed 41:2596–2599
5. Tornoe CW, Christensen C, Meldal MJ (2002) Org. Chem. 67:3057–3064
6. Dichtel WR, Miljanić OŠ, Spruell JM, Heath JR, Stoddart JF (2006) J Am Chem Soc 128:10388–10390
7. Lutz JF (2007) Angew Chem Int Ed 46:1018–1025
8. Kolb HC, Sharpless KB (2003) Drug Discovery Today 8:1128–1137
9. Mobian P, Collin JP, Sauvage J-P (2006) Tetrahedron Lett 47:4907–4909
10. Aucagne V, Hanni KD, Leigh DA, Lusby PJ, Walker DB (2006) J Am Chem Soc 128:2186–2187
11. Miljanić OŠ, Dichtel WR, Mortezaei S, Stoddart JF (2006) Org Lett 8:4835–4838
12. Miljanić OŠ, Dichtel WR, Khan SI, Mortezaei S, Heath JR, Stoddart JF (2007) J Am Chem Soc 129:8236–8246
13. Siemsen P, Livingston RC, Diederich F (2000) Angew Chem Int Ed 39:2633–2657
14. Rowan SJ, Cantrill SJ, Cousins GRL, Sanders JKM, Stoddart JF (2002) Angew Chem Int Ed 41:898–952
15. Corbett PT, Leclaire J, Vial L, West KR, Wietor JL, Sanders JKM, Otto S (2006) Chem Rev 106:3652–3711
16. Miljanić OŠ, Stoddart JF (2007) Proc Natl Acad Sci USA 104:12966–12970
17. D'Acerno C, Doddi G, Ercolani G, Mencarelli P (2000) Chem Eur J 6:3540–3546
18. Asakawa M, Ashton PR, Balzani V, Credi A, Hamers C, matterstig G, Montalti M, Shipway AN, Spencer N, Stoddart JF, Tolley MS, Venturi M, White AJP, Williams DJ (1998) Angew Chem Int Ed 37:333–337
19. Asakawa M, Ashton PR, Menzer S, Raymo FM, Stoddart JF, White AJP, Williams DJ (1996) Chem Eur J 2:877–893
20. Patel K, Miljanić OŠ, Stoddart JF (2008) Chem Commun 1853–1855
21. Liu Y, Flood AH, Bonvallett PA, Vignon SA, Northrop BH, Tseng H-R, Jeppesen JO, Huang TJ, Brough B, Baller M, Magonov S, Solares SD, Goddard WA, Ho CM, Stoddart JF (2005) J Am Chem Soc 127:9745–9759
22. Aucagne V, Leigh DA (2006) Org Lett 8:4505–4507
23. Orsini A, Viterisi A, Bodlenner A, Weibel JM, Pale PA (2005) Tetrahedron Lett 46:2259–2262
24. Spruell JM, Dichtel WR, Heath JR, Stoddart JF (2008) Chem Eur J 14:1468–1477
25. Braunschweig AB, Dichtel WR, Miljanić OŠ, Olson MA, Spruell JM, Khan SI, Heath JR, Stoddart JF (2007) Chem Asian J 2:634–647
26. Kang SS, Vignon SA, Tseng H-R, Stoddart JF (2004) Chem Eur J 10:2555–2564
27. Aprahamian I, Dichtel WR, Ikeda T, Heath JR, Stoddart JF (2007) Org Lett 9:1287–1290
28. Steuerman DW, Tseng H-R, Peters AJ, Flood AH, Jeppesen JO, Nielsen KA, Stoddart JF, Heath JR (2004) Angew Chem Int Ed 43:6486–6491
29. Tseng H-R, Wu DM, Fang NXL, Zhang X, Stoddart JF (2004) Chem Phys Chem 5:111–116
30. Aprahamian I, Yasuda T, Ikeda T, Saha S, Dichtel WR, Isoda K, Kato T, Stoddart JF (2007) Angew Chem Int Ed 46:4675–4679
31. Eelkema R, Pollard MM, Vicario J, Katsonis N, Ramon BS, Bastiaansen CWM, Broer DJ, Feringa BL (2006) Nature 440:163

32. Zhang W, Dichtel WR, Steig AZ, Benítez D, Gimzewski JK, Heath JR, Stoddart JF (2008) Proc Natl Acad Sci USA 105:6514–6519
33. Wenz G, Han BH, Müller A (2006) Chem Rev 106:782–817
34. Whang D, Jeon YM, Heo J, Kim K (1996) J Am Chem Soc 118:11333–11334
35. Lokey RS, Iverson BL (1995) Nature 375:303–305
36. Appella DH, Christianson LA, Klein DA, Powell DR, Huang XL, Barchi JJ, Gellman SH (1997) Nature 387:381–384
37. Hill DJ, Moore JS (2002) Proc Natl Acad Sci USA 99:5053–5057
38. Lummerstorfer T, Hoffmann HJ (2004) Phys Chem B 108:3963–3966
39. Collman JP, Devaraj NK, Chidsey CED (2004) Langmuir 20:1051–1053
40. Rohde RD, Agnew HD, Yeo WS, Bailey RC, Heath JR (2006) J Am Chem Soc 128:9518–9525
41. Patel K, Angelos S, Dichtel WR, Coskun A, Yang Y-W, Zink JI, Stoddart JF (2008) J Am Chem Soc 130:2382–2383
42. Rozkiewicz DI, Janczewski D, Verboom W, Ravoo BJ, Reinhoudt DN (2006) Angew Chem Int Ed 45:5292–5296
43. Aprahamian I, Olsen J-C, Trabolsi A, Stoddart JF (2008) Chem Eur J 14:3889–3895

Chapter 2
Efficient Templated Synthesis of Donor–Acceptor Rotaxanes Using Click Chemistry

2.1 Introduction

The discovery of highly efficient synthetic strategies for making electrochemically switchable, mechanically interlocked compounds will facilitate their continued development as components in molecular electronic devices [1–6] (MEDs) and nanoelectromechanical systems [7–26] (NEMS). Traditionally, such compounds, incorporating cyclobis(paraquat-*p*-phenylene) ($CBPQT^{4+}$) as the π-accepting ring component, have been synthesized [27, 28] by "clipping" a partially formed $CBPQT^{4+}$ ring (Fig. 2.1a) around a dumbbell or ring containing π-electron-rich recognition sites. Although this synthetic strategy has found wide application [29–32], the moderate yield typical of the $CBPQT^{4+}$ clipping reaction limits its practical value to the preparation of [2]rotaxanes and [2]catenanes. Herein, we describe an alternative synthetic approach (Fig. 2.1b and c) to donor–acceptor rotaxanes—including previously inaccessible [3]- and [4]rotaxanes. Their synthesis relies upon the efficient stoppering of their pseudorotaxane precursors.

This Chapter is reproduced in part with permission from: Dichtel WR, Miljanić OŠ, Spruell JM, Heath JR, Stoddart JF. *J. Am. Chem. Soc.* **2006** *128*, 10388–10390.
Author Contributions: W.R. Dichtel and J.F. Stoddart prepared the original manuscript. W.R. Dichtel, O.Š. Miljanić, and J.M. Spruell conceived of the project. W.R. Dichtel and J.M. Spruell synthesized the compounds reported in the communication (J.M. Spruell synthesized compounds **2** and **5**). J.F. Stoddart and J.R. Heath supervised the original research.

J. M. Spruell, *The Power of Click Chemistry for Molecular Machines and Surface Patterning*, Springer Theses, DOI: 10.1007/978-1-4419-9647-3_2,

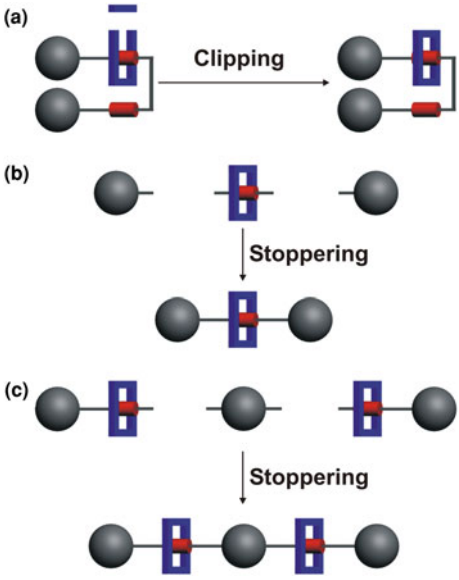

Fig. 2.1 Graphical representations of different strategies employed in the template-directed syntheses of donor–acceptor rotaxanes: **a** clipping of a macrocycle around a dumbbell, **b** double stoppering of a pseudorotaxane to form a [2]rotaxane, and **c** attachment of two semirotaxanes onto a bifunctional stopper to form a [3]rotaxane

2.2 Results and Discussion

Motivated by the use of click chemistry [33, 34] in the synthesis of a variety of functional materials [35–52] including an example [53–55] in which the Cu catalyst templates rotaxane formation, we reasoned that donor–acceptor rotaxanes might be obtained by attaching alkyne-terminated stoppers to $CBPQT^{4+}$ pseudorotaxanes using the Cu-(I)-catalyzed Huisgen 1,3-dipolar cycloaddition ("click" chemistry). The click reaction has been noted for its high regioselectivity [33, 34] tolerance of sensitive functional groups, mild reaction conditions, and excellent yields. The click reaction occurs at room temperature (and below), requiring only the addition of catalytic amounts of $CuSO_4$ and ascorbic acid, all conditions which are ideal for strong binding of $CBPQT^{4+}$ to a wide variety of thread molecules containing π-donors.

This threading-followed-by-stoppering approach is complementary to clipping and has a number of advantages. Because the recognition elements are fully formed from the outset of the reaction, templation utilizes the full thermodynamic binding of $CBPQT^{4+}$ to the guest of interest. The click methodology is also much more convergent: relatively simple, modular rotaxane components are synthesized in parallel, and the mechanically interlocked structure is assembled in the final step of the reaction protocol. The general synthetic strategy (Scheme 2.1) involves the mixing of $CBPQT{\cdot}4PF_6$ in DMF at -10 °C, with a 1,5-dioxynaphthalene (DNP) derivative **1** carrying azide-terminated glycol chains. Under these conditions, the equilibrium lies predominantly in favor of the [2]pseudorotaxane $[\mathbf{1}\subset CBPQT^{4+}]{\cdot}4PF_6$. A propargyl ether-functionalized stopper **2** is then added to the reaction mixture along with $CuSO_4{\cdot}5H_2O$ and ascorbic acid. Following these

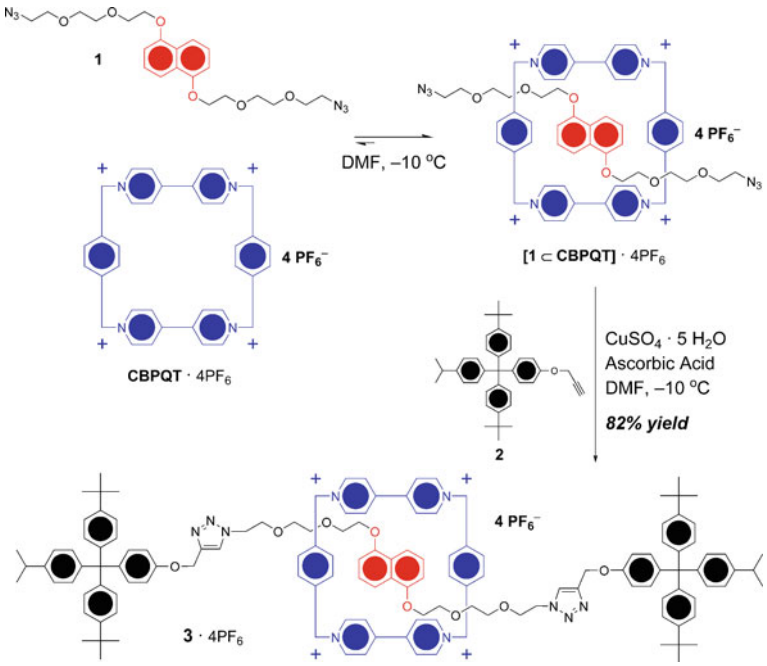

Scheme 2.1 Threading-followed-by-stoppering route to [2]rotaxane **3**·4PF$_6$

mild reaction conditions, the [2]rotaxane **3**·4PF$_6$ was isolated in 82% yield. Formation of the dumbbell was not observed by thin layer chromatography.

Encouraged by this successful proof of concept, we decided to apply this methodology to the synthesis of [3]rotaxanes. Doubly bistable [3]rotaxanes incorporating tethered CBPQT^{4+} rings have been used as redox-driven molecular muscles [56]. Although actuation was achieved, clipping two CBPQT^{4+} rings around the synthetically valuable palindromic dumbbell gave the desired [3]rotaxane in only 9% yield. Using the click methodology, a similar (albeit simplified) palindromic [3]rotaxane was synthesized (Scheme 2.2) from relatively simple precursors CBPQT·4PF$_6$, the stoppered DNP azide **4**, and bis-(propargyl ether) **5** in 79% isolated yield.

The comparative efficiency of the click methodology is emphasized by the synthesis (Scheme 2.3) of the branched [4]rotaxane **8**·12PF$_6$ in 72% isolated yield after reacting **4** with tris-1,3,5(4′-ethynylphenyl)benzene [57] **7** in the presence of CBPQT·4PF$_6$. A clipping approach is expected to provide this [4]rotaxane in very low (<3%) yield.

The partial ^{1}H NMR spectra (Fig. 2.2) of **8**·12PF$_6$ reflect its 3-fold symmetry. The resonances for the DNP protons, which are shielded and resonate at $\delta = 6.49$ (H-2/6), 6.22 (H-3/7), and 2.75 (H-4/8, not shown) ppm, are typical for rotaxanes containing CBPQT^{4+} and DNP residues. At +25 °C, rotations of the bipyridinium units and *p*-phenylene ring systems in the CBPQT^{4+} rings are slow

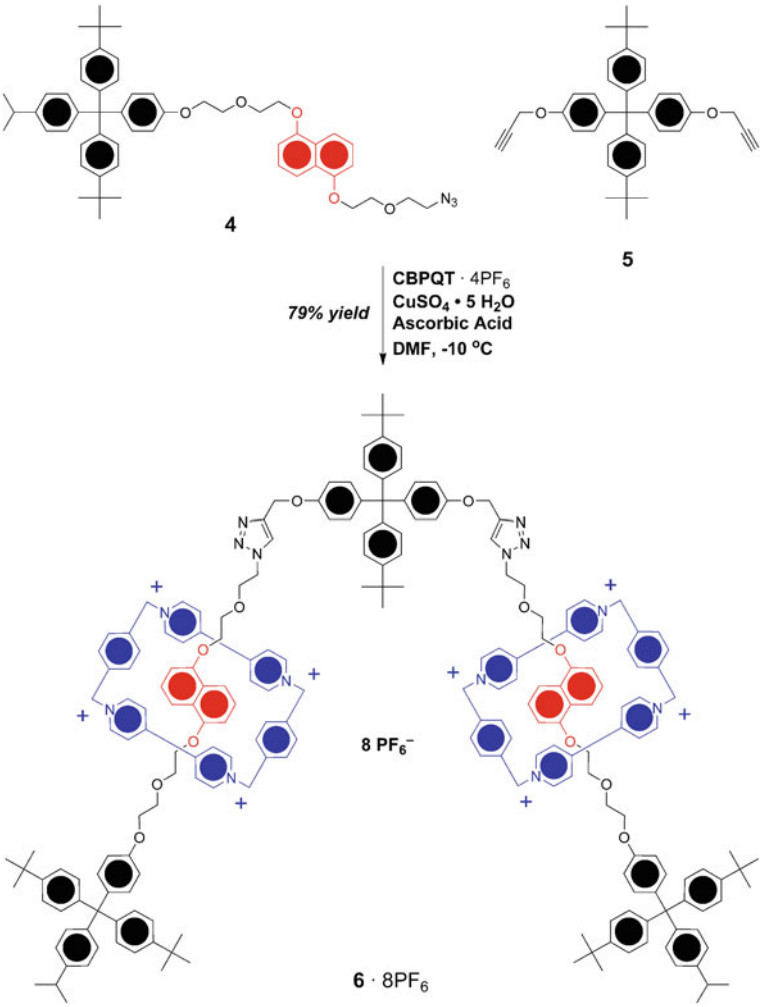

Scheme 2.2 Synthesis of [3]rotaxane **6**·8PF_6 with high efficiency

on the ^{1}H NMR time scale, resulting in broadening of the signals for the CBPQT protons. The spectrum becomes much simpler as the signals for these protons coalesce at higher temperatures. At lower temperatures, the exchange processes between all of the relevant protons slows yet further, allowing for resolution of non-equivalent proton signals. Throughout the temperature range investigated, the triazole resonance remains a sharp singlet near $\delta = 8.60$ ppm, a reasonable value for triazole protons. This observation suggest that the triazole does not compete with DNP to bind with the $CBPQT^{4+}$ ring—a hypothesis we are currently investigating more thoroughly.

Scheme 2.3 Synthesis of [4]rotaxane **8**·12PF_6 with high efficiency

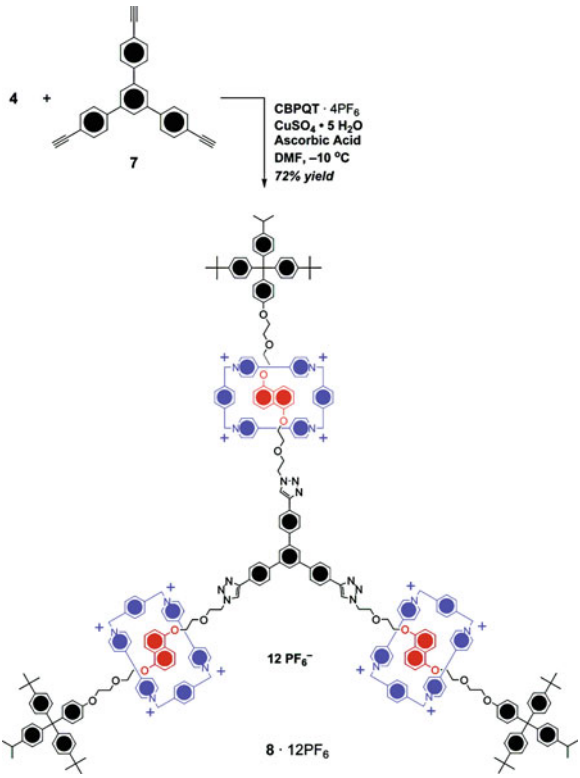

2.3 Conclusions

During this preliminary research, it has become apparent that, as a result of using click chemistry as the covalent modification step in rotaxane synthesis, it not only renders the simple donor–acceptor [2]- and [3]rotaxanes (Schemes 2.1 and 2.2) much more accessible but it also provides the opportunity to prepare respectable quantities of more exotic mechanically interlocked compounds, such as the branched [4]rotaxane (Scheme 2.3). The synthesis and applications of these new materials to MEDs and NEMs will now become part of the ongoing research efforts in our laboratories.

2.4 Experimental Section

2.4.1 General Methods

All reagents were purchased from commercial suppliers (Aldrich or Fisher) and used without purification. 1,5-Bis[2-(2-(2-(toluene-4-sulfonyl)ethoxy)ethoxy)ethoxy]-

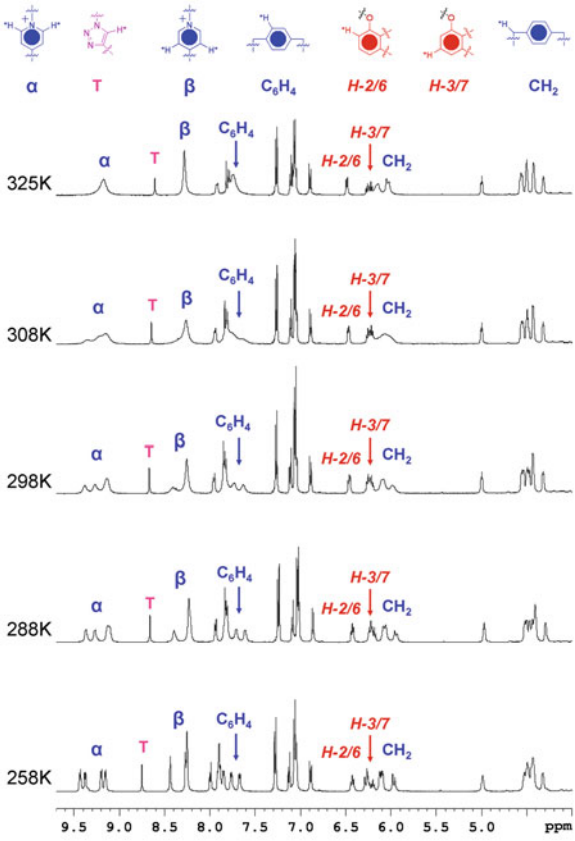

Fig. 2.2 Partial ^{1}H NMR spectra (500 MHz, CD_3COCD_3) of **8**·12PF_6 recorded at different temperatures. Several diagnostic peaks are labeled, including the signals for the CBPQT^{4+} α and β protons, and resonances for two of the three DNP protons. Slow rotation of the bipyridinium and *p*-phenylene units in the CBPQT^{4+} rings is reflected in their broad proton resonances at 298 K. At lower temperatures, these rotations are slowed even further until the signals become clearly resolved. The signals for the CBPQT^{4+} α and β protons coalesce into single, albeit broad, peaks at higher temperatures

naphthalene [58,] cyclobis(paraquat-*p*-phenylene) [59,] and 4-[bis[4-(*t*-butyl)phenyl][4-(isopropyl)phenyl]methyl]phenol [60,] tris-1,3,5(4′-ethynylphenyl) benzene [61] were prepared using previously published procedures. Thin layer chromatography (TLC) was performed on silica gel 60 F254 (E. Merck). Preparative thin layer chromatography (Prep TLC) was performed on glass plates with a 1 mm thick layer of silica gel 60 F254 (E. Merck). Column chromatography was performed on silica gel 60F (Merck 9385, 0.040–0.063 mm). Nuclear magnetic resonance (NMR) spectra were recorded on a Bruker Avance 600 (^{1}H: 600 MHz; ^{13}C: 150 MHz) or 500 (^{1}H: 500 MHz; ^{13}C: 126 MHz) spectrometer. Chemical shifts are reported as parts per million (ppm) downfield from the Me_4Si resonance as the internal standard for both ^{1}H and ^{13}C NMR spectroscopies. Electrospray ionization (ESI) mass spectra were measured on a Finnigan LCQ ion-trap mass spectrometer using 1:1 MeCN:H_2O as the mobile phase. High-resolution fast atom bombardment (HR-FAB) mass spectra were obtained on a JEOL JMS-600H high resolution mass spectrometer equipped with a FAB probe. Electrospray ionization mass spectra were obtained on a Finnigan LCQ ion trap mass spectrometer.

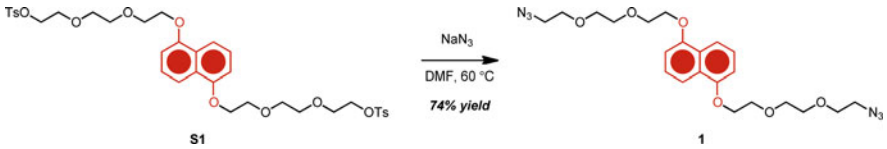

Scheme 2.4 Synthesis of DNP diazide derivative **1**

Scheme 2.5 Synthesis of alkyne functionalized stopper **2**

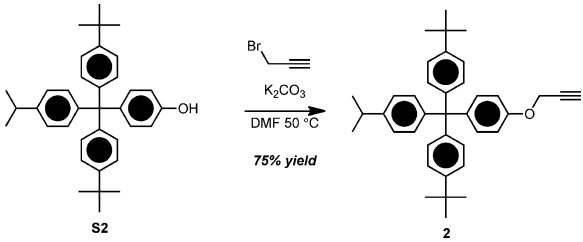

Preparation of 1,5-Bis[2-(2-(2-(azide)ethoxy)ethoxy)ethoxy]naphthalene **1** 1,5-Bis[2-(2-(2-(toluene-4-sulfonyl)ethoxy)ethoxy)ethoxy]naphthalene [58] (**S1**, 0.200 g, 0.273 mmol) and sodium azide (0.355 g, 5.458 mmol) were dissolved in DMF (2.7 mL) and heated to 60 °C for 12 h (Scheme 2.4). The crude reaction mixture was partitioned between 100 mL of water and CH_2Cl_2, and the aqueous phase was washed with CH_2Cl_2 (3 × 50 mL). The combined organic extracts were washed with brine, dried ($MgSO_4$), and the solvent evaporated. The crude product was chromatographed (SiO2, 7:3 CH_2Cl_2:Et_2O eluent) to give 96 mg (74.4% yield) of **1** as a pale yellow solid. **1**: ^{1}H NMR (500 MHz, $CDCl_3$, 25 °C, TMS): δ 7.86 (d, ^3J (H,H) = 9 Hz, 2H, DNP aryl -H *p*-O), 7.35 (t, ^3J (H,H) = 9 Hz, 2H, DNP aryl -H *m*–O), 6.84 (d, ^3J (H,H) = 8 Hz, 2H, DNP aryl -H *o*–O), 4.31 (t, ^3J (H,H) = 5 Hz, 4H, DNP-OCH_2), 4.00 (t, ^3J (H,H) = 5 Hz, 4H), 3.82 (t, ^3J (H,H) = 9 Hz, 4H), 3.71 (m, 8H), 3.37 (t, ^3J (H,H) = 5 Hz, 4H, CH_2N_3); ^{13}C NMR (125 MHz, $CDCl_3$, 25 °C): δ 154.2, 126.7, 125.0, 114.5, 105.6, 71.0, 70.7, 70.0, 69.8, 67.8, 50.6; HRMS (FAB): Calcd for $C_{22}H_{30}N_6O_6$ *m/z* = 474.2227. Found *m/z* = 474.2226.

Preparation of 4-[Bis[4-(*t*-butyl)phenyl][4-(isopropyl)phenyl]methyl]phenyl-propargyl Ether **2** Tetraarylmethane **S2** (4-[bis[4-(*t*-butyl)phenyl][4-(isopropyl)-phenyl]methyl]phenol [60,] 0.750 g, 1.528 mmol) and K_2CO_3 (0.634 g, 4.585 mmol) were suspended in DMF (7.6 mL). Propargyl bromide (0.6 g of an 80 wt% solution in xylenes, 3.47 mmol) was added and the solution was heated to 50 °C for 12 h (Scheme 2.5). The reaction mixture was poured in 75 mL of EtOAc and was washed with 1 M $NaHSO_4$ (75 mL), H_2O (2 × 75 mL), brine (75 mL), and dried ($MgSO_4$). The solution was evaporated onto silica gel, loaded onto a silica gel column, and chromatographed using 1:9 EtOAc:hexanes as the eluent to obtain 0.602 g (75% yield) of **2** as a white solid. **2**: ^{1}H NMR (500 MHz, $CDCl_3$, 25 °C, TMS): 7.22 (d, ^2J(H,H) = 9 Hz, 4H, Ar–H *ortho*-tBu), 7.12 (d, ^2J(H,H) = 7 Hz, 2H, Ar–H, Ar–H *ortho*-iPr), 7.07 (m, 8H, all meta Ar–H), 6.85 (d, ^2J(H,H) = 6 Hz,

2H, Ar–H *ortho*–O), 4.66 (d, ^2J(H,H) = 2 Hz, -O-CH_2-), 2.88 (septet, ^2J(H,H) = 7 Hz, 1H, -$CH(CH_3)_2$), 2.52 (t, ^2J(H,H) = 2 Hz, 1H, CCH), 1.30 (s, 18H, tBu), 1.24 (d, ^2J(H,H) = 7 Hz, 6H, iPr); ^{13}C NMR (125 MHz, CDCl3): δ 155.4, 148.2, 146.0, 144.4, 144.0, 140.4, 132.2, 130.9, 130.6, 125.1, 124.0, 113.2, 78.7, 75.3, 63.1, 55.7, 34.2, 33.4, 31.3, 23.9; HRMS (FAB): Calcd for $C_{39}H_{45}O$ *m/z* = 529.3470. Found *m/z* = 529.3449.

Preparation of the [2]Rotaxane **3**·4PF_6 Diazide DNP derivative **1** (0.0070 g, 0.015 mmol), $CBPQT^{4+}$ (0.017 g, 0.015 mmol), and the alkyne-functionalized stopper **2** (0.016 g, 0.031 mmol) were dissolved in DMF (0.160 mL) at −10 °C, forming a deep red solution. Stock solutions of $CuSO_4$·$5H_2O$ in DMF (20 μL, 0.074 M) and ascorbic acid in DMF (20 μL, 0.148 M) were added. The solution was stirred at −10 °C for 24 h, at which time the solvent was evaporated. The red solid was redissolved in Me_2CO and the [2]rotaxane was purified by preparative TLC using a 1% w/v NH_4PF_6 solution in Me_2CO as the mobile phase. The rotaxane product was recovered from the silica gel by washing with an excess of eluent solution. The Me_2CO was concentrated to a minimum volume, and the product was precipitated from this solution through the addition of an excess of cold water. The click [2]rotaxane **3**·4PF_6 was isolated as a purple solid (0.033 g, 84% yield). **3**·4PF_6**:** ^{1}H NMR (500 MHz, CD_3COCD_3, 52 °C): δ 9.21 (br s, 8H, α-$CBPQT^{4+}$), 8.29 (s, 8H, β-$CBPQT^{4+}$), 8.02 (s, 2H, triazole-H), 7.75 (br s, 8H, aryl-$CBPQT^{4+}$), 7.29 (d, ^3J (H,H) = 7 Hz, 8H, stopper aryl-H *o*-tBu), 7.11 (m, 20H, stopper—all meta Ar–H plus *o*-iPr aryl -H), 6.84 (d, ^3J (H,H) = 9 Hz, 4H, stopper aryl -H *o*–O), 6.49 (d, ^3J (H,H) = 8 Hz, 2H, DNP *o*-O), 6.26 (t, ^3J (H,H) = 8 Hz, 2H, DNP- *m*–O), 6.02 (br s, 8H, $CBPQT^{4+}$ benzyl H), 4.97 (s, 4H, stopper -OCH_2), 4.61 (t, ^3J (H,H) = 5 Hz, 4H), 4.50 (br m, 4H), 4.30 (br m, 4H), 4.15 (t, ^3J (H,H) = 5 Hz, 4H), 4.09 (br m, 4H), 4.00 (br m, 4H), 2.89 (septet, ^3J (H,H) = 7 Hz, 2H, stopper iPr H), 2.80 (d, ^3J (H,H) = 8 Hz, 2H, DNP *p*-O), 1.31 (s, 36H, tBu), 1.23 (d, ^3J (H,H) = 7 Hz, 12H, iPr CH3); ^{13}C NMR (125 MHz, CD_3COCD_3, 52 °C): 149.6, 147.3, 146.7, 145.8, 145.4, 137.9, 133.1, 132.6, 131.9, 131.7, 129.3, 126.3, 125.8, 125.2, 114.6, 110.0, 105.9, 72.1, 71.8, 71.1, 70.5, 69.3, 66.6, 64.3, 62.6, 35.0, 34.3, 31.8, 24.3; MS (ESI, 1:1 MeCN:H_2O, 0.1% AcOH): Found 1170.9 $(M–2PF_6)^{2+}$, 723.3 $(M–3PF_6)^{3+}$, 512.9 $(M–4PF_6)^{4+}$.

General Click Chemistry Procedure for the Synthesis of High Order Rotaxanes and Preparation of [3]Rotaxane **6**·8PF_6 DNP Derivative **4** (0.013 g, 0.0155 mmol, 1.05 eq. per alkyne), $CBPQT^{4+}$ (0.0195 g, 0.0178 mmol, 1.2 eq. per alkyne), and the dialkyne functionalized tetraarylmethane **5** (0.0040 g, 0.0074 mmol) were dissolved in DMF (0.090 mL) at −10 °C, forming a deep red solution. Stock solutions of $CuSO_4$·$5H_2O$ in DMF (20 μL, 0.036 M, 0.05 eq per alkyne) and ascorbic acid in DMF (20 μL, 0.072 M, 0.1 eq. per alkyne) were added. The solution was stirred at −10 °C for 24 h, at which time the solvent was evaporated. The red solid was redissolved in Me_2CO and the product [2]rotaxane was purified by preparative TLC using a 2% w/v NH_4PF_6 solution in Me_2CO as the mobile phase. The rotaxane product was recovered from the silica gel by washing with an excess of Me_2CO/NH_4PF_6 solution. The Me_2CO was concentrated to a minimum

volume, and the product was precipitated from this solution through the addition of an excess of cold water. The click [3]rotaxane **6**·8PF_6 (0.033 g, 84% yield) was isolated by filtration as a purple solid and dried under high vacuum overnight. **6**·8PF_6**:** ^{1}H NMR (500 MHz, CD_3CN, 75 °C): δ 8.77 (br s, 16H, α-CBPQT^{4+}), 8.07 (s, 2H, triazole-H), 7.99 (s, 16H, *β*-CBPQT^{4+}), 7.30 (m, 28H, aryl-CBPQT^{4+}, all stopper aryl-H *o*-tBu), 7.10 (m, 28H, stopper m- aryl -H, stopper aryl -H *o*-iPr), 6.86 (m, 8H, stopper aryl -H *o*–O), 6.41 (d, ^3J (H,H) = 8 Hz, 2H, DNP *o*–O), 6.37 (d, ^3J (H,H) = 8 Hz, 2H, DNP *o*–O), 6.01 (m, 4H, DNP- *m*–O), 5.79 (d, ^2J (H,H) = 13 Hz, 8H, CBPQT^{4+} benzyl H), 5.79 (d, ^2J (H,H) = 13 Hz, 8H, CBPQT^{4+} benzyl H), 5.11 (s, 4H, OCH_2-triazole), 4.83 (t, ^3J (H,H) = 5 Hz, 4H, triazole-CH_2), 4.46 (br m, 8H), 4.30 (br m, 12H), 4.25 (m, 8H), 2.88 (septet, ^3J (H,H) = 7 Hz, 2H, stopper iPr H), 2.56 (d, ^3J (H,H) = 8 Hz, 2H, DNP *p*-O), 2.55 (d, ^3J (H,H) = 8 Hz, 2H, DNP *p*-O), 1.31 (s, 18H, central tBu), 1.29 (s, 36H, external tBu), 1.22 (d, ^3J (H,H) = 7 Hz, 12H, stopper iPr); ^{13}C NMR (125 MHz, CD_3CN, 75 °C): δ 156.2, 156.1, 150.9, 148.5, 148.4, 146.2, 145.2, 144.7, 144.3, 144.3, 143.8, 140.1, 140.0, 136.4, 131.8, 131.6, 131.2, 130.3, 130.0, 128.0, 127.9, 126.1 125.4, 124.6, 124.3, 124.2, 124.2, 113.5, 113.4, 108.2, 104.4, 104.3, 70.4, 69.8, 69.6, 68.2, 68.0, 65.0, 62.9, 62.6, 61.1, 50.5, 33.8, 33.8, 33.1, 30.5, 30.4, 23.1; MS (ESI, 1:1 MeCN:H_2O, 0.1% AcOH): Found 1,324.6 $(M–3PF_6)^{3+}$, 957.3 $(M–4PF_6)^{4+}$, 736.9 $(M–5PF_6)^{5+}$, 589.9 $(M–6PF_6)^{6+}$, 484.9 $(M–7PF_6)^{7+}$.

Preparation of [4]Rotaxane **8**·12PF_6 The above procedure was followed using tris-1,3,5(4′-ethynylphenyl)benzene **7**[57] (0.0040 g, 0.011 mmol) as the alkyne containing component. Preparative TLC as described above provided the [4]rotaxane **8**·12PF6 (47.5 mg, 72% yield) as a purple solid. **8**·12PF_6**:** ^{1}H NMR (500 MHz, CD_3COCD_3, 52 °C): δ 9.17 (br s, 24H, α-CBPQT^{4+}), 8.61 (s, 3H, triazole-H), 8.28 (s, 24H, *β*-CBPQT^{4+}), 7.79 (m, 39H, aryl-CBPQT^{4+}, all central unit Ar–H), 7.26 (d, ^3J (H,H) = 7 Hz, 12H, stopper aryl -H *o*-tBu), 7.07 (m, 30H, stopper—all meta Ar–H plus *o*-iPr aryl -H), 6.88 (d, ^3J (H,H) = 9 Hz, 6H, stopper aryl -H *o*–O), 6.49 (d, 3 *J* (H,H) = 8 Hz, 6H, DNP *o*–O), 6.22 (overlapping t, ^3J (H,H) = 8 Hz, 6H, both DNP- *m*–O), 6.03 (br m, 24H, CBPQT^{4+} benzyl H), 4.00 (t, ^3J (H,H) = 8 Hz, 6H, stopper- OCH_2), 4.55 (m, 12H), 4.50 (m, 12H), 4.43 (m, 12H), 4.32 (t, ^3J (H,H) = 5 Hz, 6H, triazole-NCH_2), 2.86 (septet, ^3J (H,H) = 7 Hz, 3H, stopper iPr H), 2.55 (br s, 3H, DNP *p*- O), 1.28 (s, 54H, tBu), 1.20 (d, ^3J (H,H) = 7 Hz, 12H, iPr CH_3); ^{13}C NMR (125 MHz, CD_3COCD_3, 25 °C):156.2, 150.8, 148.4, 147.2, 146.2, 145.2, 144.7, 144.3, 143.6, 141.4, 140.2, 140.0, 136.3, 131.8, 131.2, 130.3, 130.0, 127.9, 127.9, 127.7, 126.2, 125.7, 125.4, 124.6, 124.3, 124.2, 121.5, 113.4, 108.2, 104.4, 104.2, 70.35, 69.9, 69.7, 68.1, 68.0, 65.0, 62.9,50.5, 33.8, 33.1, 30.4, 23.1; MS (ESI, 1:1 MeCN:H_2O, 0.1% AcOH): Found 1915.2 $(M–3PF_6)^{3+}$, 1400.3 $(M–4PF_6)^{4+}$, 1091.3 $(M–5PF_6)^{5+}$, 885.3 $(M–6PF_6)^{6+}$, 738.1 $(M–7PF_6)^{7+}$, 627.7 $(M–8PF_6)^{8+}$, 541.8 $(M–9PF_6)^{9+}$.

Preparation of Stopper-DNP-OH **S4** Tetraarylmethane **S2** (1.500 g, 3.057 mmol), dioxynaphthalene monotosylate derivative (1.799 g, 3.668 mmol) [61], K_2CO_3 (1.690 g,12.23 mmol), and [18]crown-6 (0.040 g, 0.153 mmol) were taken up in MeCN (30 mL). The heterogeneous solution was refluxed with vigorous stirring

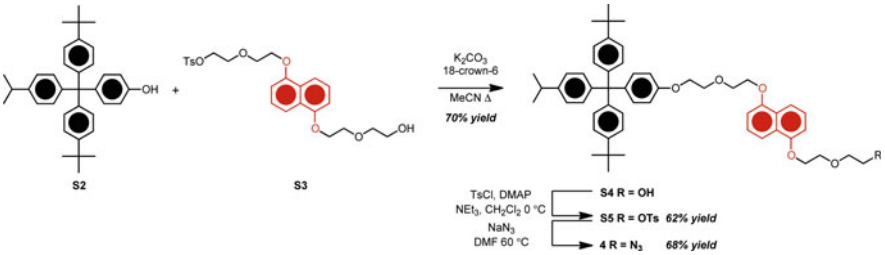

Scheme 2.6 Preparation of DNP azide derivative **4**

for 12 h (Scheme 2.6). The reaction mixture was filtered through Celite and the solvent was evaporated. Flash chromatography of the crude product (SiO_2, 85:15 CH_2Cl_2:hexanes) yielded 1.725 g (70% yield) of the alkylation product **S4** as an amorphous white solid. ^{1}H NMR (500 MHz, $CDCl_3$, 25 °C, TMS): δ 7.88 (d, ^3J (H,H) = 9 Hz, 1H, DNP *p*-O), 7.86 (d, ^3J (H,H) = 9 Hz, 1H, DNP aryl -H *p*-O), 7.32 (m, 2H, DNP aryl -H *m*–O), 7.23 (m, 4H, stopper aryl -H *o*-tBu), 7.09 (m, 10H, stopper all meta Ar–H and *o*-iPr), 6.85 (d, ^3J (H,H) = 8 Hz, 1H, DNP aryl -H *o*–O), 6.84 (d, ^3J (H,H) = 8 Hz, 1H, DNP aryl -H *o*–O), 6.80 (d, ^3J (H,H) = 9 Hz, 2H, stopper aryl -H *o*–O), 4.31 (m, 4H, both DNP-OCH_2), 4.16 (t, ^3J (H,H) = 5 Hz, 2H, stopper -OCH_2), 4.07 (t, ^3J (H,H) = 5 Hz, 2H, stopper -OCH_2CH_2), 4.00 (m, 4H, both DNP-OCH_2CH_2), 3.78 (m, 2H, $HOCH_2CH_2$), 3.75 (m, 2H, $HOCH_2$), 2.88 (septet, ^3J (H,H) = 7 Hz, 1H, iPr-H), 1.31 (s, 18H, t-Bu), 1.24 (d, ^3J (H,H) = 7 Hz, 6H, iPr –CH_3); ^{13}C NMR (125 MHz, CDCl3, 25 °C): δ 156.4, 154.3, 154.1, 148.2, 145.9, 144.5, 144.0, 139.7, 132.1, 130.9, 130.6, 128.9, 128.8, 126.7, 126.6, 125.1, 125.1, 125.0, 124.0, 114.7, 114.4, 113.0, 105.7, 72.5, 70.0, 69.9, 69.7, 67.9, 67.8, 67.2, 63.0, 61.8, 34.2, 33.4, 23.9; HRMS (FAB): Calcd for $C_{54}H_{64}O_6$ *m/z* = 808.4703. Found *m/z* = 808.4701.

Preparation of Stopper-DNP-OTs **S5** **S4** (0.300 g, 0371 mmol), DMAP (0.005 g, 0.037 mmol), and triethylamine (0.261 mL, 1.854 mmol) were dissolved in CH_2Cl_2 (3.7 mL). The solution was cooled to 0 °C, and *p*-toluenesulfonyl chloride (0.085 g, 0.445 mmol) was added. The solution was allowed to warm slowly to RT while stirring for 12 h. The reaction mixture was diluted into CH_2Cl_2 (50 mL), washed with H_2O (2 × 50 mL), saturated NH_4Cl (2 × 50 mL), brine (1 × 50 mL), dried ($MgSO_4$), filtered, and the solvent evaporated. The crude product was passed through a short plug of SiO_2 in CH_2Cl_2 to obtain 0.221 g (61.9% yield) of the pure tosylated product **S5**. **S5:** ^{1}H NMR (500 MHz, $CDCl_3$, 25 °C, TMS): δ 7.83 (d, ^3J (H,H) = 9 Hz, 1H, DNP *p*-O), 7.79 (d, ^3J (H,H) = 9 Hz, 1H, DNP aryl -H *p*-O), 7.78 (d, ^3J (H,H) = 8 Hz, 2H, tosylate aryl -H *o*-S), 7.30 (m, 2H, DNP aryl -H *m*–O), 7.23 (m, 4H, stopper aryl -H *o*-tBu), 7.08 (m, 10H, stopper all meta Ar–H and *o*-iPr), 6.85 (d, ^3J (H,H) = 8 Hz, 1H, DNP aryl -H *o*–O), 6.80 (d, ^3J (H,H) = 9 Hz, 2H, stopper aryl -H *o*–O), 6.78 (d, ^3J (H,H) = 8 Hz, 1H, DNP aryl -H *o*–O), 4.32(t, ^3J (H,H) = 5 Hz, 2H), 4.19

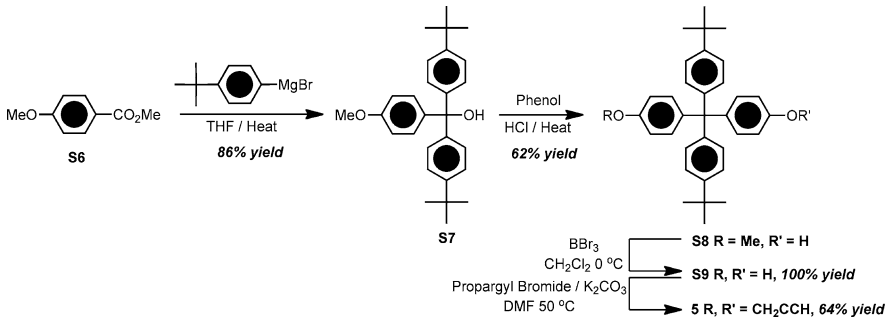

Scheme 2.7 Synthesis of dialkyne stopper derivative **5**

(m, 6H), 4.07 (t, ^3J (H,H) = 5 Hz, 2H), 3.99 (t, ^3J (H,H) = 5 Hz, 2H), 3.91 (t, ^3J (H,H) = 5 Hz, 2H), 3.83 (t, ^3J (H,H) = 5 Hz, 2H), 2.87 (septet, ^3J (H,H) = 7 Hz, 1H, iPr-H), 2.35 (s, 3H, OTs -CH3), 1.29 (s, 18H, t-Bu), 1.24 (d, ^3J (H,H) = 7 Hz, 6H, iPr –CH_3); ^{13}C NMR (125 MHz, $CDCl_3$, 25 °C): δ 156.4, 154.2, 154.0, 148.2, 145.9, 144.7, 144.5, 144.1, 139.7, 132.1, 130.9, 130.6, 129.7, 128.9, 127.9, 126.7, 126.6, 125.1, 125.0, 124.0, 114.7, 114.4, 113.0, 105.7, 105.6, 70.0, 69.8, 69.3, 68.9, 67.9, 67.8, 67.2, 63.0, 34.2, 33.3, 31.3, 29.6, 23.9, 21.5. HRMS (FAB): Calcd for $C_{61}H_{70}O_8S$ *m/z* = 962.4791. Found *m/z* = 962.4833.

Preparation of Stopper-DNP-N3 **4** **S5** (0.275 g, 0.285 mmol) and sodium azide (0.186 g, 2.855 mmol) were stirred in DMF (3.81 mL) at 50 °C for 6 h. The reaction mixture was filtered through Celite and the solvent was evaporated. The resulting solid was sonicated in CH_2Cl_2 and soluble fractions chromatographed (SiO_2, 8:2 CH_2Cl_2 eluent) to yield 0.170 g (68% yield) of **4** as an amorphous white powder. **4**: ^{1}H NMR (400 MHz, $CDCl_3$, 25 °C, TMS): δ 7.89 (d, ^3J (H,H) = 8 Hz, 1H, DNP *p*-O), 7.87 (d, ^3J (H,H) = 8 Hz, 1H, DNP aryl -H *p*-O), 7.34 (m, 2H, DNP aryl -H *m*–O), 7.23 (m, 4H, stopper aryl -H *o*-tBu), 7.09 (m, 10H, stopper all meta Ar–H and *o*-iPr), 6.85 (d, ^3J (H,H) = 8 Hz, 1H, DNP aryl -H *o*–O), 6.84 (d, ^3J (H,H) = 8 Hz, 1H, DNP aryl -H *o*–O), 6.80 (d, ^3J (H,H) = 9 Hz, 2H, stopper aryl -H *o*–O), 4.32 (m, 4H), 4.16 (t, ^3J (H,H) = 5 Hz, 2H), 4.07 (t, ^3J (H,H) = 5 Hz, 2H), 4.01 (m, 4H), 3.84 (t, ^3J (H,H) = 5 Hz, 2H), 3.44 (t, ^3J (H,H) = 5 Hz, 2H, -CH_2N_3), 2.88 (septet, ^3J (H,H) = 7 Hz, 1H, iPr-H), 1.30 (s, 18H, t- Bu), 1.24 (d, ^3J (H,H) = 7 Hz, 6H, iPr –CH_3); ^{13}C NMR (125 MHz, CDCl3, 25 °C): δ 156.5, 154.2, 154.1, 148.2, 145.9, 144.5, 144.0, 139.7, 132.1, 130.9, 130.6, 126.7, 126.6, 125.1, 125.1, 125.0, 124.0, 114.7, 114.5, 113.0, 105.6, 70.3, 70.0, 69.9, 69.8, 67.9, 67.2, 63.0, 50.7, 34.2, 33.3, 31.3, 23.9; HRMS (FAB): Calcd for $C_{54}H_{63}N_3O_5$ *m/z* = 873.4768. Found *m/z* = 873.4736.

Preparation of Trityl Alcohol **S7** 4-*t*-Butylphenyl bromide (24.5 mL, 30.1 g, 141.4 mmol) was added slowly to freshly cleaned magnesium turnings (3.50 g, 144 mmol; cleaned by sonication in Et_2O) in THF (65 mL) under an Ar atmosphere. The solution was heated under reflux for 4 h until the solid Mg had

disappeared. The Grignard reagent was cooled down to 0 °C and a solution of methyl 4-methoxybenzoate (**S6**, 10.00 g, 60.2 mmol) in the minimum amount of THF was added by cannula transfer. The mixture was heated under reflux for 1 h (Scheme 2.7), then was taken up in CH_2Cl_2 (100 mL), washed with sat. NH_4Cl (3 × 100 mL) and brine, dried ($MgSO_4$), and the solvent evaporated. The crude product was recrystallized from hexanes to yield 20.8 g (86% yield) of **S7** as white crystals. **S7**: ^{1}H NMR (500 MHz, $CDCl_3$, 25 °C): δ 7.33–7.31 (m, 4 H, H–Ar), 7.21–7.18 (m, 6 H, H–Ar), 6.84 (d, ^3J (H,H) = 9 Hz, 2 H, H–Ar), 3.80 (s, 3 H, -OCH3), 1.321 (s, 18 H, -CH_3); ^{13}C NMR (125 MHz, $CDCl_3$): δ 158.4, 149.8, 144.1, 139.5, 129.0, 127.4, 124.6, 113.0, 81.3, 55.1, 34.3, 31.3; Anal. C: 83.74, H: 8.18 (calcd C: 83.54, H: 8.51). HRMS (FAB): Calcd for $C_{28}H_{34}O_2$ *m/z* = 402.2559. Found *m/z* = 402.2567.

Preparation of Tetraarylmethane Alcohol **S8** Trityl alcohol **S7** (10.00 g, 24.2 mmol) and phenol (45.4 g, 483 mmol) were mixed neat and heated to 80 °C until the phenol melted. Concentrated HCl (1.1 mL) was added and the solution was heated to 100 °C for 5 h. The reaction mixture was taken up in PhMe, washed with aqueous 0.5 M NaOH (7 × 75 mL), and dried ($MgSO_4$), and the solvent evaporated to give the crude product as a yellow oil. Chromatography (silica gel, 25% hexanes in CH_2Cl_2) afforded 6.06 g (62%yield) of **S8** as a white powder. **S8**: ^{1}H NMR (400 MHz, $CDCl_3$, 25 °C): δ 7.24–7.22 (m, 4 H, H–Ar), 7.10–7.04 (m, 8 H, H–Ar), 6.77 (d, ^3J (H,H) = 9 Hz, 2 H, H–Ar), 6.70 (d, ^3J (H,H) = 9 Hz, 2 H, H–Ar), 4.63 (s, 1 H, -OH), 3.79 (s, 3 H, -OCH_3), 1.30 (s, 18 H, -CH_3); ^{13}C NMR (100 MHz, $CDCl_3$): δ 157.3, 153.3, 148.4, 144.2, 139.9, 139.7, 132.4, 132.2, 130.6, 129.1, 124.1, 114.0, 112.5, 62.8, 55.2, 34.3, 31.4; Anal. C: 84.89, H: 8.15 (calcd C: 85.31, H: 8.00). HRMS (FAB): Calcd for $C_{34}H_{38}O_2$ *m/z* = 478.2872. Found *m/z* = 478.2886.

Preparation of Tetraarylmethane Diol **S9** A 1 M solution of BBr_3 in CH_2Cl_2 (23.0 mL, 23.0 mmol) was added dropwise to a solution of methyl aryl ether **S8** (5.00 g, 10.4 mmol) in CH_2Cl_2 (350 mL) at 0 °C. The reaction mixture was warmed up to room temperature and stirred for 36 h under Ar. MeOH (5 mL) and then H_2O (200 mL) were added to quench the reaction. The organic layer was separated and collected. The aqueous layer was washed with CH_2Cl_2 (3 × 200 mL) and the combined organic layers were dried (MgSO4). Removal of the solvent in vacuo afforded 4.85 g (100% yield) of **S9** as an orange powder requiring no further purification. **S9**: ^{1}H NMR (500 MHz, $CDCl_3$, 25 °C): δ 7.23 (d, ^3J(H,H) = 9 Hz, 4H, H–Ar), 7.07 (d, ^3J(H,H) = 9 Hz, 4H,H–Ar), 7.04 (d, ^3J (H,H) = 9 Hz, 4 H, H–Ar), 6.70 (d, ^3J (H,H) = 9 Hz, 4 H, H–Ar), 1.30 (s, 18 H, -CH_3); ^{13}C NMR (125 MHz, $CDCl_3$): δ 153.1, 148.3, 144.0, 139.8, 132.3, 130.5, 124.0, 113.9, 62.7, 34.2, 31.3; HRMS (FAB): Calcd for $C_{33}H_{36}O_2$ *m/z* = 464.2715. Found *m/z* = 464.2721.

Preparation of Diacetylene **5** Propargyl bromide (80% w/w solution in xylenes, 4.80 g, 32.3 mmol) and K_2CO_3 (2.68 g, 19.4 mmol) were added to a solution of diol **S9** (1.50 g, 3.23 mmol) in DMF (20 mL). The reaction mixture was heated to

50 °C and stirred for 40 h under Ar. The reaction was taken up in EtOAc (150 mL), washed with 1 M $NaHSO_4$ (1 × 150 mL), H_2O (2 × 100 mL), and brine (2 × 100 mL), dried ($MgSO_4$), and evaporated onto silica gel. Chromatography (silica gel, 10% EtOAc in hexanes) afforded 1.12 g (64% yield) of **5**. **5**: ^{1}H NMR (500 MHz, CDCl3, 25 °C): δ 7.24 (d, ^3J (H,H) = 9 Hz, 4H, H–Ar), 7.10 (d, ^3J(H,H) = 9 Hz, 4H, H–Ar), 7.07 (d, ^3J(H,H) = 9 Hz, 4 H, H–Ar), 6.85 (d, ^3J (H,H) = 9 Hz, 4 H, H–Ar), 4.66 (d, ^4J (H,H) = 2 Hz, 4 H, -CH_2-), 2.52 (t, ^4J (H,H) = 2 Hz, 2 H, H-acetylene), 1.30 (s, 18 H, -CH_3); ^{13}C NMR (125 MHz, $CDCl_3$): δ 155.4, 148.3, 143.9, 140.3, 132.0, 130.5, 124.0, 113.3, 78.7, 75.3, 62.7, 55.7, 34.2, 31.3; HRMS (FAB): Calcd for $C_{39}H_{40}O_2$ *m/z* = 540.3028. Found *m/z* = 540.3042.

References

1. Choi JW, Flood AH, Steuerman DW, Nygaard S, Braunschweig AB, Moonen NNP, Laursen BW, Luo Y, DeIonno E, Peters AJ, Jeppesen JO, Xu K, Stoddart JF, Heath JR (2006) Chem Eur J 12:261–279
2. Steuerman DW, Tseng H-R, Peters AJ, Flood AH, Jeppesen JO, Nielsen KA, Stoddart JF, Heath JR (2004) Angew Chem Int Ed 43:6486–6491
3. Diehl MR, Steuerman DW, Tseng H-R, Vignon SA, Star A, Celestre PC, Stoddart JF, Heath JR (2003) Chem Phys Chem 4:1335–1339
4. Yu HB, Luo Y, Berverly K, Stoddart JF, Tseng H-R, Heath JR (2003) Angew Chem Int Ed 42:5706–5711
5. Luo Y, Collier CP, Jeppesen JO, Nielsen KA, DeIonno E, Ho G, Perkins J, Tseng H-R, Yamamoto T, Stoddart JF, Heath JR (2002) Chem Phys Chem 3:519–525
6. Collier CP, Mattersteig G, Wong EW, Luo Y, Berverly K, Sampaio J, Raymo FM, Stoddart JF, Heath JR (2000) Science 289:1172–1175
7. Tseng H-R, Wu DM, Fang NXL, Zhang X, Stoddart JF (2004) Chem Phys Chem 5:111–116
8. Badjić JD, Balzani V, Credi A, Silvi S, Stoddart JF (2004) Science 303:1845–1849
9. Collin J-P, Heitz V, Sauvage J-P (2005) Top Curr Chem 262:29–62
10. Kay ER, Leigh DA, Zerbetto F (2007) Angew Chem Int Ed 46:72–191
11. Braunschweig AB, Northrop BH, Stoddart JF (2006) J Mater Chem 16:32–44
12. Moonen NNP, Flood AH, Fernandez JM, Stoddart JF (2005) Top Curr Chem 262:99–132
13. Tseng H-R, Vignon SA, Celestre PC, Perkins J, Jeppesen JO, Di Fabio A, Ballardini R, Gandolfi MT, Venturi M, Balzani V, Stoddart JF (2004) Chem Eur J 10:155–172
14. Stoddart JF (2001) Acc Chem Res 34:410–411
15. Ballardini R, Balzani V, Dehaen W, Dell'Erba AE, Raymo FM, Stoddart JF, Venturi M (2000) Eur J Org Chem 591–602
16. Bermudez V, Capron N, Gase T, Gatti FG, Kajzar F, Leigh DA, Zerbetto F, Zhang SW (2000) Nature 406:608–611
17. Berna J, Leigh DA, Lubomska M, Mendoza SM, Perez EM, Rudolf P, Teobaldi G, Zerbetto F (2005) Nat Mater 4:704–710
18. Kern J-M, Raehm L, Sauvage J-P, Divisia-Blohorn B, Vidal PL (2000) Inorg Chem 39:1555–1560
19. Kinbara K, Aida T (2005) Chem Rev 105:1377–1400
20. Kottas GS, Clarke LI, Horinek D, Michl J (2005) Chem Rev 105:1281–1376
21. Poleschak I, Kern J-M, Sauvage J-P (2004) Chem Commun 474–476
22. Raehm L, Kern J-M, Sauvage J-P (1999) Chem Eur J 5:3310–3317

23. Garcia-Garibay MA (2005) Proc Natl Acad Sci USA 102:10771–10776
24. Perez EM, Dryden DTF, Leigh DA, Teobaldi G, Zerbetto F (2004) J Am Chem Soc 126:12210–12211
25. Chatterjee MN, Kay ER, Leigh DA (2006) J Am Chem Soc 128:4058–4073
26. Fletcher SP, Dumur F, Pollard MM, Feringa BL (2005) Science 310:80–82
27. Ashton PR, Goodnow TT, Kaifer AE, Reddington MV, Slawin AMZ, Spencer N, Stoddart JF, Vicent C, Williams DJ (1989) Angew Chem Int Ed Engl 28:1396–1399
28. Anelli P-L, Spencer N, Stoddart JF (1991) J Am Chem Soc 113:5131–5133
29. Philp D, Stoddart JF (1991) Synlett 445–458
30. Amabilino DB, Stoddart JF (1995) Chem Rev 95:2725–2828
31. Vignon SA, Stoddart JF (2005) Collect Czech Chem Commun 70:1493–1576
32. Philp D, Stoddart JF (1996) Angew Chem Int Ed 35:1155–1196
33. Rostovtsev VV, Green LG, Fokin VV, Sharpless KB (2002) Angew Chem Int Ed 41:2596–2599
34. Tornoe CW, Christensen C, Meldal M (2002) J Org Chem 67:3057–3064
35. Hawker CJ, Wooley KL (2005) Science 309:1200–1205
36. Goodall GW, Hayes W (2006) Chem Soc Rev 35:280–312
37. Diaz DD, Punna S, Holzer P, McPherson AK, Sharpless KB, Fokin VV, Finn MGJ (2004) Polym Sci, Part A: Polym Chem 42:4392–4403
38. Laurent BA, Grayson SM (2006) J Am Chem Soc 128:4238–4239
39. Riva R, Schmeits P, Stoffelbach F, Jerome C, Jerome R, Lecomte P (2005) Chem Commun 5334–5336
40. Opsteen JA, van Hest JCM (2005) Chem Commun 57–59
41. Lutz JF, Borner HG, Weichenhan K (2005) Macromol Rapid Commun 26:514–518
42. Ossipov DA, Hilborn J (2006) Macromolecules 39:1709–1718
43. Wu P, Feldman AK, Nugent AK, Hawker CJ, Scheel A, Voit B, Pyun J, Fréchet JMJ, Sharpless KB, Folkin VV (2004) Angew Chem Int Ed 43:3928–3932
44. Wu P, Malkoch M, Hunt JN, Vestberg R, Kaltgrad E, Finn MG, Fokin VV, Sharpless KB, Hawker CJ (2005) Chem Commun 5775–5777
45. Malkoch M, Schleicher K, Drockenmuller E, Hawker CJ, Russell TP, Wu P, Fokin VV (2005) Macromolecules 38:3663–3678
46. Lee JW, Kim BK, Kim HJ, Han SC, Shin WS, Jin SH (2006) Macromolecules 39:2418–2422
47. Lee JW, Kim JH, Kim BK, Shin WS, Jin SH (2006) Tetrahedron 62:894–900
48. Fernandez-Megia E, Correa J, Rodriguez-Meizoso I, Riguera R (2006) Macromolecules 39:2113–2120
49. Helms B, Mynar JL, Hawker CJ, Fréchet JMJ (2004) J Am Chem Soc 126:15020–15021
50. Mynar JL, Choi TL, Yoshida M, Kim V, Hawker CJ, Fréchet JMJ (2005) Chem Commun 5169–5171
51. Malkoch M, Thibault RJ, Drockenmuller E, Messerschmidt M, Voit B, Russell TP, Hawker CJ (2005) J Am Chem Soc 127:14942–14949
52. O'Reilly RK, Joralemon MJ, Wooley KL, Hawker CJ (2005) Chem Mater 17:5976–5988
53. Aucagne V, Hanni KD, Leigh DA, Lusby PJ, Walker DB (2006) J Am Chem Soc 128:2186–2187
54. Ashton PR, Glink PT, Stoddart JF, Tasker PA, White AJP, Williams DJ (1996) Chem Eur J 2:729–736
55. Badjić JD, Balzani V, Credi A, Lowe JN, Silvi S, Stoddart JF (2004) Chem Eur J 10:1926–1935
56. Liu Y, Flood AH, Bonvallett PA, Vignon SA, Northrop BH, Tseng H-R, Jeppesen JO, Huang TJ, Brough B, Baller M, Magonov S, Solares SD, Goddard WA, Ho CM, Stoddart JF (2005) J Am Chem Soc 127:9745–9759
57. Simpson CD, Mattersteig G, Martin K, Gherghel L, Bauer RE, Rader HJ, Müllen K (2004) J Am Chem Soc 126:3139–3147
58. Rowan SJ, Stoddart JF (1999) Org Lett 1:1913–1916

59. Asakawa M, Dehaen W, L'abbé G, Menzer S, Nouwen J, Raymo FM, Stoddart JF, Williams DJ (1996) J Org Chem 61:9591–9595
60. Ashton PR, Ballardini R, Balzani V, Belohradsky M, Gandolfi MT, Philp D, Prodi L, Raymo FM, Reddington MV, Spencer N, Stoddart JF, Venturi M, Williams DJ (1996) J Am Chem Soc 118:4931–4951
61. Jeppesen JO, Perkins J, Becher J, Stoddart JF (2001) Angew Chem Int Ed 40:1216–1221

Chapter 3
A One-Pot Synthesis of Constitutionally Unsymmetrical Rotaxanes Using Sequential Cu(I)-Catalyzed Azide–Alkyne Cycloadditions

3.1 Introduction

Highly efficient and convergent strategies for the synthesis of mechanically interlocked compounds are essential in order to facilitate the development of sophisticated and functional artificial molecular machinery [1–15]. In this context, we recently developed [16] a simple and high-yielding method for the synthesis of donor–acceptor rotaxanes [16–24] based on a threading-followed-by-stoppering approach [25–29] that utilizes the Cu(I)-catalyzed azide-alkyne cycloaddition (CuAAC) [30, 31]. Although we have employed [16, 20, 22] this method to prepare previously unavailable mechanically interlocked compounds, it is best suited for the template-directed synthesis [32–37] of [*n*]rotaxanes stoppered by identical bulky groups. Rotaxanes that incorporate two different stoppers, such as the amphiphilic bistable [2]rotaxanes [38–43] used as the storage elements in crossbar memory circuits [1, 44–52], represent a significant increase in structural complexity and are thus even more challenging synthetic targets. Herein, we report (1) the extension of a general, one-pot method [53] that uses sequential CuAAC reactions to address this challenge, and (2) demonstrate its application to the highly convergent synthesis of an amphiphilic [4]rotaxane.

A sequence of two or more CuAAC reactions may be controlled (Fig. 3.1) through (i) performing the reaction of the desired azide and alkyne partners in the presence of another masked reactive functionality, (ii) removing the masking group to present another reaction partner, and (iii) repeating the CuAAC reaction

---

This Chapter is reproduced in part with permission from: Spruell JM, Dichtel WR, Heath JR, Stoddart JF. *Chem. Eur. J.* **2008** *14*, 4168–4177.
Author Contributions: J.M. Spruell and W.R. Dichtel conceived the project. J.M. Spruell synthesized all compounds reported and performed all experiments. J.M. Spruell and J.F. Stoddart prepared the original manuscript. J.F. Stoddart and J.R. Heath supervised the original research.

J. M. Spruell, *The Power of Click Chemistry for Molecular Machines and Surface Patterning*, Springer Theses, DOI: 10.1007/978-1-4419-9647-3_3,

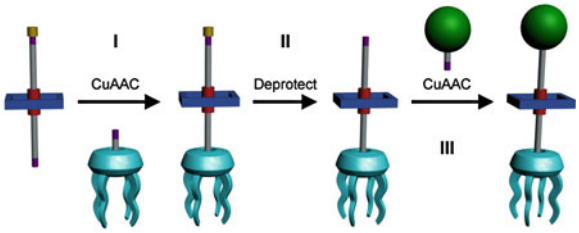

Fig. 3.1 Graphical representation of the sequential CuAAC strategy applied to the synthesis of mechanically interlocked molecular compounds. A constitutionally unsymmetrical monoprotected pseudorotaxane may be stoppered in the initial step (I), the protecting group removed in the second step (II), and then functionalized with a different type of stopper in the third step (III) to form a constitutionally unsymmetrical [2]rotaxane. The use of a multifunctional stopper allows higher order rotaxanes (e.g., the branched [4]rotaxane described in this Chapter) to be assembled sequentially in one pot

of the unmasked functionality. These sequences prove most efficient if they could be performed in one-pot, a goal that adds the requirements that each of the three (or more) steps must proceed to nearly quantitative conversion and that the reagents used in the beginning of the sequence must not interfere with those employed in subsequent steps. Such a sequence was devised [53] for the covalent attachment of peptide building blocks to a central unit directed by a silyl protecting group. The extension of such a method to mechanical bond formation adds several challenges, most prominently, the need for all components of sensitive donor–acceptor mechanically interlocked compounds to tolerate each of the steps of a sequential CuAAC method. The ring most commonly employed in donor–acceptor mechanically interlocked compounds, namely cyclobis(paraquat-*p*-phenylene) ($CBPQT^{4+}$), is sensitive to most bases, nucleophiles, and reducing agents, severely limiting the range and scope of reagents and conditions available to carry out the deprotection(s). The prevalent use of silyl groups for the protection of alkynes, and the availability of relatively mild methods for the deprotection of trimethylsilyl-(TMS)-protected alkynes [54–58] in particular, led us to investigate this protecting group with the intention of developing a one-pot sequential CuAAC method compatible with the $CBPQT^{4+}$ ring and its donor–acceptor complexes.

3.2 Results and Discussion

As a preliminary appraisal of the ability of the TMS group to prevent a contiguous alkyne functionality from participating in the desired CuAAC reaction, 3-trimethylsilyl-2-propyn-1-ol (**1**) and 1-azidohexane (**3**) were treated (Table 3.1, entry 1) with the $CuSO_4 \bullet 5H_2O$/ascorbic acid catalyst system in DMF. Somewhat surprisingly, under these reaction conditions, significant amounts of the 1,2,3-triazole product 4 (54% conversion) were formed over the course of 24 h, presumably as a result of the slow hydrolysis of the TMS group. The protecting group did,

Table 3.1 Chemoselectivity between **1** and **2** in CuAAC reaction with **3** to form either **4** or **5**

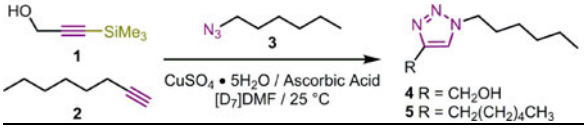

Entry	**1**:**2**:**3**	Time (h)	**4**:**5**	Conversion[a] (%)
1	1:0:1	24	1:0	54
2	1:1:1	16	1:99	96

[a] With respect to **3**, monitored by integration of ^{1}H NMR spectra

however, slow down the CuAAC reaction substantially, and a competition experiment (Table 3.1, entry 2) between **1** and 1-octyne (**2**) in a CuAAC reaction with **3** resulted in excellent chemoselectivity for the formation of 1,4-dihexyl-1,2,3-triazole (**5**), despite the observation of partial hydrolysis of **1** to propargyl alcohol (8%) at the conclusion of the experiment. This test-bed work demonstrates that the TMS protecting group is sufficiently kinetically stable under the conditions of the CuAAC reaction, so much so that the cycloaddition occurs almost exclusively with the unprotected alkyne.

Next, appropriate conditions for the sequential desilylation and CuAAC reactions required for the desired one-pot procedure (Table 3.2) were investigated. The Ag^I-catalyzed hydrolysis of TMS protected alkynes [54–58] was assumed to be sufficiently mild to ensure the survival of the $CBPQT^{4+}$. Indeed, 10 mol% $AgPF_6$ in the presence of H_2O (1 eq. per alkyne) catalyzed the hydrolysis of the TMS group, resulting (Table 3.2, entry 3) in nearly quantitative conversion in 18 h when the

Table 3.2 Reaction condition development: one-pot TMS deprotection of **1** followed by CuAAC reaction of the generated alkyne

Entry	Deprotection conditions (°C, h) (additive)	Conv (%)[a]	CuAAC reagents[b] (additive)	CuAAC time (h)	Conv (%)[c]
1	25, 48	98[d]	$CuSO_4$•5H_2O Ascorbic Acid	90	45
2	25, 48	98[d]	Cu nanopowder	90	>98
3	40, 18	>98[e]	$Cu(MeCN)_4PF_6$	26	93
4	40, 18	>98[e]	Cu nanopowder $Cu(MeCN)_4PF_6$	1	>98
5	40, 54, ($CBPQT•4PF_6$)	90[e]	Cu nanopowder $Cu(MeCN)_4PF_6$ ($CBPQT•4PF_6$)	5	>98

[a] With respect to **1**, monitored by integration of ^{1}H NMR spectra
[b] **3** (1.1 eq.) was used
[c] With respect to propargyl alcohol intermediate
[d] 0.05 eq. of $AgPF_6$ was used
[e] 0.10 eq. of $AgPF_6$ was used

reaction mixture was heated to 40 °C. $AgPF_6$ was introduced into the reaction mixture in order to prevent counterion exchange and subsequent precipitation of Ag^I or $CBPQT^{4+}$-containing salts. Interestingly, the desilylation proceeded noticeably more slowly when the reaction was performed (Table 3.2, entry 5) in the presence of $CBPQT^{4+}$. No decomposition of the $CBPQT^{4+}$, however, was observed. Next, we developed conditions to effect the second CuAAC reaction in the presence of silver salts remaining from the deprotection. The $CuSO_4 \bullet 5H_2O$/ascorbic acid catalytic system (5/10 mol%, respectively) formed (Table 3.2, entry 1) the CuAAC product, albeit somewhat slowly. Upon addition of the $CuSO_4 \bullet 5H_2O$ and ascorbic acid, a silver mirror formed on the walls of the reaction vessel, most likely as a result of the reduction of Ag^I to Ag^0 by Cu(I) and/or ascorbic acid, both processes that would impact negatively upon the availability of Cu(I) required to catalyze the cycloaddition. Although the CuAAC reaction proceeds to higher conversions when an excess of ascorbic acid (1.3 eq. per alkyne; 6.3 eq. per $CBPQT^{4+}$) is used, the intensities of the broadened $CBPQT^{4+}$ resonances in the ^1H NMR spectrum of the reaction mixture were attenuated to 17% of their initial values. The excess of ascorbic acid ($E^\circ = 0.3$ V) presumably reduces the $CBPQT^{4+}$ ($E^\circ = -0.29$ and -0.71 V) [38], and while the reversibility of this process was not determined, reduced $CBPQT^{4+}$ derivatives do not bind electron rich guests. As an alternative to adding ascorbic acid at all, Cu^0 was used (Table 3.2, entry 2) as a copper source, which presumably *generates* the catalytically active Cu(I) following oxidation by Ag^I. Indeed, this procedure did ultimately produce the desired CuAAC reaction, although we subsequently found that a small amount of additional $Cu(MeCN)_4PF_6$ helped to speed up the reaction (Table 3.2, entry 4) further, despite the fact that the addition of $Cu(MeCN)_4PF_6$ alone catalyzed the CuAAC reaction only slowly (Table 3.2, entry 3). Finally, it was confirmed that, when the above sequence is carried out in the presence of $CBPQT^{4+}$, the sequential deprotection/CuAAC reactions proceed (Table 3.2, entry 5) to high conversion with no decrease in the intensities of the $CBPQT^{4+}$ ^1H NMR resonances.

With the three-step sequential CuAAC methodology operating well in our hands, we envisioned that the sequential CuAAC reactions could be used to attach different stoppers to each end of a pseudorotaxane. Furthermore, in order to test this method for the synthesis of compounds with particularly complicated structures, a branched [4]rotaxane was chosen so that each CuAAC reaction and deprotection step would have to occur, not just once, but three times within each molecule. The threefold symmetry, previously incorporated into acid/base-switched molecular elevators [59–61] and present in the non-trivial amphiphilic [4]rotaxane **11**•12PF_6 was accessed (Scheme 3.1) in one-pot by sequentially stoppering the constitutionally unsymmetrical dioxynaphthalene (DNP) derivative **7**, firstly with the trifunctional azide **6** and then subsequently with the monofunctional azide **10**. The DNP derivative **7** was synthesized (Scheme 3.2) bearing one TMS-protected alkyne and one terminal alkyne such that the constitutional asymmetry endowed by the TMS group would be expressed in the amphiphilic character of the final branched [4]rotaxane. The triazide **6** and monoazide **10** were each obtained (Scheme 3.3) through azide displacement of their benzyl chloride precursors.

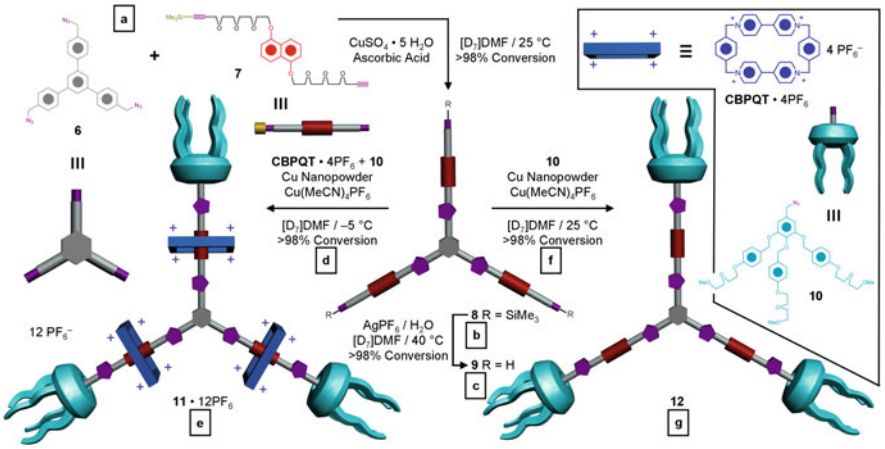

Scheme 3.1 Sequential CuAAC synthesis of the [4]rotaxane **11**•12PF_6 and the dumbbell compound **12**. Labels for ^{1}H NMR spectroscopic monitoring of the reactions are identified by boxed letters

Scheme 3.2 The synthesis of the constitutionally unsymmetrical DNP derivative **7**

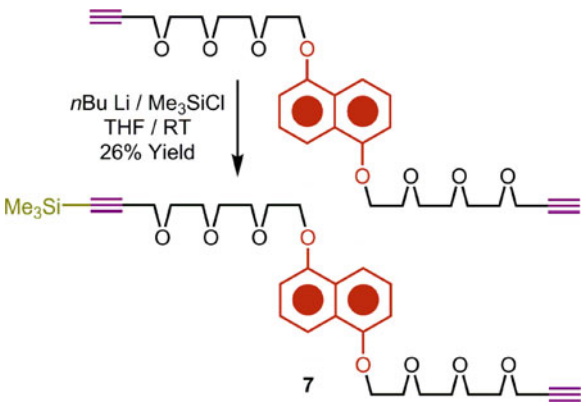

Before attempting the template-directed synthesis of the [4]rotaxane, we first of all pursued (Scheme 3.1) the same reaction sequences—which we had in mind to prepare **11**•12PF_6—to form the dumbbell compound **12**. The relative simplicity of the ^{1}H NMR spectrum of **12** compared to that (*vida infra*) of the [4]rotaxane was the motivation for us making the dumbbell compound first. By stoppering the monofunctional DNP derivative **7** in a controlled, sequential manner in the absence of CBPQT•4PF_6, first with the triazide **6** and then subsequently with the monoazide **10**—following silyl deprotection of the protected alkyne—we anticipated obtaining compound **12** in high yield. This three-step reaction sequence was carried out in an NMR tube in DMF-d_7 such that each step of the reaction could be

Scheme 3.3 The synthesis of the triazide **6** and the monoazide **10**

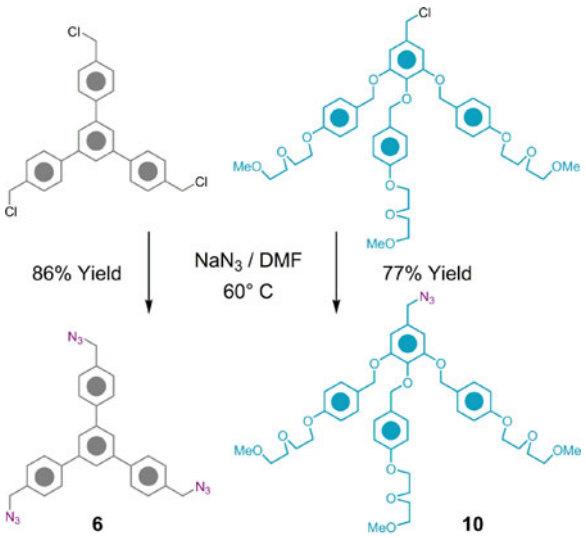

monitored (Fig. 3.2) closely by ^{1}H NMR spectroscopy. Upon mixing the triazide **6** with the monoalkyne **7** in a 1:3 molar ratio, the first CuAAC reaction proceeded to form the tris–TMS-protected compound **8**, the outcome of which was confirmed by the transformation of the terminal alkyne proton resonance ($\delta = 3.39$ ppm in Fig. 3.2a) of the DNP derivative **7** to the triazole proton resonance ($\delta = 8.25$ ppm in Fig. 3.2b) of the tris–DNP intermediate **8**. The chemical shifts of the methylene group resonances neighboring the terminal alkyne and azide ($\delta = 4.22$ and 4.61 ppm, respectively, in Fig. 3.2a) are transformed into the methylene group resonances ($\delta = 4.62$ and 5.76 ppm in Fig. 3.2b) neighboring the newly-formed triazole. In keeping with the model experiments, some partial hydrolysis (17%) of the TMS protecting groups also occurred during the first CuAAC reaction of **6** with **7**. Even so, as indicated by the model experiments, the TMS group protects the alkynes to the extent that the CuAAC reaction occurs, forming **8** with a high conversion (>98% with respect to **6**). The Ag^I-catalyzed desilylation was then performed, affording the tris–alkyne **9**, once again in high conversion (>98%). Completion of the desilylation was confirmed by the migration and transformation of the methylene group singlet resonance ($\delta = 4.23$ ppm in Fig. 3.2b) neighboring the silyl protected alkyne of **8** to a doublet ($\delta = 4.20$ ppm with $J^4 \sim 3$ Hz in Fig. 3.2c) for the methylene group neighboring the terminal alkyne in **9**. This diagnostic splitting pattern is a result of long-range coupling between the liberated terminal alkyne proton and the neighboring methylene protons in **9**. Upon addition of 3.3 equivalents of the azide-containing hydrophilic precursor **10** (Fig. 3.2f), the methylene peak ($\delta = 4.45$ ppm) neighboring the added azide was evident along with the terminal alkyne proton peak ($\delta = 3.38$ ppm) for the tris–alkyne **9**. Both of these peaks reappeared as another set of signals—for the methylene group next to a triazole ($\delta = 5.62$ ppm) and for the second triazole proton ($\delta = 8.33$ ppm) in

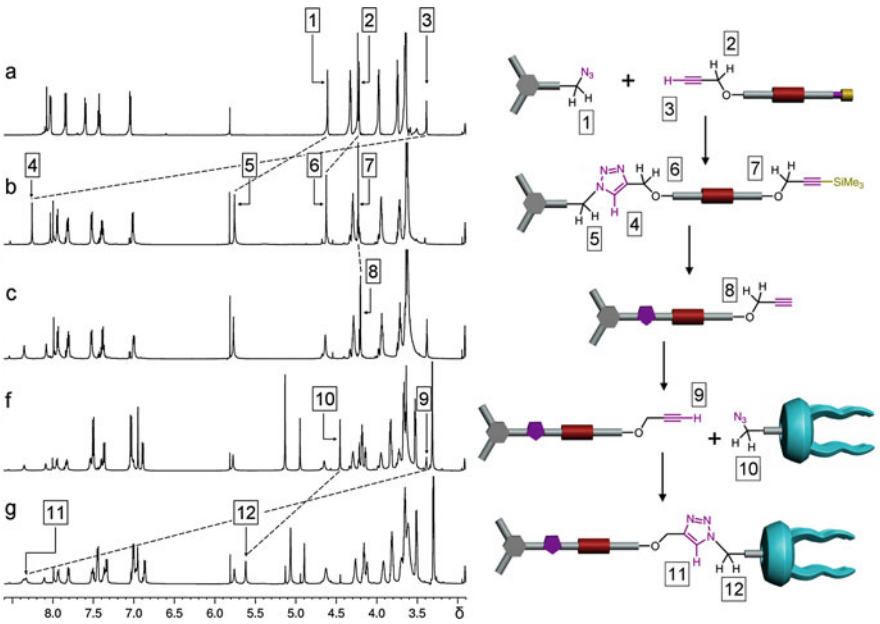

Fig. 3.2 ^{1}H NMR (600 MHz, DMF-d_7, 25 °C) spectroscopic monitoring of the synthesis of the dumbbell compound **12**. Several diagnostic resonances are numbered and the changes monitored throughout the reaction steps indicated by letters *a*, *b*, *c*, *f*, and *g* in Scheme 3.1. See the text for further discussion

Fig. 3.2g—after the second (Cu-nanopowder/Cu(MeCN)$_4$PF$_6$-promoted) CuAAC reaction was carried out to form the final dumbbell compound **12** with >98% conversion with respect to tris–alkyne intermediate **9**.

With an intimate knowledge of the spectroscopic characteristics accompanying the sequential CuAAC reaction in the formation of the dumbbell compound **12**, the synthesis of the [4]rotaxane **11**•12PF$_6$ was attempted in a similar manner with periodic monitoring (Fig. 3.3) by ^{1}H NMR spectroscopy. The steps leading to the formation of the tris–alkyne intermediate **9** were exactly the same as those followed in the synthesis of **12**. The addition of 3.3 equivalents of CBPQT•4PF$_6$ at −5 °C to the intermediate **9** resulted in the formation of the [4]pseudorotaxane **[9** ⊂ 3CBPQT]•12PF$_6$ which was stoppered with the monoazide **10** using the Cu-nanopowder/Cu(MeCN)$_4$PF$_6$-promoted CuAAC reaction to yield the amphiphilic branched [4]rotaxane **11**•12PF$_6$. The addition of CBPQT•4PF$_6$ caused broadening of all the peaks (Fig. 3.3d) as a consequence of the many dynamic equilibria associated with the formation of pseudorotaxanes. The terminal alkyne proton resonance, however, was resolved clearly ($\delta = 3.17$ ppm) from the other signals and so it was used as a diagnostic resonance with which to monitor the progress of the final CuAAC reaction. The disappearance of the terminal alkyne proton resonance (Fig. 3.3d) in the [4]pseudorotaxane **[9** ⊂ 3CBPQT]•12PF$_6$ and the appearance of a second triazole peak ($\delta = 8.10$ ppm in Fig. 3.3e) for the

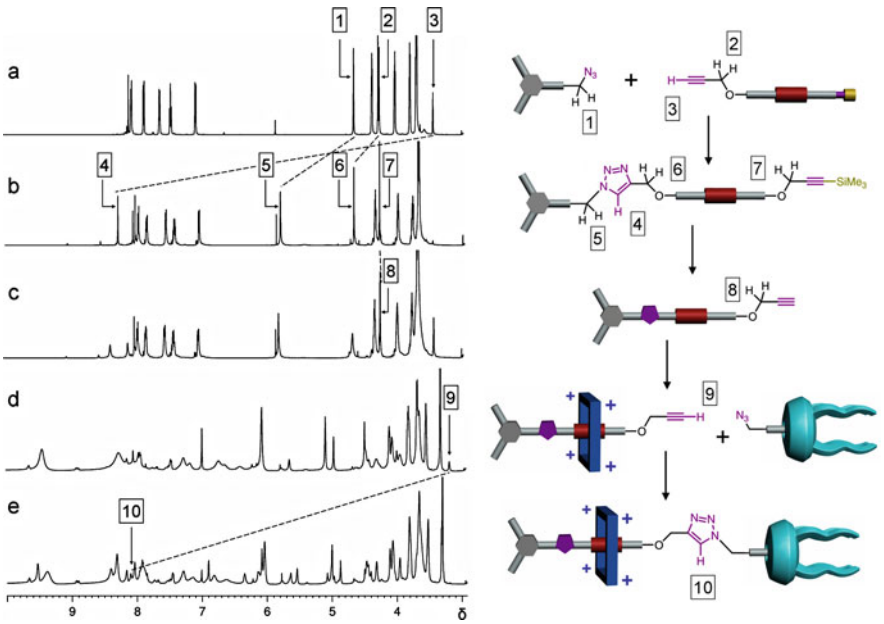

Fig. 3.3 ^{1}H NMR (600 MHz, DMF-d_7, 25 °C) spectroscopic monitoring of the synthesis of the [4]rotaxane **11**•12PF$_6$. Several diagnostic resonances are numbered and the changes monitored throughout the reaction steps indicated by letters *a*, *b*, *c*, *d*, and *e* in Scheme 3.1. See the text for further discussion

[4]rotaxane **11**•12PF$_6$ heralded the completion of the second CuAAC reaction. Although we had never performed the second CuAAC reaction at low temperatures in the test-bed investigations (Table 3.2, entry 5), the tris–alkyne **9** was consumed completely during the final CuAAC reaction performed at −5 °C. All three of the second CuAAC reactions occurred with considerable efficiency, forming the threefold symmetric amphiphilic [4]rotaxane in 44% yield from a one-pot synthesis. Although, the isolated yield of **11**•12PF$_6$ at first glance may seem low in comparison with the near-quantitative conversions observed by ^{1}H NMR spectroscopy, it represents the overall yield for a sum of nine "consecutive" reactions, including the formation of three mechanical bonds, starting from no less than 10 building blocks. Also, extensive purification by preparative thin-layer chromatography was required in order to isolate the highly polar amphiphilic branched [4]rotaxane as a pure compound. In addition, a small quantity of a minor [2]rotaxane by-product, comprised of a CBPQT^{4+}-encircled thread **7**, stoppered by two hydrophilic stoppers **10**, was isolated. The formation of this compound can be attributed to the use of a very slight excess of **7** over **6** at the start of the three-step reaction sequence. Importantly, no evidence of constitutional defects—for example, missing rings, missing DNP threads, or crosslinking—was observed during the template-directed synthesis of **11**•12PF$_6$. The successful silver-catalyzed silyl deprotection, performed in the second and intermediate step of the sequence,

although not forming a bond itself, enabled the direction of the useful bond-forming CuAAC reaction in the third step of the sequence. Moreover, this reaction is another example that can be added to the small list of chemical reactions that may be performed in the presence of $CBPQT^{4+}$.

3.3 Conclusions

The protocol presented demonstrates the general and highly convergent nature of the sequential CuAAC strategy for the template-directed synthesis of a tripodal [4]rotaxane. Employing this one-pot methodology, constitutionally unsymmetrical rotaxanes may be prepared quickly and efficiently, aiding and abetting their continued use as components of molecular machinery and electronics. This methodology sets forth a new synthetic paradigm for $CBPQT^{4+}$-containing compounds in which the formation of the mechanical bond need not occur in the final step of the synthesis. These advances have been driven by the discovery and use of reactions amenable to the sensitive nature of $CBPQT^{4+}$. We intend to continue to develop new synthetic strategies performed under thermodynamic [62] as well as kinetic [16] control so that mechanical bonds may be precisely and predictably introduced into a wide range of complex functional molecules.

3.4 Experimental

3.4.1 General Methods

All reagents were purchased from commercial suppliers (Aldrich or Fisher) and used without purification. Dry solvents were obtained from a commercial Dri-Solv® solvent delivery system (EMD Chemicals). The molarity of *n*BuLi solutions was determined immediately before use by titration using salicyaldehyde phenylhydrazone [63] as an indicator. Cyclobis(paraquat-*p*-phenylene) [64], 1,5-bis[2-(2-(2-(2-propyne)ethoxy)ethoxy)ethoxy]naphthalene [19], and 3,4,5-tris-[(2-(2-methoxy)ethoxy)ethoxybenzyloxy]benzyl chloride [52] were prepared using previously published procedures. Copper nanopowder was used as received from Aldrich and is described as metallic copper (99.8%) particles <100 nm in size. Thin layer chromatography (TLC) was performed on silica gel 60 F_{254} (E. Merck). Preparative thin layer chromatography (Prep TLC) was performed on glass plates with a 1 mm thick layer of silica gel 60 F_{254} (E. Merck). Column chromatography was performed on silica gel 60F (Merck 9385, 0.040–0.063 mm). Nuclear magnetic resonance (NMR) spectra were recorded on a Bruker Avance 600 (^{1}H: 600 MHz; ^{13}C: 150 MHz) or 500 (^{1}H: 500 MHz; ^{13}C: 126 MHz) spectrometer. Chemical shifts are reported as parts per million (ppm) downfield from

the Me_4Si resonance as the internal standard for both ^1H and ^{13}C NMR spectroscopies. Electrospray ionization (ESI) mass spectra were measured on a Finnigan LCQ ion-trap mass spectrometer using 1:1 MeCN:H_2O as the mobile phase. High-Resolution Fast Atom Bombardment (HR-FAB) mass spectra were obtained on a JEOL JMS-600H high-resolution mass spectrometer equipped with a FAB probe. Electrospray Ionization (EI) Mass Spectra were obtained on a Finnigan LCQ ion trap mass spectrometer.

3.4.1.1 Method Development

General Procedure for Single Step Methodology Experiments and Table 3.1, Entry 1

3-Trimethylsilyl-2-propyn-1-ol (**1**) (0.010 g, 0.078 mmol) and 1-azidohexane (**3**) (0.010 g, 0.078 mmol) were dissolved in DMF-d_7 (0.780 mL) in an NMR tube. Stock solutions of $CuSO_4$•$5H_2O$ in DMF-d_7 (18 μL, 0.072 M, 0.05 eq. per azide) and ascorbic acid in DMF-d_7 (18 μL, 0.144 M, 0.10 eq. per azide) were added and the mixture left at RT. The reaction progress was monitored by comparing the integrated area of the disappearing –C$H_2$$N_3$ resonance at 3.50 ppm with that of the appearing –CH_2N(triazole) at 4.57 ppm in the ^1H NMR spectrum of the reaction mixture.

Methodology Experiment for Table 3.1, Entry 2

The above procedure was followed using 3-trimethylsilyl-2-propyn-1-ol (**1**) (0.010 g, 0.078 mmol), 1-octyne (**2**) (0.0090 g, 0.078 mmol), and 1-azidohexane (**3**) (0.010 g, 0.078 mmol) dissolved in DMF-d_7 (0.780 mL) and stock solutions of $CuSO_4$•$5H_2O$ in DMF-d_7 (18 μL, 0.072 M, 0.05 eq. per azide) and ascorbic acid in DMF-d_7 (18 μL, 0.144 M, 0.10 eq. per azide).

General Procedure for Two Step Methodology Experiments and Table 3.2, entry 1

3-Trimethylsilyl-2-propyn-1-ol (**1**) (0.0070 g, 0.055 mmol) was dissolved in DMF-d_7 (0.546 mL) in an NMR tube. A stock solution of $AgPF_6$ in DMF-d_7 (30 μL, 0.1 M, 0.05 eq. per alkyne) and H_2O (3 μL, 0.164 mmol) were added and the mixture left at room temperature. The reaction progress was monitored by comparing the integrated area of the disappearing –CH_2CCSi singlet resonance at 4.19 ppm with that of the appearing –CH_2CCH doublet resonance at 4.16 ppm in the ^1H NMR spectrum of the reaction mixture. Following sufficient conversion, to this solution was added 1-azidohexane (**3**) (0.0080 g, 0.060 mmol) and stock solutions of $CuSO_4$•$5H_2O$ in DMF-d_7 (18 μL, 0.072 M, 0.05 eq. per azide) and ascorbic acid in DMF-d_7 (18 μL, 0.144 M, 0.10 eq. per azide) and the reaction was left at room temperature. Conversion of the CuAAC reaction was monitored

by comparing the integrated area of the disappearing $-CH_2N_3$ resonance at 3.50 ppm with that of the appearing $-CH_2N$(triazole) at 4.57 ppm in the ^{1}H NMR spectrum of the reaction mixture.

Methodology Experiment for Table 3.2, Entry 2

The above procedure was followed using 3-trimethylsilyl-2-propyn-1-ol (**1**) (0.0070 g, 0.055 mmol), DMF-d_7 (0.546 mL), stock solution of $AgPF_6$ in DMF-d_7 (30 μL, 0.10 M, 0.05 eq. per alkyne), H_2O (3 μL, 0.164 mmol), 1-azidohexane (**3**) (0.0080 g, 0.060 mmol), and copper nanopowder (0.0010 g, 0.016 mmol). The reaction mixture was heterogeneous, as the copper nanopowder remained at the bottom of the NMR tube.

Methodology Experiment for Table 3.2, Entry 3

The above procedure was followed using 3-trimethylsilyl-2-propyn-1-ol (**1**) (0.0080 g, 0.055 mmol), DMF-d_7 (0.530 mL), stock solution of $AgPF_6$ in DMF-d_7 (23.5 μL, 0.235 M, 0.1 eq. per alkyne), H_2O (3 μL, 0.16 mmol), 1-azidohexane (**3**) (0.0080 g, 0.060 mmol), and $Cu(MeCN)_4PF_6$ (0.002 g, 0.005 mmol, 0.1 eq. per alkyne). After the addition of the $AgPF_6$ solution, the mixture was warmed to 40 °C. The subsequent CuAAC reaction was performed at room temperature.

Methodology Experiment for Table 3.2, Entry 4

The above procedure was followed using 3-trimethylsilyl-2-propyn-1-ol (**1**) (0.0070 g, 0.055 mmol), DMF-d_7 (0.546 mL), stock solution of $AgPF_6$ in DMF-d_7 (23.5 μL, 0.235 M, 0.1 eq. per alkyne), H_2O (3.0 μL, 0.16 mmol), 1-azidohexane (**3**) (0.0080 g, 0.060 mmol), copper nanopowder (0.0010 g, 0.016 mmol), and $Cu(MeCN)_4PF_6$ (0.002 g, 0.005 mmol, 0.1 eq. per alkyne). After the addition of the $AgPF_6$ solution, the mixture was warmed to 40 °C. The subsequent CuAAC reaction was performed at room temperature.

Methodology Experiment for Table 3.2, Entry 5

The above procedure was followed using 3-trimethylsilyl-2-propyn-1-ol (**1**) (0.0070 g, 0.055 mmol), DMF-d_7 (0.546 mL), stock solution of $AgPF_6$ in DMF-d_7 (23.5 μL, 0.235 M, 0.1 eq. per alkyne), H_2O (3.0 μL, 0.16 mmol), 1-azidohexane (**3**) (0.0080 g, 0.060 mmol), copper nanopowder (0.0010 g, 0.016 mmol), $Cu(MeCN)_4PF_6$ (0.002 g, 0.005 mmol, 0.1 eq. per alkyne), and CBPQT•$4PF_6$ (0.0115 g, 0.0110 mmol, 0.2 eq. per alkyne). CBPQT•$4PF_6$ was dissolved initially

with **1** and remained as a spectator throughout the sequence. After the addition of the $AgPF_6$ solution, the mixture was warmed to 40 °C. The subsequent CuAAC reaction was performed at room temperature.

3.4.1.2 Synthesis and Characterization

1-[2-(2-(2-(3-Trimethylsilyl-2-Propyne)Ethoxy)Ethoxy)Ethoxy]-5-[2-(2-(2-(2-Propyne)Ethoxy)Ethoxy)Ethoxy]Naphthalene (**7**)

*n*BuLi (0.52 M in hexanes, 665 μL, 0.343 mmol) was added dropwise to a solution of 1,5-bis[2-(2-(2-(2-propyne)ethoxy)ethoxy)ethoxy]naphthalene, (0.156 g, 0.311 mmol) dissolved in dry THF (15.7 mL) at −78 °C under an Ar atmosphere. After stirring for 15 min at −78 °C Me_3SiCl (48.0 μL, 0.374 mmol) was added dropwise and the reaction mixture was stirred at RT for 12 h. The crude reaction mixture was quenched with saturated aq. NH_4Cl (15 mL) and extracted with CH_2Cl_2 (4 × 20 mL). The combined organic extracts were washed with brine (20 mL), dried ($MgSO_4$), and evaporated. The crude product was subjected to chromatography (SiO_2, 93:7 to 90:10 CH_2Cl_2:Et_2O eluent) to give 47 mg (26% yield) of **7** as a pale yellow oil. **7**: ^{1}H NMR (600 MHz, $CDCl_3$, 25 °C, TMS): δ 7.86 (d, ^3J (H,H) = 8 Hz, 2H, DNP aryl –*H p*-O), 7.34 (t, ^3J (H,H) = 8 Hz, 2H, DNP aryl –*H m*–O), 6.84 (d, ^3J (H,H) = 8 Hz, 2H, DNP aryl –*H o*–O), 4.30 (t, ^3J (H,H) = 5 Hz, 4H, DNP–OCH_2), 4.20 (s, 2H, –OCH_2CCSi), 4.19 (d, ^4J (H,H) = 2.4 Hz, 2H, –OCH_2CCH), 4.00 (t, ^3J (H,H) = 5 Hz, 4H), 3.82–3.80 (m, 4H), 3.72–3.67 (m, 12H), 2.41 (t, ^4J (H,H) = 2.4 Hz, 1H, –CC*H*), 0.17 (s, 9H, –Si(CH_3)$_3$); ^{13}C NMR (151 MHz, $CDCl_3$, 25 °C, TMS): δ 154.5, 126.9, 125.2, 114.8, 105.8, 101.6, 91.5, 79.8, 74.6, 71.1, 70.9, 70.9, 70.6, 70.6, 70.0, 69.3, 69.2, 68.1, 59.3, 58.5, 0.0; HRMS (FAB): Calcd. for $C_{31}H_{44}O_8Si$ *m/z* = 572.2805; found *m/z* = 572.2823.

Tris-1,3,5-(4′-Azidomethyl)Benzene (**6**)

NaN_3 (1.079 g, 16.61 mmol) was added to a solution of tris-1,3,5-(4′-chloromethyl)benzene, (0.500 g, 1.11 mmol) dissolved in dry DMF (75 mL) and the solution was stirred at 60 °C for 24 h. The crude reaction mixture was quenched with H_2O (75 mL) and extracted with CH_2Cl_2 (2 × 50 mL). The combined organic extracts were dried ($MgSO_4$), and evaporated. The crude product was subjected to chromatography (SiO_2, 7:3 hexane:CH_2Cl_2) to give 450 mg (86% yield) of **5** as a white solid. **5**: ^{1}H NMR (400 MHz, $CDCl_3$, 25 °C, TMS): δ 7.78 (s, 3H, central aryl–*H*), 7.73 (d, ^3J (H,H) = 8 Hz, 6H, aryl –*H m*-CH_2N_3), 7.45 (d, ^3J (H,H) = 8 Hz, 6H, aryl –*H o*-CH_2N_3), 4.42 (s, 6H, CH_2N_3); ^{13}C NMR (151 MHz, $CDCl_3$, 25 °C, TMS): δ 141.8, 140.9, 134.8, 128.7, 127.7, 125.2, 54.5; HRMS (EI): Calcd. for $C_{27}H_{21}N_9$ *m/z* = 471.1920; found *m/z* = 471.1939.

3,4,5-Tris-[(2-(2-Methoxy)Ethoxy)Ethoxybenzyloxy]Benzyl Azide (**10**)

NaN_3 (0.379 g, 3.53 mmol) was added to a solution of 3,4,5-tris-[(2-(2-methoxy)ethoxy)ethoxybenzyloxy]benzyl chloride [52], (0.282 g, 0.353 mmol) dissolved in DMF (3.7 mL) and the solution was stirred at 60 °C for 24 h. The crude reaction mixture was quenched with H_2O (50 mL) and extracted with CH_2Cl_2 (2 × 25 mL). The combined organic extracts were washed with H_2O (2 × 20 mL), brine (20 mL), dried ($MgSO_4$), and evaporated. The crude product was subjected to chromatography (SiO_2, EtOAc eluent) to give 221 mg (77% yield) of **10** as a pale yellow amorphous solid. **10**: ^{1}H NMR (600 MHz, $CDCl_3$, 25 °C, TMS): δ 7.32 (d, ^3J (H,H) = 9 Hz, 4H, aryl *–H m–*O), 7.27 (d, ^3J (H,H) = 9 Hz, 2H, aryl *–H m–*O), 6.91 (d, ^3J (H,H) = 9 Hz, 4H, aryl *–H o–*O), 6.79 (d, ^3J (H,H) = 9 Hz, 2H, aryl *–H o–*O), 6.57 (s, 2H, aryl –H *o*-CH_2N$_3$), 5.01 (s, 4H, benzylic CH_2O), 4.94 (s, 2H, benzylic CH_2O), 4.21 (s, 2H, –CH_2N$_3$), 4.16 (t, ^3J (H,H) = 5 Hz, 4H), 4.12 (t, ^3J (H,H) = 5 Hz, 2H), 3.89–3.85 (m, 6H), 3.74–3.71 (m, 6H), 3.60–3.57 (m, 6H), 3.40 (s, 6H, OCH_3), 3.39 (s, 3H, OCH_3); ^{13}C NMR (151 MHz, $CDCl_3$, 25 °C, TMS): δ 158.7, 158.6, 153.2, 138.5, 130.9, 130.3, 130.2, 129.3, 129.2, 114.7, 114.3, 108.2, 74.7, 72.1, 71.2, 70.9, 70.8, 69.9, 67.6, 67.5, 59.2, 55.1; HRMS (FAB): Calcd. for $C_{43}H_{55}O_{12}N_3$(Na) *m/z* = 828.3649; found *m/z* = 828.3684; elemental analysis: C: 64.33, H: 6.81, N: 5.19 (calcd. C: 64.08, H: 6.88, N: 5.21).

[4]Rotaxane (**11**•12PF_6)

Tris-1,3,5-(4′-azidomethyl)benzene (**6**) (0.0107 g, 0.0227 mmol) and DNP derivative **7** (0.0390 g, 0.0682 mmol, 1.0 eq. per azide) were dissolved in DMF-d_7 (0.45 mL) in an NMR tube. Stock solutions of $CuSO_4$•5H_2O in DMF-d_7 (45 μL, 0.072 M, 0.05 eq. per azide) and ascorbic acid in DMF-d_7 (45 μL, 0.144 M, 0.10 eq. per azide) were added and the mixture left at RT for 20 h (until the –CH_2N$_3$ resonance at 4.61 ppm was replaced by the –CH_2N(triazole) resonance at 5.76 ppm in the ^{1}H NMR spectrum of the reaction mixture). A stock solution of $AgPF_6$ in DMF-d_7 (50 μL, 0.235 M, 0.17 eq. per TMS) and H_2O (3.7 μL, 0.2081 mmol, 9 eq. per TMS) were added and the mixture left at 40 °C for 36 h (until the –CH_2CCSi singlet resonance at 4.36 was replaced by the –CH_2CCH doublet resonance at 4.23 ppm and the –CCSi(CH_3)$_3$ resonance at 0.16 ppm was replaced by the –Si(CH_3)$_3$ resonances at 0.08 and 0.05 ppm in the ^{1}H NMR spectrum of the reaction mixture). 3,4,5-Tris-[(2-(2-methoxy)ethoxy)ethoxybenzyloxy]benzyl azide (**10**) (0.0584 g, 0.0725 mmol, 1.1 eq. per alkyne), CBPQT•4PF_6 (0.0840 g, 0.0763 mmol, 1.1 eq. per DNP), Cu nanopowder (Aldrich, 0.002 g, 0.0315 mmol), and Cu(MeCN)$_4PF_6$ (0.002 g, 0.0054 mmol) were then added and the dark purple reaction mixture was cooled to −5 °C for 40 h (until the –CC*H* resonance at 3.17 ppm was no longer observed in the ^{1}H NMR spectrum), after which time a Ag mirror had formed on the walls of the NMR tube. The reaction mixture was filtered through a fritted funnel to

remove residual solids and the solvent evaporated. The resulting purple oil was redissolved in Me_2CO and the [4]rotaxane was purified by preparative TLC using 50% MeOH/CH_2Cl_2 followed by 3% w/v NH_4PF_6 in Me_2CO followed by a 12:7:1 1 M NH_4Cl:MeOH:$MeNO_2$ mobile phases consecutively on one preparative TLC plate. The rotaxane product was recovered from the silica gel by washing with excess water, then Me_2CO, and finally a 4% w/v NH_4PF_6 solution in Me_2CO. The recovered material was then resubjected to preparative TLC using a 12:7:1 1 M NH_4Cl:MeOH:$MeNO_2$ mobile phase. The rotaxane product was again recovered from the silica gel as before. The Me_2CO was concentrated to a minimum volume, and the product was precipitated from this solution through the addition of an excess of cold water. The [4]rotaxane **11**•12PF_6 was isolated as a purple solid (78 mg, 44% yield). **11**•12PF_6: ^{1}H NMR (600 MHz, CD_3COCD_3, 52 °C, TMS) (assignments verified by COSY and HMQC): δ 9.08 (br s, 24H, α-CBPQT^{4+}), 8.19 (br s, 24H, phenylene-CBPQT^{4+}), 7.92 (s, 3H, central benzene aryl *–H*), 7.90 (d, ^3J (H,H) = 8 Hz, 6H, central aryl *–H m*-methylene triazole), 7.83 (s, 3H, triazole *–H*), 7.74 (s, 3H, triazole *–H*), 7.56 (br s, 24H, β-CBPQT^{4+}), 7.46 (d, ^3J (H,H) = 8 Hz, 6H, central aryl *–H o*-methylene triazole), 7.32 (d, ^3J (H,H) = 8 Hz, 12H, stopper aryl *–H m*–O), 7.28 (d, ^3J (H,H) = 8 Hz, 6H, stopper aryl *–H m*–O), 6.92 (d, ^3J (H,H) = 8 Hz, 12H, stopper aryl *–H o*–O), 6.83 (d, ^3J (H,H) = 8 Hz, 6H, stopper aryl *–H o*–O), 6.74 (s, 6H, stopper aryl *–H o*-methylene triazole), 6.41 (d, ^3J (H,H) = 8 Hz, 3H, DNP aryl *–H p*-O), 6.30 (d, ^3J (H,H) = 8 Hz, 3H, DNP aryl *–H o*–O), 6.16 (t, ^3J (H,H) = 8 Hz, 3H, DNP aryl *–H m*–O), 6.08 (t, ^3J (H,H) = 8 Hz, 3H, DNP aryl *–H m*–O), 5.96 (br s, 24H, CBPQT^{4+} benzyl *–H*), 5.56 (s, 6H, central CH_2-triazole), 5.39 (s, 6H, stopper CH_2–triazole), 4.96 (s, 12H, stopper phenyl–OCH_2), 4.88 (s, 6H, stopper phenyl–OCH_2), 4.45–4.39 (m, 12H, DNP–OCH_2), 4.37 (s, 6H, OCH_2–triazole), 4.34 (s, 6H, OCH_2–triazole), 4.25–4.17 (m, 12H), 4.13 (t, ^3J (H,H) = 5 Hz, 12H, stopper aryl–OCH_2), 4.10 (t, ^3J (H,H) = 5 Hz, 6H, stopper aryl–OCH_2), 4.06–3.97 (m, 12H), 3.95–3.85 (m, 12H), 3.83–3.74 (m, 30H), 3.67–3.60 (m, 18H), 3.53–3.48 (m, 18H), 3.31–3.27 (m, 27H, stopper–OCH_3), 2.72 (d, ^3J (H,H) = 8 Hz, 3H, DNP aryl *–H p*-O), 2.68 (d, ^3J (H,H) = 8 Hz, 3H, DNP aryl *–H p*-O); ^{13}C NMR (151 MHz, CD_3COCD_3, 2 °C, TMS): δ 159.6, 153.6, 151.9, 145.9, 145.6, 145.2, 141.1, 138.1, 137.7, 136.8, 132.2, 132.0, 131.9, 131.1, 130.8, 130.4, 129.7, 129.6, 128.9, 128.6, 126.8, 126.6, 125.2, 125.1, 125.0, 115.0, 114.7, 109.0, 107.9, 104.9, 104.7, 75.1, 72.4, 72.4, 71.7, 71.3, 71.2, 71.0, 70.9, 70.7, 70.1, 69.7, 68.8, 68.1, 65.8, 65.7, 64.3, 64.2, 58.7, 54.1, 53.5; MS (ESI; MeOH/H_2O = 1:1, 0.1% AcOH): *m/z* = 1,777.4 [M–4PF_6]$^{4+}$, 1,392.7 [M–5PF_6]$^{5+}$, 1,136.5 [M–6PF_6]$^{6+}$, 953.4 [M–7PF_6]$^{7+}$, 816.2 [M–8PF_6]$^{8+}$.

Dumbbell Compound (**12**)

Tris-1,3,5-(4′-azidomethyl)benzene (**6**) (0.0103 g, 0.0219 mmol) and DNP derivative **7** (0.0378 g, 0.0659 mmol, 1.0 eq. per azide) were dissolved in DMF-d_7 (0.45 mL) in an NMR tube. Stock solutions of $CuSO_4$•5H_2O in DMF-d_7 (43 μL, 0.072 M, 0.05 eq. per azide) and ascorbic acid in DMF-d_7

(43 μL, 0.144 M, 0.10 eq. per azide) were added and the reaction mixture was held at RT for 20 h (until the –CH_2N$_3$ resonance at 4.61 ppm was replaced by the –CH_2N(triazole) resonance at 5.76 ppm in the ^{1}H NMR spectrum of the reaction mixture). A stock solution of $AgPF_6$ in DMF-d_7 (50 μL, 0.235 M, 0.17 eq. per TMS) and H_2O (3.7 μL, 0.208 mmol, 9 eq. per TMS) were added and the mixture was heated to 40 °C for 36 h (until the –CH_2CCSi singlet resonance at 4.36 was replaced by the –CH_2CCH doublet resonance at 4.23 ppm and the –CCSi(CH_3)$_3$ resonance at 0.16 ppm was replaced by the –Si(CH_3)$_3$ resonances at 0.08 and 0.05 ppm in the ^{1}H NMR spectrum of the reaction mixture). 3,4,5-Tris-[(2-(2-methoxy)ethoxy)ethoxybenzyloxy]benzyl azide (**10**) (0.0584 g, 0.0725 mmol, 1.1 eq. per alkyne), Cu nanopowder (Aldrich, 0.002 g, 0.0315 mmol), and $Cu(MeCN)_4PF_6$ (0.002 g, 0.0054 mmol) were then added and the reaction mixture was allowed to rest at room temperature for 24 h (until the –CC*H* resonance at 3.38 ppm was replaced by the –C*H*(triazole) at 8.31 ppm in the ^{1}H NMR spectrum of the reaction mixture), after which time a Ag mirror had formed on the walls of the NMR tube. The reaction mixture was filtered through a fritted funnel to remove the residual solids and the solvent evaporated. The resulting brown oil was subjected to chromatography (SiO_2, 10:90 Me_2CO:CH_2Cl_2 followed by 10:90 MeOH:CH_2Cl_2 eluent) to give 63.2 mg (65% yield) of **12** as a colorless oil. **12**: ^{1}H NMR (600 MHz, $CDCl_3$, 25 °C, TMS) (assignments verified by COSY and HMQC): δ 7.84 (d, ^3J (H,H) = 8 Hz, 6H, DNP aryl –*H p*-O), 7.71 (s, 3H, central benzene aryl –*H*), 7.64 (d, ^3J (H,H) = 8 Hz, 6H, central aryl –*H m*-methylene triazole), 7.53 (s, 3H, triazole –*H*), 7.43 (s, 3H, triazole –*H*), 7.34 (d, ^3J (H,H) = 8 Hz, 6H, central aryl –*H o*-methylene triazole), 7.35–7.26 (m, 24H), 6.91 (d, ^3J (H,H) = 8 Hz, 12H, stopper aryl –*H o*–O), 6.81–6.79 (m, 12H, stopper aryl –*H o*–O and DNP aryl –*H o*–O), 6.53 (s, 6H, stopper aryl –*H o*-methylene triazole), 5.51 (s, 6H, tris–phenyl benzene–CH_2N), 5.33 (s, 6H, stopper phenyl–CH_2N), 4.96 (s, 12H, stopper O-CH_2–phenyl), 4.92 (s, 6H, stopper O-CH_2–phenyl), 4.67 (s, 6H, triazole–CH_2O), 4.67 (s, 6H, triazole–CH_2O), 4.26–4.23 (m, 12H, DNP–OCH_2), 4.15 (t, ^3J (H,H) = 5 Hz, 12H, stopper phenyl–OCH_2), 4.13 (t, ^3J (H,H) = 5 Hz, 6H, stopper phenyl–OCH_2), 3.97–3.94 (m, 12H), 3.89–3.85 (m, 18H), 3.79–3.76 (m, 12H), 3.74–3.72 (m, 18H), 3.70–3.66 (m, 36H), 3.60–3.58 (m, 18H), 3.40 (s, 27H, stopper –OCH_3); ^{13}C NMR (151 MHz, $CDCl_3$, 25 °C, TMS): δ 158.6, 158.6, 154.3, 153.2, 145.7, 145.9, 141.7, 141.2, 138.7, 134.2, 130.2, 130.0, 129.9, 129.2, 129.0, 128.7, 127.9, 126.7, 125.3, 125.1, 122.6, 122.6, 114.6, 114.3, 108.0, 105.7, 74.7, 71.9, 71.1, 70.9, 70.7, 70.7, 70.6, 70.6, 69.8, 69.8, 67.9, 67.4, 67.4, 64.7, 64.7, 59.1, 54.2, 53.7; MS (ESI; MeOH/H_2O = 1:1, 0.1% AcOH): *m/z* = 1,464.4 $[M + 3H]^{3+}$, 1,098.5 $[M + 4H]^{4+}$, 879.2 $[M + 5H]^{5+}$; HRMS (ESI; MeOH/H_2O = 1:1, 0.1% AcOH): *m/z* calcd. for $[C_{240}H_{298}N_{18}O_{60}]^{4+}$: 1,098.5220 $[M + 4H]^{4+}$; found: 1,098.5203.

References

1. Green JE, Choi JW, Boukai A, Bunimovich Y, Johnston-Halpering E, DeIonno E, Luo Y, Sheriff BA, Xu K, Shin YS, Tseng H-R, Stoddart JF, Heath JR (2007) Nature 445:414–417
2. Liu Y, Flood AH, Bonvallett PA, Vignon SA, Northrop BH, Tseng H-R, Jeppesen JO, Huang TJ, Brough B, Baller M, Magonov S, Solares SD, Goddard WA, Ho CM, Stoddart JF (2005) J Am Chem Soc 127:9745–9759
3. Eelkema R, Pollard MM, Vicario J, Katsonis N, Ramon BS, Bastiaansen CWM, Broer DJ, Feringa BL (2006) Nature 440:163
4. Kay ER, Leigh DA, Zerbetto F (2007) Angew Chem Int Ed 46:72–191
5. Berna J, Leigh DA, Lubomska M, Mendoza SM, Perez EM, Rudolf P, Teobaldi G, Zerbetto F (2005) Nat Mater 4:704–710
6. Bath J, Turberfield AJ (2007) Nat Nanotechnol 2:275–284
7. Saha S, Leung KCF, Nguyen TD, Stoddart JF, Zink JI (2007) Adv Funct Mater 17:685–693
8. Balzani V, Credi A, Venturi M (2007) Nano Today 2:18–25
9. Saha S, Stoddart JF (2007) Chem Soc Rev 36:77–92
10. Serreli V, Lee CF, Kay ER, Leigh DA (2007) Nature 445:523–527
11. Leung KCF, Nguyen TD, Stoddart JF, Zink JI (2006) Chem Mater 18:5919–5928
12. Brough B, Northrop BH, Schmidt JJ, Tseng H-R, Houk KN, Stoddart JF, Ho C-M (2006) Proc Natl Acad Sci USA 103:8583–8588
13. Balzani V, Clemente-Leon M, Credi A, Ferrer B, Venturi M, Flood AH, Stoddart JF (2006) Proc Natl Acad Sci USA 103:1178–1183
14. van Delden RA, ter Wiel MKJ, Pollard MM, Vicario J, Koumura N, Feringa BL (2005) Nature 437:1337–1340
15. Leigh DA, Wong JKY, Dehez F, Zerbetto F (2003) Nature 424:174–179
16. Dichtel WR, Miljanić OŠ, Spruell JM, Heath JR, Stoddart JF (2006) J Am Chem Soc 128:10388–10390
17. Mobian P, Collin JP, Sauvage J-P (2006) Tetrahedron Lett 47:4907–4909
18. Aucagne V, Hanni KD, Leigh DA, Lusby PJ, Walker DB (2006) J Am Chem Soc 128:2186–2187
19. Miljanić OŠ, Dichtel WR, Mortezaei S, Stoddart JF (2006) Org Lett 8:4835–4838
20. Braunschweig AB, Dichtel WR, Miljanić OŠ, Olson MA, Spruell JM, Khan SI, Heath JR, Stoddart JF (2007) Chem Asian J 2:634–647
21. Aprahamian I, Dichtel WR, Ikeda T, Heath JR, Stoddart JF (2007) Org Lett 9:1287–1290
22. Aprahamian I, Yasuda T, Ikeda T, Saha S, Dichtel WR, Isoda K, Kato T, Stoddart JF (2007) Angew Chem Int Ed 46:4675–4679
23. Prikhod'ko AI, Durola F, Sauvage J-P (2008) J Am Chem Soc 130:448–449
24. Aucagne V, Berna J, Crowley JD, Goldup SM, Haenni KD, Leigh DA, Lusby PJ, Ronaldson VE, Slawin AMZ, Viterisi A, Walker DB (2007) J Am Chem Soc 129:11950–11963
25. Ashton PR, Glink PT, Stoddart JF, Tasker PA, White AJP, Williams DJ (1996) Chem Eur J 2:729–736
26. Rowan SJ, Cantrill SJ, Stoddart JF (1999) Org Lett 1:129–132
27. Chiu S-H, Rowan SJ, Cantrill SJ, Glink PT, Garrell RL, Stoddart JF (2000) Org Lett 2:3631–3634
28. Elizarov AM, Chiu S-H, Glink PT, Stoddart JF (2002) Org Lett 4:679–682
29. Braunschweig AB, Ronconi CM, Han JY, Arico F, Cntrill SJ, Stoddart JF, Khan SI, White AJP, Williams DJ (2006) Eur J Org Chem 18
30. Rostovtsev VV, Green LG, Fokin VV, Sharpless KB (2002) Angew Chem Int Ed 41:2596–2599
31. Tornoe CW, Christensen C, Meldal M (2002) J Org Chem 67:3057–3064
32. Busch DH (2005) Top Curr Chem 249:1–65
33. Hubin TJ, Busch DH (2000) Coord Chem Rev 200:5–52
34. Busch DH, Stephenson NA (1990) Coord Chem Rev 100:119–154

35. Anderson S, Anderson HL, Sanders JKM (1993) Acc Chem Res 26:469–475
36. Breault GA, Hunter CA, Mayers PC (1999) Tetrahedron 55:5265–5293
37. Blanco MJ, Cambron JC, Jiménez MC, Sauvage J-P (2003) Top Stereochem 23:125–173
38. Tseng H-R, Vignon SA, Celestre PC, Perkins J, Jeppesen JO, Di Fabio A, Ballardini R, Gandolfi MT, Venturi M, Balzani V, Stoddart JF (2004) Chem Eur J 10:155–172
39. Mendes PM, Lu WX, Tseng H-R, Shinder S, Iijima T, Miyaji M, Knobler CM, Stoddart JF (2006) J Phys Chem B 110:3845–3848
40. Jeppesen JO, Nygaard S, Vignon SA, Stoddart JF (2005) Eur J Org Chem 196–220
41. Lee IC, Frank CW, Yamamoto T, Tseng H-R, Flood AH, Stoddart JF, Jeppesen JO (2004) Langmuir 20:5809–5828
42. Jeppesen JO, Nielsen KA, Perkins J, Vignon SA, Di Fabio A, Balladini R, Gandolfi MT, Benturi M, Balzani V, Becher J, Stoddart JF (2003) Chem Eur J 9:2982–3007
43. Chen Y, Jung GY, Ohlberg DAA, Li XM, Stewart DR, Jeppesen JO, Nielsen KA, Stoddart JF, Williams RS (2003) Nanotechnology 14:462–468
44. Steuerman DW, Tseng H-R, Peters AJ, Flood AH, Jeppesen JO, Nielsen KA, Stoddart JF, Heath JR (2004) Angew Chem Int Ed 43:6486–6491
45. Diehl MR, Steuerman DW, Tseng H-R, Vignon SA, Star A, Celestre PC, Stoddart JF, Heath JR (2003) Chem Phys Chem 4:1335–1339
46. Yu HB, Luo Y, Berverly K, Stoddart JF, Tseng H-R, Heath JR (2003) Angew Chem Int Ed 42:5706–5711
47. Luo Y, Collier CP, Jeppesen JO, Nielsen KA, DeIonno E, Ho G, Perkins J, Tseng H-R, Yamamoto T, Stoddart JF, Heath JR (2002) Chem Phys Chem 3:519–525
48. Collier CP, Mattersteig G, Wong EW, Luo Y, Berverly K, Sampaio J, Raymo FM, Stoddart JF, Heath JR (2000) Science 289:1172–1175
49. Dichtel WR, Heath JR, Stoddart JF (2007) Philos Trans R Soc London Ser A 365:1607–1625
50. DeIonno E, Tseng H-R, Harvey DD, Stoddart JF, Heath JR (2006) J Phys Chem B 110:7609–7612
51. Flood AH, Stoddart JF, Steuerman DW, Heath JR (2004) Science 306:2055–2056
52. Collier CP, Jeppesen JO, Luo Y, Perkins J, Wong EW, Heath JR, Stoddart JF (2001) J Am Chem Soc 123:12632–12641
53. Aucagne V, Leigh DA (2006) Org Lett 8:4505–4507
54. Orsini A, Viterisi A, Bodlenner A, Weibel JM, Pale PA (2005) Tetrahedron Lett 46:2259–2262
55. Viterisi A, Orsini A, Weibel JM, Pale P (2006) Tetrahedron Lett 47:2779–2781
56. Carpita A, Mannocci L, Rossi R (2005) Eur J Org Chem 1859–1864
57. Lee T, Kang HR, Kim S (2006) Tetrahedron 62:4081–4085
58. Halbes-Letinois U, Weibel JM, Pale P (2007) Chem Soc Rev 36:759–769
59. Badjić JD, Balzani V, Credi A, Silvi S, Stoddart JF (2004) Science 303:1845–1849
60. Badjić JD, Balzani V, Credi A, Lowe JN, Silvi S, Stoddart JF (2004) Chem Eur J 10:1926–1935
61. Badjić JD, Nelson A, Cantrill SJ, Turnbull WB, Stoddart JF (2005) Acc Chem Res 38:723–732
62. Miljanić OŠ, Stoddart JF (2007) Proc Natl Acad Sci USA 104:12966–12970
63. Love BE, Jones EG (1999) J Org Chem 64:3755–3756
64. Asakawa M, Dehaen W, L'abbé G, Menzer S, Nouwen J, Raymo FM, Stoddart JF, Williams DJ (1996) J Org Chem 61:9591–9595

Chapter 4
Heterogeneous Catalysis Through Microcontact Printing

4.1 Introduction

The chemical toolkit for the modification of inorganic surfaces with organic molecules has grown dramatically in recent years. Much of the underlying science has been driven by developing technologies [1–5] such as biomolecular and chemical sensing [6, 7], molecular electronics [8, 9], light harvesting [10], and others. These applications all have certain requirements that place unique demands on the chemistry, which often impact more than just the choice of substrate or organic modifier. For example, electronic communication between surface-bound organic molecules and the underlying substrate may be necessary. Other application-specific requirements include rapid and efficient surface attachment chemistries that provide (i) high surface coverage, (ii) protection of the underlying substrate against oxidation [11], and/or (iii) control over molecular orientation.

The ability to pattern the organic monolayer spatially is a common requirement. The technique of microcontact printing (μCP) permits [12–16] the patterned transfer of a molecular ink onto a surface using an elastomeric stamp. The transferred molecules may form a self-assembled, high coverage monolayer—e.g., thiols on gold [14, 16] or silanes on silicon dioxide [17]. Alternatively, μCP can promote the spatially selective reaction between an already surface-bound

This Chapter is reproduced in part with permission from: Spruell JM, Sheriff BA, Rozkiewicz DI, Dichtel WR, Rohde RD, Reinhoudt DN, Stoddart JF., Heath JR *Angew. Chem. Int. Ed.* **2008**, *47*, 9927–9932.

Author Contributions: J.M. Spruell, D.I. Rozkiewicz, W.R. Dichtel, and J.R. Heath conceived the project. J.M. Spruell, J.R. Heath and J.F. Stoddart prepared the original manuscript. J.M. Spruell, D.I. Rozkiewicz, and B.A. Sheriff performed microcontact printing. J.M. Spruell synthesized all compounds used in these investigations. J.M. Spruell and B.A. Sheriff performed IR, electrochemical, and water contact angle characterization. D.I. Rozkiewicz performed AFM and confocal fluorescence microscopies. R.D. Rohde performed XPS analysis. D.N. Reinhoudt, J.F. Stoddart, and J.R. Heath supervised the original research.

J. M. Spruell, *The Power of Click Chemistry for Molecular Machines and Surface Patterning*, Springer Theses, DOI: 10.1007/978-1-4419-9647-3_4,

molecule and a molecular ink. This concept has been demonstrated for (i) the patterning of peptides using amide [13, 15, 18] coupling chemistry, (ii) the formation of thermodynamically stable imine [19] bonds, and (iii) for the promotion of the Huisgen 1,3-dipolar cycloaddition, yielding [20] a triazole link between a surface-bound moiety and the ink molecule. Both the triazole- and amide-coupling chemistries typically require catalysts or additional stoichiometric reagents, such as carbodiimides, when performed in solution. However, within the unique environment [21] created when the surface-bound and molecular ink reagents are brought into close contact using a stamp, the reactions have been reported [20, 21] to proceed—at least to some extent—without these additional components.

The organic functionalization of surfaces is heterogeneous, involving a solid-surface reacting with solution- or gas-phase reagents. The two-dimensional nature of surfaces also means that steric effects can either impose kinetic barriers upon thermodynamically favored chemical processes, or they can impart kinetic stability to certain non-equilibrium surface structures [22–24]. The presence of kinetic barriers, in turn, implies that different chemical approaches towards functionalizing surfaces with organic components might lead to different coverages and/or surface structures.

In this chapter, we investigate four different chemical pathways (Scheme 4.1a–d) relevant to the Cu-catalyzed azide-alkyne cycloaddition (CuAAC) reaction [25–28]. Three of those pathways lead to surfaces functionalized with organic molecules [11, 21, 29–34]. At the outset, our practical goal was to identify surface-functionalization protocols that are capable of attaining (i) spatial selectivity, (ii) high surface coverage, and (iii) rapid reaction kinetics. Our ultimate goal is to achieve a fundamental understanding of how different reaction pathways influence the chemical outcome as it applies to the organic functionalization of surfaces.

4.2 Results and Discussion

The four pathways illustrated in Schemes 4.1a–d vary with regard to how the reaction components (**1–7**, Fig. 4.1, and the Cu source) are introduced to one another. A Cu catalyst is required for the CuAAC reaction to proceed to any appreciable extent in each scheme. Probes **5–7**, when attached to surfaces, are respectively designed for specific redox, X-ray photoelectron spectroscopy (XPS), or fluorescent signatures, thus allowing for the full characterization of the functionalized surfaces using complementary techniques. Scheme 4.1a summarizes a homogeneous, s*olution*-based pathway in which 1-azidohexane (**3**), 1-octyne (**4**), and $CuSO_4 \bullet 5H_2O$/ascorbic acid [25] react in solution, and provides a reference against which the surface chemistries can be compared. Under conditions chosen to simulate those relevant to surface functionalization (20-fold excess of **4** relative to **3**), the CuAAC reaction proceeded to 95% conversion during 6 h. This finding is a useful baseline for comparison of the kinetics of the reactions performed through each of the (Scheme 4.1b–d) heterogeneous surface reactions.

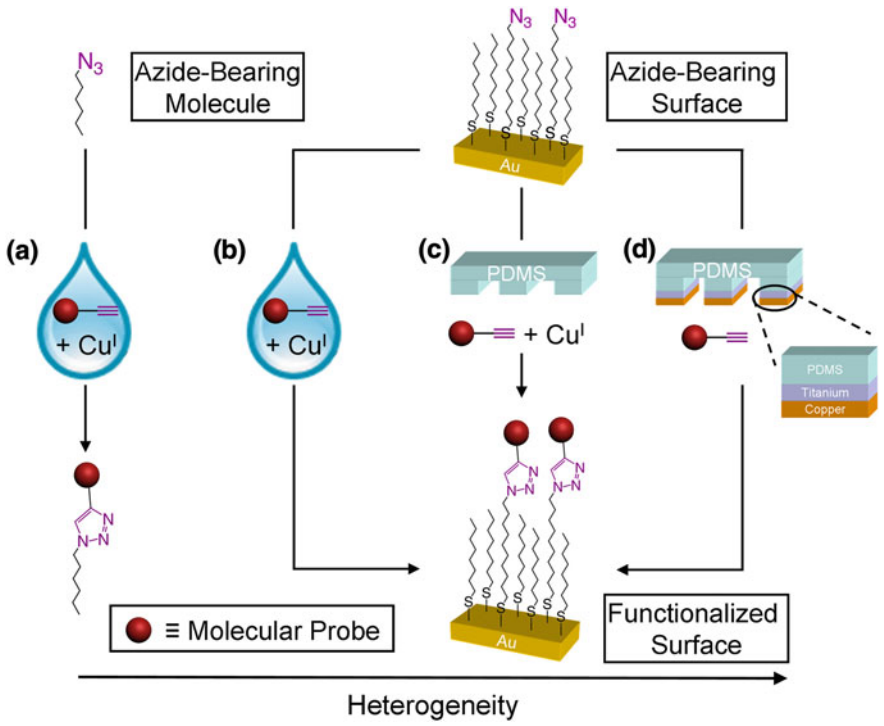

Scheme 4.1 Various routes to affect the Cu(I)-catalyzed azide-alkyne coupling (CuAAC) in different environments: **a** *Solution*: A solution reaction where azide, alkyne, and catalyst participate in a homogeneous reaction; **b** *Solution-Surface*: A heterogeneous reaction where dissolved alkyne and catalyst react with a surface bound azide; **c** *Reagent-Stamping*: A heterogeneous reaction where the alkyne and catalyst are brought into contact with a surface-bound azide in the condensed phase; **d** *StampCat*: A heterogeneous reaction where immobilized copper catalyzes the reaction of an alkyne with a surface bound azide in the condensed phase

The substrates for the CuAAC reactions described in Schemes 4.1b–d were composed of azide functionalities tethered to undecyl alkyl chains as self-assembled monolayers (SAMs) on gold and silicon oxide through terminal thiol and silane groups, respectively. Following on the work of Collman et al. [29, 30], the monolayers on Au were deposited from a 1:1 mixture of two thiols (azidoundecanethiol and octanethiol) to form mixed monolayers in which the relatively long, projecting azido functions are accessible for reaction. Glass slides functionalized with azide moieties were created in a two-step process [20] whereby a bromoundecylsilane SAM is converted to the azido-terminated SAM through nucleophilic displacement of the bromide by sodium azide. The *Solution-Surface* approach (Scheme 4.1b) introduces both the alkyne-terminated molecules and the Cu(I) catalyst, dissolved in a solution placed in contact with the surface. Similar chemistry has been reported previously on Au [29, 30] and other [35, 36] substrates. The *Reagent-Stamping* method (Scheme 4.1c) employs μCP

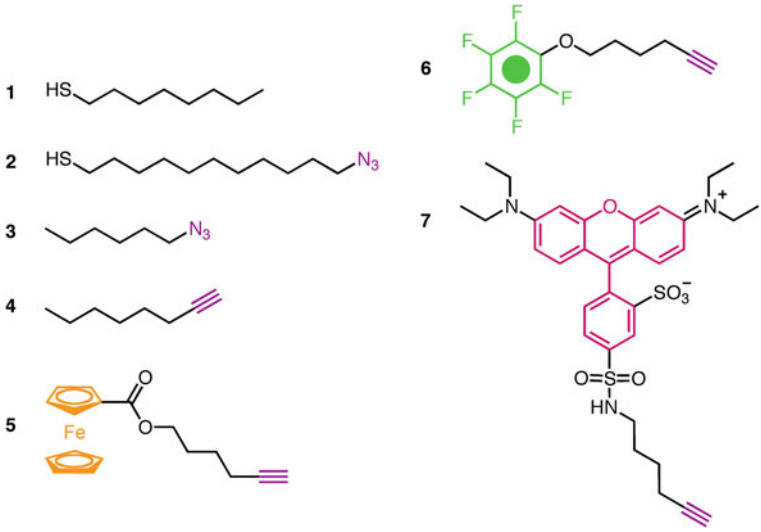

Fig. 4.1 Formulas of molecules studied

methods—using polydimethylsiloxane (PDMS) stamps—to introduce both the alkyne-containing reactant and the Cu(I) catalyst to the surfaces by the (solventless) contacting of inked stamps onto the surfaces. Finally, the *StampCat* procedure (Scheme 4.1d) utilizes a PDMS stamp coated with a thin Cu metal film. The stamp itself catalyzes the spatially-selective reaction between a small-molecule alkyne and the azide surface, also under solvent-free conditions.

Elastomeric stamps are often modified [37, 38] to improve their ability to transfer various inks for μCP, generally by increasing the loading potential of the stamp. The CuAAC reaction may be catalyzed in both the solution [25, 39–44] and solid phase [45] using heterogeneous catalysis in the form of a copper metal source. We hypothesized that a Cu-coated elastomer would similarly catalyze the coupling between surface-bound azides and terminal alkynes. Thus, we modified cured PDMS stamps via electron-beam deposition of a 10 nm Ti adhesion layer followed by a 50 nm Cu layer. The resulting metal-coated flat or patterned stamps retained most of their elasticity and were used in the *StampCat* process.

Surfaces functionalized via Schemes 4.1b–d were characterized by water contact angle, XPS, FTIR, and cyclic voltammetry (CV) measurements. For Scheme 4.1c and d, flat, non-patterned stamps were utilized. For the experiments on surfaces following the CuAAC reaction with each molecular probe (**5**–**7**), all measurements other than CV were carried out after the relevant reaction steps had proceeded to completion (*vida infra*). For the reaction of an Au surface with **5**, CV measurements were carried out to validate the formation of a covalent linkage between **5** and the surface, and to follow the reaction kinetics of Schemes 4.1b–d.

Cyclic voltammetry measurements were utilized to confirm the formation of a covalent bond between the surface and **5**, and to quantify the extent of the reaction.

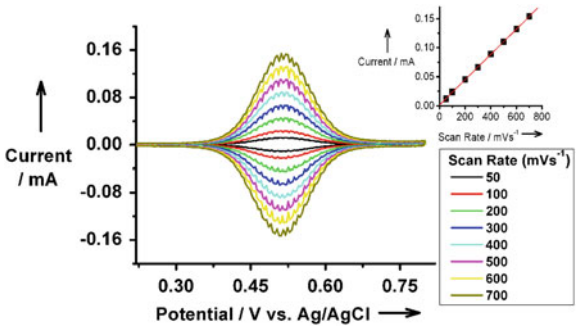

Fig. 4.2 Electrochemical measurements at various scan rates, indicating covalent functionalization of ferrocene-containing ink **3** through *StampCat*. Proof of covalent attachment is supported by the linear plot of current versus scan rate (Inset: current recorded at +0.51 V for each scan rate). The electrolyte was 1 M $HClO_4$

Figure 4.2 displays CV data, collected for a mixed monolayer of **1** and **2** that was functionalized by *StampCat* of **5**. The linear increase in current as a function of scan rate, and the identical values for the peak potential for both oxidation and reduction of the ferrocene, indicate covalent surface attachment of the ferrocenyl moieties. A square-root dependence of current on scan rate would be expected for similar redox behavior if the electroactive components were dissolved in solution. Similar spectra were obtained for surfaces functionalized with **5** employing the *Reagent-Stamping* and *Solution-Surface* schemes. Integration of these spectra confirmed that similar efficiencies were obtained using all three schemes.

Further spectroscopic proof of surface functionalization was obtained by XPS. The *StampCat* process using the pentafluorophenolic ether **6** demonstrated a pronounced change (Fig. 4.3a, b) in the XPS spectra of the F 1*s* region as a consequence of the addition of a highly fluorinated molecular entity onto the surface. Surfaces functionalized with **5**, using the *Reagent-Stamping* process, displayed similar changes in their XPS spectra. Figure 4.3c presents high-resolution XPS spectra of the N 1*s* region, and shows two peaks at 400 and 404 eV with an intensity ratio of 2:1, similar to other reports for azide groups on gold [31] and graphitic [35] surfaces. After functionalization with **5**, a single feature in the N 1*s* region is observed (Fig. 4.3d). These changes for CuAAC functionalized surfaces were common to every situation we investigated, and are also consistent with literature observations [29, 30]. For surfaces functionalized with **5**, changes in the Fe 2*p* region of the spectrum revealed (Fig. 4.3f) the presence of an Fe-containing molecule.

External Reflectance IR spectroscopy also revealed the presence or absence of azide functions at the surface (Fig. 4.4) via measurement of a large peak centered on 2,103 cm^{-1} that arises from the azide symmetric stretching mode. Upon either *StampCat* or *Reagent-Stamping* of **5**, the integrated peak intensity is attenuated by $\sim$90% while a *Solution-Surface* reaction with **5** leads to its complete

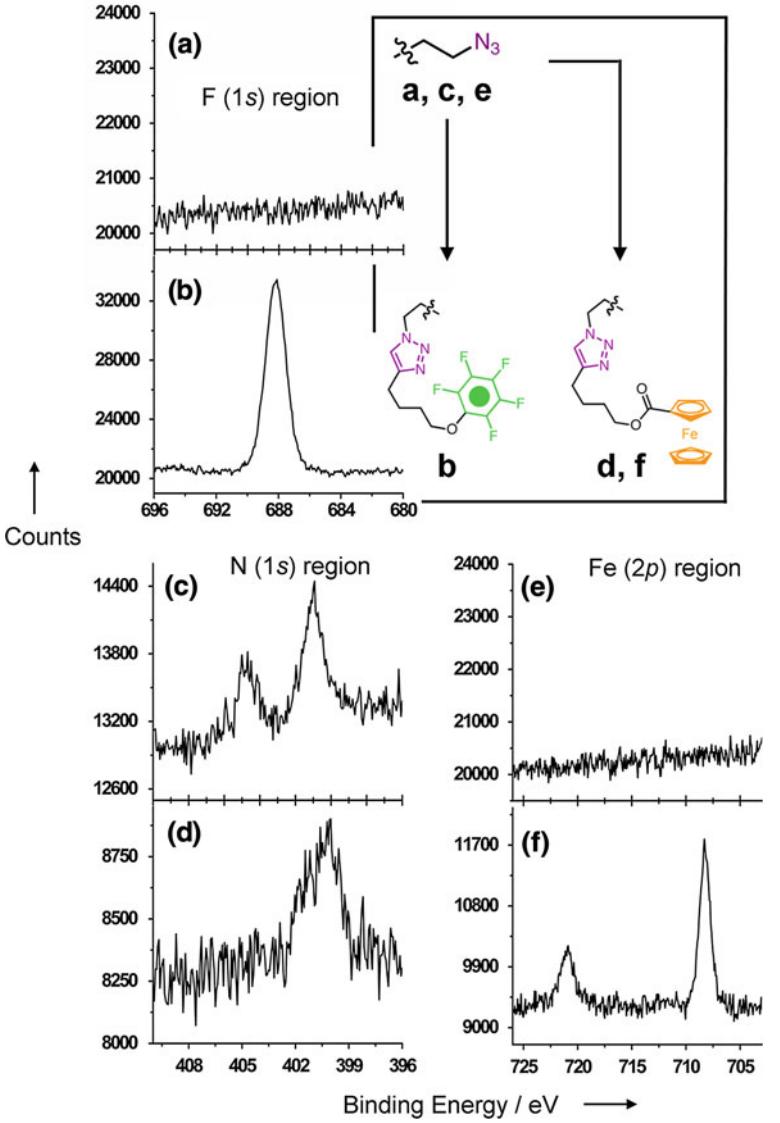

Fig. 4.3 XPS data demonstrating the functionalization of azide-terminated Au substrates (**a**, **c**, and **e**) with pentafluorobenzene **6**-containing (**b**) and ferrocene **5**-containing alkynes (**d** and **f**). The *StampCat* CuAAC reaction is demonstrated in the F 1*s* region before (**a**) and after (**b**) the reaction with the pentafluoro alkyne **6**. The *Reagent-Stamping* CuAAC reaction is demonstrated in the N 1*s* and Fe 2*p* regions of the XPS before (**c**, **e**) and after (**d**, **f**) the reaction with the ferrocene-containing alkyne **5**

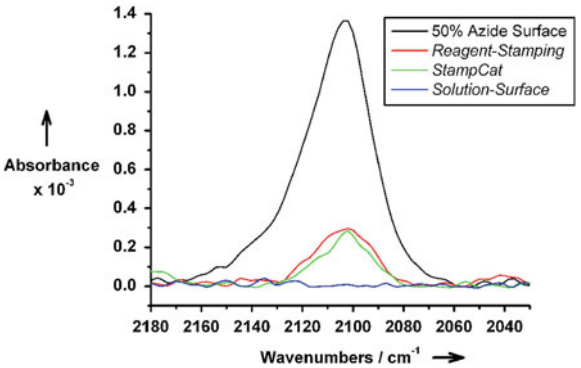

Fig. 4.4 IR spectra demonstrating the reduction of the azide stretch after functionalization with the ferrocene-containing ink **5** using the *Reagent-Stamping*, *StampCat*, and *Solution-Surface* methods

disappearance. These results suggest azide consumption resulting from triazole ring formation and hence the functionalization of the surface in general. Water contact angle measurements also lent qualitative support to the idea that all three methods proceed with comparable reaction efficiency (see Experimental Section).

The solution-based homogeneous reaction (Scheme 4.1a) provided a baseline for comparison with the heterogeneous, surface-based reactions of Schemes 4.1b–d. Under the conditions employed to approximate those expected for surface-based reactions, the reaction proceeds (Fig. 4.5c) to >95% conversion within 400 min with a half-life around 1 h. The homogeneous CuAAC reaction is known to demonstrate complicated kinetics. Under catalytic conditions in copper, Finn and coworkers [46] found the reaction to demonstrate different rate orders in copper depending on concentration and ligand choice. Thus, rather than elucidate the rate law for the conditions described above, we used them as a rough benchmark for the kinetics of the different surface functionalization approaches.

The measured rates (using cyclic voltammetry) of the chemical processes summarized in Schemes 4.1b–d are shown in Fig. 4.5. For these experiments, the attachment of **5** to azide-presenting Au surfaces was monitored as a function of reaction (or stamping) time. When making the *StampCat* measurements, a new Cu-coated PDMS stamp was used in the microcontact printing of the surfaces produced for each time point. Two different *StampCat* kinetic series were investigated: one in which freshly deposited CuPDMS stamps were employed (fresh) and another in which the stamps were allowed to age for 24 h (aged). The integrated intensity of the CV spectra increased (Fig. 4.5a) as a function of reaction (or stamping) time for all methods, and permitted calculation of ferrocene coverage at the surfaces. That all three methods produced coverages at a maximum of 2×10^{14} molecules/cm^2 at extended reaction times indicates that the CuAAC proceeds to completion, in agreement with previous measurements [30] made on the same mixed monolayer surfaces. Plotting the number of functionalizing ferrocene molecules/cm^2 as a function of the reaction time provides (Fig. 4.5b) a means to monitor the kinetics of each CuAAC process.

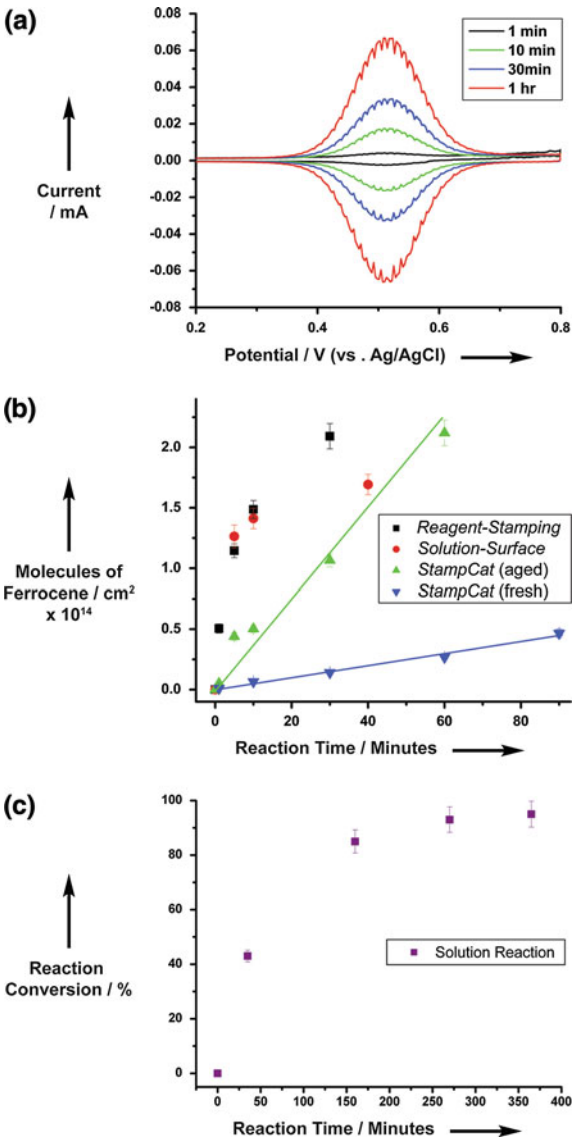

Fig. 4.5 The kinetics of CuAAC catalysis for Scheme 4.1a–d. **a** Cyclic voltammograms, collected (at 300 mV/s) as a function of stamping time, for the *StampCat* process. Coverage increases with longer stamping times (using aged stamps). **b** Plot demonstrating the conversion of azide surfaces to surfaces functionalized with **5**, as a function of time, for all three surface-based reactions (Scheme 4.1b–d). For the *StampCat* process, reaction kinetics for stamps that were used within an hour of metal deposition, and for stamps that were aged in air for 24 h, are shown. Both exhibit linear response functions on this plot, as indicated by the straight lines that are drawn to guide the eye. **c** Reaction conversion versus reaction time for the *Solution* reaction (Scheme 4.1a) between 1-azidohexane (**3**) and 1-octyne (**4**), as measured by ^{1}H NMR spectroscopy

The *Reagent-Stamping* process produced fully functionalized surfaces at the fastest rate, with complete conversion being attained within 30 min. In comparison, the *StampCat* process using aged stamps catalyzed the reaction at half the rate, generating complete coverage after 1 h. Interestingly, a comparison of the two kinetic curves reveals different operable rate orders, with the *Reagent-Stamping* displaying what appears to be pseudo-first order exponential growth and the *StampCat* process zero-order linear growth. Zero-order reaction behavior was

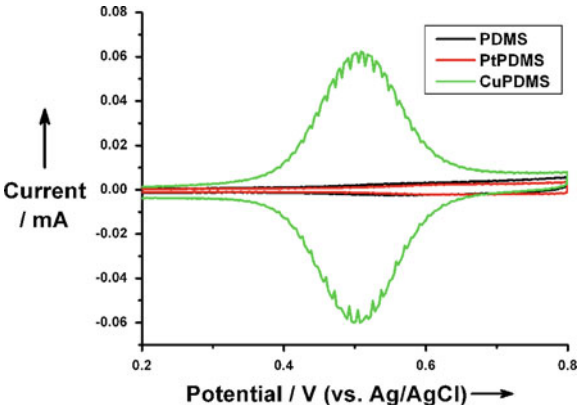

Fig. 4.6 No ferrocene functionalization was observed for stamping with Pt-coated PDMS or bare PDMS for 1 h in comparison to the high functionalization observed for stamping using Cu-coated PDMS

also observed when freshly deposited Cu-coated PDMS stamps were used in the *StampCat* process, but the rate was slower, producing 10-fold less coverage after 60 min of stamping time. The *Solution-Surface* reaction proceeded at a very high rate initially, producing surfaces functionalized with over 1.2×10^{14} ferrocene molecules/cm^2 after 5 min. However, the efficiency plummets in the later stages of the reaction, only producing fully functionalized surfaces (containing 2×10^{14} molecules/cm^2) after 180 min of reaction. This non-linear kinetic behavior for the *Solution-Surface* method is comparable to the pseudo-first order exponential growth of the *Reagent-Stamping* method, a feature that can be attributed to an abundance of Cu(I) catalytic centers available for reaction when employing both of these methods. The *Solution-Surface* process produced fully functionalized surfaces slower than either *Reagent-Stamping* or *StampCat* (using aged stamps).

The *StampCat* process involving the CuAAC reaction is dependent on the catalytic Cu metal coating being present. When bare PDMS or platinum-coated stamps were used for the functionalization of the azide-coated gold surfaces, there was no electrochemical evidence (Fig. 4.6) of the CuAAC reaction having occurred with ferrocene alkyne **5**. This result was unexpected based upon a previous report [20] of quantitative copper-free click reaction onto glass surfaces. An electrochemical analysis of surfaces functionalized with **5** provides a quantitative assessment of reaction efficiencies. The earlier work employed highly sensitive but non-quantitative surface characterization methods. We appreciate now that the reaction without a catalyst results in very limited conversion, even over prolonged reaction times.

In an effort to interrogate the nature of the *StampCat* process, the reaction efficiencies achieved from stamps with freshly deposited Cu films, and those with Cu films that had been aged for 24 h (Fig. 4.5b) were compared. Both situations exhibit linear response functions in terms of ferrocene functionalization versus time, indicating a similar chemical mechanism. However, the aged stamps yielded 5-fold more ferrocene coverage at 60 min than the freshly coated stamps, implying

that the aging process increases the concentration of the active catalytic species on the Cu-coated stamps. While the homogeneous CuAAC reaction is catalyzed by free Cu(I) ions, heterogeneous versions of the reaction have been reported [39–44] in which surface-bound CuO and Cu_2O species are thought [41, 47] to be responsible for the catalysis.

Studies of the oxidation of Cu surfaces [48] indicate that Cu_2O is the predominant initial surface species formed under conditions that are most similar to those for the stamps aged in air for 24 h. It is this Cu_2O coating which most likely acts as the active heterogeneous catalyst in the *StampCat* process. The stamps with freshly-deposited Cu films are less catalytically active because they contain fewer catalytically active Cu_2O surface sites. The aged Cu-coated PDMS stamps also lose their activity over repeated stampings (see supporting information), implying that the surface Cu_2O film is somehow disturbed or depleted during the first stamping event.

The ability to produce spatial surface patterns is a key advantage of μCP methods. It is possible that the active catalyst from the *StampCat* scheme is either the solid surface of the stamp itself, or potentially Cu(I) ions that leave the stamp and diffuse through an adsorbed water layer at the stamp or wafer surface. Thus, we used the *StampCat* method to react the azide-presenting glass surface with a micro-patterned stamp containing the fluorescent alkyne **7**. We reasoned that, for long stamping periods, the finer features of the stamp would be washed out of the stamped pattern, if the catalyst originated from diffusing Cu(I) ions. Otherwise, the stamped pattern would reflect the fine structure of the stamp itself. The stamped patterns were measured using confocal fluorescence microscopy, and compared (Fig. 4.6) alongside atomic force microscopy (AFM) images of the surface of the Cu-coated PDMS stamp.

AFM of the Cu-coated PDMS stamp reflected the molded pattern of 3 × 5 μm lines (Fig. 4.7a), but also revealed a finer structure of submicrometer width lines at a pitch of about 1 μm. This pattern likely arises from contraction of the PDMS stamp when it is removed from the vacuum of the metal deposition chamber. In any case, both the patterned and the fine-structure features are observed in the fluorescence micrographs of the glass surface. This observation, coupled with the above described results that PDMS-only stamps, or Pt-coated PDMS stamps do not promote the surface click reaction to any appreciable extent, confirms that the catalyst for *StampCat* is likely the (oxidized), Cu-coated surface of the PDMS stamp. The *StampCat* process can clearly be harnessed to generate impressively small feature sizes for μCP.

4.3 Conclusions

We have explored multiple pathways for achieving Cu-catalyzed, surface functionalization of azide-modified surface. One particular novel pathway is the *StampCat* method, in which a Cu-coated elastomeric stamp is utilized to catalyze

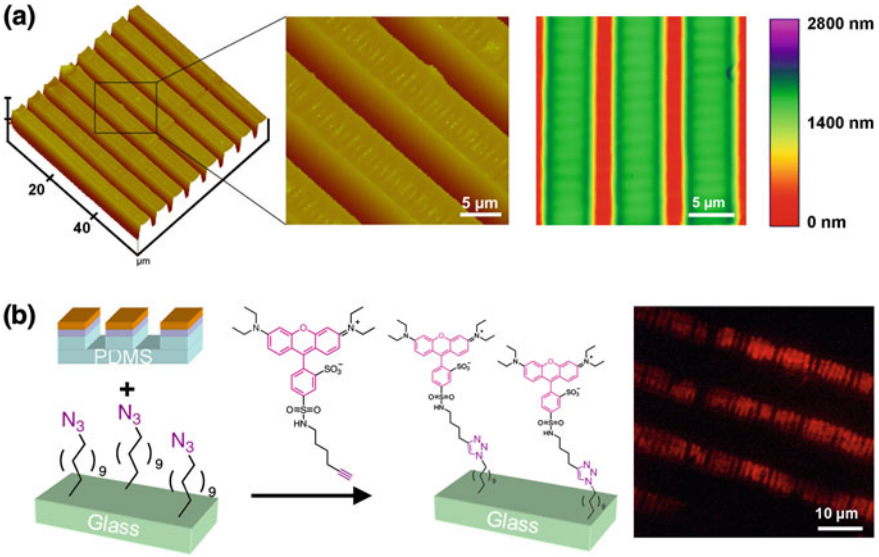

Fig. 4.7 **a** AFM Investigation of a CuPDMS patterned stamp topography where both the large line patterns—present before metal deposition—and metal ripples—as a consequence of metal deposition—are observed. **b** *StampCat* of the fluorescent alkyne **7** onto azide-functionalized glass slides using the patterned CuPDMS stamp produces lines of stripes that are observed by fluorescent microscopy. The ripple pattern transfer is consistent with heterogeneous catalysis

the reaction heterogeneously, and with spatial selectivity, between molecules with pendant alkynes and surface-bound azides. The *StampCat* method enables solvent-free, fast and efficient surface functionalization. The mechanism and kinetics of the *StampCat* pathway are contrasted with three other schemes that vary primarily in terms of the increasing range of reactant and reagent immobilization for the CuAAC reaction. A linear rate order is observed for metallic Cu film based catalysis while pseudo-first order behavior is exhibited by freely diffusing Cu(I) catalytic processes. The CuAAC reaction is becoming an increasingly important approach towards chemically functionalizing surfaces, and these studies should provide a firmer understanding of how that reaction can be harnessed for application-specific uses.

4.4 Experimental Section

4.4.1 Reagents and General Methods

All reagents were purchased from commercial suppliers (Aldrich or Fisher) and used without purification. Dry solvents were obtained from a commercial DriSolv® solvent delivery system (EMD Chemicals). Thin layer chromatography

(TLC) was performed on silica gel 60 F_{254} (E. Merck). Column chromatography was performed on silica gel 60F (Merck 9385, 0.040–0.063 mm). Nuclear magnetic resonance (NMR) spectra were recorded on a Varian Inova 500 (^{1}H: 500 MHz; ^{13}C: 126 MHz) or 400 (^{1}H: 400 MHz; ^{13}C: 101 MHz; ^{19}F: 377 MHz) spectrometer. Chemical shifts are reported as parts per million (ppm) downfield from the Me_4Si resonance as the internal standard for both ^{1}H and ^{13}C NMR spectroscopies and $CFCl_3$ as the internal standard for ^{19}F NMR spectroscopy. Electrospray ionization (ESI) mass spectra were measured on a Agilent LC/MS ion-trap mass spectrometer using 1:1 MeCN:H_2O as the mobile phase. Fast atom bombardment (FAB) mass spectra were measured on a Waters 70-SE-4F mass spectrometer. The synthesis of 1-azido-11-undecanethiol [29] (**2**) and lissamine rhodamine alkyne [20] (**7**) have been described elsewhere. Azide terminated SAMs on glass were prepared as published previously [20].

4.4.2 Synthesis of Ferrocene Alkyne (5)

5-Hexyn-1-ol (1.410 mL, 13.04 mmol) and then dicyclohexylcarbodiimide (0.987 g, 4.78 mmol) were added to a solution of ferrocene carboxylic acid (1.001 g, 4.347 mmol), 4-dimethylaminopyridine (0.027 g, 0.217 mmol), and 4-(dimethylamino)-pyridinium *p*-toluenesulfonate (0.068 g, 0.217 mmol) dissolved in dry methylene chloride (45 mL) and the solution was stirred at ambient temperature under N_2 for 12 h. The crude reaction mixture was filtered through a pad of Celite and the solvent evaporated. The crude product was subjected to chromatography (SiO_2, 1:9 EtOAc:Hexanes eluent) to give 0.990 g (73% yield) of **5** as an orange oil. **5**: ^{1}H NMR (500 MHz, $CDCl_3$, 25 °C, TMS): δ 4.80–4.78 (m, 2H, aryl -*H*), 4.38–4.36 (m, 2H, aryl -*H*), 4.23 (t, ^{3}J(H,H) = 6.4 Hz, 2H, CH_2O), 4.18 (s, 5H, aryl -*H*), 2.28 (dt, ^{3}J(H,H) = 6.9 Hz, ^{4}J(H,H) = 2.7 Hz, 2H, CH_2CCH), 1.98 (t, ^{4}J(H,H) = 2.7 Hz, 1H, CC*H*), 1.87–1.81 (m, 2H, CH_2), 1.72–1.65 (m, 2H, CH_2); ^{13}C NMR (126 MHz, $CDCl_3$, 25 °C, TMS): 171.7, 84.0, 71.4, 71.3, 70.2, 69.8, 68.9, 28.0, 25.2, 18.2; HRMS (ESI): Calcd for $C_{17}H_{18}FeO_2$ m/z = 310.0656, found m/z = 310.0649.

4.4.3 Synthesis of Pentafluorophenylether Alkyne (6)

1-Chloro-5-hexyne (1.57 mL, 16.3 mmol) was added to a slurry of pentafluorophenol (1.002 g, 5.433 mmol) and potassium carbonate (4.505 g, 32.60 mmol) in dry DMF (50 mL) and the mixture was stirred at 80 °C under N_2 for 16 h. The crude reaction mixture was partitioned between EtOAc (300 mL) and an aqueous solution of NH_4Cl (1 M, 200 mL). The organic layer was washed with aqueous NH_4Cl (1 M, 1 × 200 mL), H_2O (3 × 200 mL), and brine (1 × 200 mL) and

then dried ($MgSO_4$) and evaporated. The excess of 1-chloro-5-hexyne was distilled away (110 torr, 150 °C) and the residual crude product was subjected to chromatography (SiO_2, Hexanes eluent) to give 1.002 g (70% yield) of **6** as a colorless oil. **6**: ^{1}H NMR (500 MHz, $CDCl_3$, 25 °C, TMS): δ 4.18 (t, ^3J(H,H) = 6.3 Hz, 2H, CH_2O), 2.28 (dt, ^3J(H,H) = 7.0 Hz, ^4J(H,H) = 2.7 Hz, 2H, CH_2CCH), 1.96 (t, ^4J(H,H) = 2.7 Hz, 1H, CC*H*), 1.93–1.87 (m, 2H, CH_2), 1.77–1.70 (m, 2H, CH_2); ^{13}C NMR (126 MHz, $CDCl_3$, 25 °C, TMS): 83.9, 75.3, 68.9, 28.9, 24.6, 18.1; ^{19}F NMR (377 MHz, $CDCl_3$, 25 °C, $CFCl_3$): δ –157.4 (d, ^3J(F,F) = 21.2 Hz, 2F, *o*-OCH_2), −163.9 (dd, ^3J(F,F) = 21.4, ^3J(F,F) = 21.4, 2F, *m*-OCH_2), −164.1 (t, ^3J(F,F) = 21.4, 1F, *p*-OCH_2); HRMS (FAB): Calcd. for $[C_{12}H_9F_5O + H]^+$ *m/z* = 265.0652, found *m/z* = 265.0652.

4.4.4 Gold Substrates

Gold substrates were prepared by electron-beam evaporation of a titanium adhesion layer (15 nm, deposition rate of 1 Å/s) followed by gold (150 nm, deposition rate of 1 Å/s) onto 4 in. silicon(100) wafers in a cryogenically pumped deposition chamber. The silicon wafers were cleaned prior to metal deposition for 10 min in piranha solution (1:3 30 wt% aqueous H_2O_2:H_2SO_4; 130 °C), rinsed with deionized water, and dried under a filtered N_2 stream (*Warning*: Piranha solution reacts violently with organic material. It should be prepared freshly before use and disposed of properly. Do not store or combine with organic material.).

4.4.5 Formation of Mixed Azide Terminated SAMs on Gold

Method adapted from previously published source [30]. Freshly cleaved Au substrates were submerged in piranha solution (1:3 30 wt% aqueous H_2O_2:H_2SO_4; 130 °C) for 1 min, rinsed with H_2O, submerged in concentrated HCl for 1 min, rinsed with copious amounts of H_2O followed by ethanol, and finally dried under a steam of filtered N_2. The cleaned gold substrates were then submerged in a deposition solution containing octanethiol (**1**, 0.5 mM) and 1-azido-undecanethiol (**2**, 0.5 mM) dissolved in EtOH (total concentration of thiol = 1 mM) for 16 h. After deposition the SAM substrates were rinsed with EtOH and dried under a stream of N_2.

4.4.6 PDMS Stamp Preparation [14]

A 10:1 (wt:wt) mixture of PDMS-Sylgard Silicone Elastomer 184 and Sylgard Curing Agent 184 (Dow Corning Corp. Midland, MI) was poured over a

fluoro-coated flat or patterned silicon wafer (SAM of (tridecafluoro-1,1,2,2-tetrahydrooctyl)-1-trichlorosilane, Gelest) in a Petri dish. The mixture was left at ambient temperature for 1 h before being placed in an oven at 60 °C for 16 h, after which the cured PDMS was slowly pulled away from the surface and cut into ~ 1 cm^2 squares to be used as elastomeric stamps. Stamps to be used for *Reagent-Stamping* were then oxidized in UV/ozone plasma (50 W, 10 s) and stored in water until just before use.

4.4.7 Metal-Coated PDMS Stamp Preparation

PDMS Elastomer stamps were suspended in a cryogenically pumped deposition chamber and electron-beam evaporation of a titanium adhesion layer (10 nm, deposition rate of 1 Å/s) followed by Cu or Pt (50 nm, deposition rate of 1 Å/s) was carried out. They were then cut into ~ 1 cm^2 squares to be used as elastomeric stamps either immediately after preparation or allowed to oxidize for at least 24 h in air prior to use.

4.4.8 StampCat on Gold

Ink solution (molecular alkyne, 5 mM in MeCN) was applied to the metallic side of a metal-coated PDMS stamp and the solvent allowed to evaporate, after which it was blown dry in a stream of N_2. The inked stamp was then brought into contact with the azide-terminated SAM on gold substrate for 2 h with a load of 40 g to ensure conformal contact, after which the stamp was peeled away from the surface. The surface was then washed extensively with MeCN and EtOH, and then dried in a stream of N_2.

4.4.9 StampCat on Glass

Ink solution (**7**, 1 mM in EtOH) was applied to the metallic side of a Cu-coated PDMS stamp and the solvent allowed to evaporate, after which it was blown dry in a stream of N_2. The inked stamp was then brought into contact with the azide terminated SAM on glass substrate for 1 min with a load of 40 g to ensure conformal contact, after which the stamp was peeled away from the surface. The surface was then washed extensively with EtOH and dried in a stream of N_2.

4.4.10 Reagent-Stamping on Gold

To a freshly oxidized PDMS stamp was applied ink solution (molecular alkyne, 5 mM in MeCN) to cover the stamp surface followed by $Cu(OAc)_2$ (1 drop, 1 mM in EtOH) and ascorbic acid (1 drop, 1 mM in EtOH). The solutions were allowed to mix on the surface of the stamp for 1 min, blown dry in a stream of N_2, and brought into contact with the azide terminated SAM on gold substrate for 1 h with a load of 40 g to ensure conformal contact, after which the stamp was peeled away from the surface. The surface was then washed extensively with MeCN and EtOH, and then dried in a stream of N_2.

4.4.11 Solution-Surface Functionalization on Gold

Method adapted from reported [1] procedure. A solution of **5** (3 mM), $CuSO_4 \bullet 5H_2O$ (1 mM), and ascorbic acid (2 mM) in DMF was placed on top of azide-terminated SAM coated gold substrates. The reaction was performed protected from light under foil to prevent photo-oxidation of the thiol monolayers during the reaction. The substrates were rinsed extensively with EtOH, CH_2Cl_2, and H_2O after the desired reaction time had elapsed, and then dried in a stream of N_2.

4.4.12 Solution Reaction of 1-Azidohexane (3) and 1-Octyne (4)

1-Azidohexane (**3**) (0.0050 g, 0.039 mmol) and 1-octyne (**4**) (0.0756 g, 0.786 mmol) were dissolved in DMF-d_7 (0.786 mL) in an NMR tube. Stock solutions of $CuSO_4 \bullet 5H_2O$ in DMF-d_7 (54 μL, 0.072 M, 0.1 eq. per azide) and ascorbic acid in DMF-d_7 (54 μL, 0.144 M, 0.20 eq. per azide) were added and the mixture left at room temperature. The reaction progress was monitored by comparing the integrated area of the disappearing $-CH_2N_3$ resonance at 3.47 ppm with that of the appearing—CH_2N(triazole) at 4.52 ppm in the ^{1}H NMR spectrum of the reaction mixture.

4.4.13 Electrochemical Measurements

Electrochemical measurements were performed in a custom built, cylindrically bored Teflon cone cell (10 mm inner diameter) pressed against the surface of the sample. The bored opening was filled with aqueous perchloric acid (1 M) as an electrolyte solution. The counter electrode (platinum coiled wire) and reference electrode (a glass frit-isolated Ag(s)/AgCl(s)/3 M NaCl(aq)) were each suspended in the electrolyte solution. The exposed surface extending from under the Teflon

cone was contacted by a Tungsten probe (Micromanipulator Company, part number 7B) which served as the working electrode. The cell potential was controlled and the current generated was measured using a VMP Multi-Potentiostat (Princeton Applied Research, Oak Ridge, TN).

4.4.14 X-Ray Photoelectron Spectroscopy

X-ray photoelectron spectroscopy (XPS) measurements were performed in an ultra high vacuum chamber of an M-probe surface spectrometer that has been described elsewhere [49]. All measurements were taken on the center of the sample at room temperature. Monochromatic Al K_α X-rays (1,486.6 eV) were incident at 35° from the sample surface and a takeoff angle of 35° from the plane of the sample surface was employed to collected the emitted electrons. ESCA-2000 software was used to collect and analyze the data. Survey scans from 0 to 1,000 eV were conducted followed by detailed scans for C 1s (282–292 eV), N 1s (393–410 eV), F 1s (680–696), and Fe 2p (700–730 eV).

4.4.15 Contact Angle Measurements

The sessile contact angle (θ) water were obtained with an NRL C.A. Goniometer Model #100-00 (Rame-Hart, Inc.) at room temperature. Contact angles were measured from sessile drops by lowering a 1 μL drop of H_2O from a syringe needle onto a surface and recording the contact angle at both edges of the drop. This was repeated three times and averaged to obtain the θ for the surface.

Contact angle measurements obtained from surfaces functionalized with ferrocenyl-alkyne **5** using each of the three methods suggested similar high levels of functionalization (Table 4.1). Surfaces functionalized with the pentafluorophenolate **6** using the *StampCat* technique were the most hydrophobic (80°). The contact angles for these functionalized surfaces differed from those for both the hydrophilic gold surfaces (56°) and the azide-containing mixed monolayers (77°), each of which is in agreement with previously recorded [29, 50] values. The similar contact angle changes for surfaces functionalized with **5** through each of the methods add qualitative support to that all three procedures (Schemes 4.1b–d) proceed with comparable reaction efficiency.

4.4.16 Infrared Surface Characterization

Surfaces were characterized by external reflection Fourier transform infrared spectroscopy using a Vertex 70 FT-IR spectrometer (Bruker Optics Inc.) equipped with a liquid N_2 cooled MCT detector and an AutoSeagull accessory

Table 4.1 Contact angle goniometry for functionalized and unfunctionalized gold surfaces

Surface	Method	Compound	H_2O Contact Angle (°)
Au	–[a]	–[a]	56.5 ± 1.5
50% N_3 on Au	–[a]	–[a]	76.5 ± 1.7
50% N_3 on Au	*Solution-Surface*	**5**	72.6 ± 3.0
50% N_3 on Au	*Reagent-Stamping*	**5**	68.5 ± 5.3
50% N_3 on Au	*StampCat*	**5**	73.5 ± 3.4
50% N_3 on Au	*StampCat*	**6**	80.3 ± 3.6

[a] No functionalization reaction was performed

(Harrick Scientific Products, Inc.). The light incident the sample was 86° from the normal and only plane-polarized light was collected. A total of 128 scans were recorded with 4 cm^{-1} resolution. A background spectrum of a freshly cleaned gold substrate was subtracted from the spectra were baseline corrected using the concave rubberband method (25 iterations, excluding CO_2 bands, 256 baseline points).

4.4.17 Atomic Force Microscopy (AFM) Imaging

AFM Measurements were carried out with a digital multimode Nanoscope III (Digital Instruments, Santa Barbara, CA, USA) scanning force microscope in contact mode, with 512 × 512 data acquisitions, using V-shaped Si_3N_4 AFM tips (Nanoprobes, Digital Instruments) with a nominal spring constant of 0.32 N/m. The scan angle was set to 90°. Typical scan rates of 1–2 Hz were used to acquire the data. All imaging was conducted at room temperature in air.

4.4.18 Laser Scanning Confocal Microscopy/Optical Microscopy

Fluorescence images were obtained on Carl Zeiss LSM 510 with an excitation Ar-Kr laser beam of 563 nm wavelength and a 40× objective. The emitted fluorescence was collected on a PMT Hamamatsu R6357 spectrophotometer. All imaging was conducted at room temperature in air.

References

1. Nie ZH, Kmacheva E (2008) Nat Mater 7:277–290
2. Nakanishi J, Takarada T, Yamaguchi K, Maeda M (2008) Anal Sci 24:67–72
3. Guo LJ (2007) Adv Mater 19:495–513
4. Chen XD, Lenhert S, Hirtz M, Lu N, Fuchs H, Chi LF (2007) Acc Chem Res 40:393–401
5. Henzie J, Barton JE, Stender CL, Odom TW (2006) Acc Chem Res 39:249–257

6. Anderson AS, Dattelbaum AM, Montaño GA, Price DN, Schmidt JG, Marinez JS, Grace WK, Grace KM, Swanson BI (2008) Langmuir 24:2240–2247
7. Katz E, Willner I, Wang J (2004) Electroanalysis 16:19–44
8. Green JE, Choi JW, Boukai A, Bunimovich Y, Johnston-Halpering E, DeIonno E, Luo Y, Sheriff BA, Xu K, Shin YS, Tseng H-R, Stoddart JF, Heath JR (2007) Nature 445:414–417
9. Dichtel WR, Heath JR, Stoddart JF (2007) Philos Trans R Soc London Ser A 365:1607–1625
10. Hagfeldt A, Grätzel M (2000) Acc Chem Res 33:269–277
11. Rohde RD, Agnew HD, Yeo WS, Bailey RC, Heath JR (2006) J Am Chem Soc 128:9518–9525
12. Balachander N, Sukenik CN (1990) Langmuir 6:1621–1627
13. Yan L, Zhao XM, Whitesides GM (1998) J Am Chem Soc 120:6179–6180
14. Kumar A, Whitesides GM (1993) Appl Phys Lett 63:2002–2004
15. Lahiri J, Ostuni E, Whitesides GM (1999) Langmuir 15:2055–2060
16. Michel B, Bernard A, Bietsch A, Delamarche E, Geissler M, Juncker D, Kind H, Renault JP, Rothuizen H, Schmid H, Schmidt-Winkel P, Stutz R, Wolf H (2001) IBM J Res Dev 45:697–719
17. Jeon NL, Finnie K, Branshwa K, Nuzzo RG (1997) Langmuir 13:3382–3391
18. Yan L, Huck WTS, Zhao XM, Whitesides GM (1999) Lanmuir 15:1208–1214
19. Rozkiewicz DI, Ravoo BJ, Reinhoudt DN (2005) Langmuir 21:6337–6343
20. Rozkiewicz DI, Janczewski D, Verboom W, Ravoo BJ, Reinhoudt DN (2006) Angew Chem Int Ed 45:5292–5296
21. Sullivan TP, van Poll ML, Dankers PYW, Huck WTS (2004) Angew Chem Int Ed 43:4190–4193
22. Johnson MD, Ormie C, Hunt AW, Graff D, Sudijono J, Sander LM, Orr BG (1994) Phys Rev Lett 72:116–119
23. Jeong HC, Williams ED (1999) Surf Sci Rep 34:171–294
24. Bales GS, Chrzan DC (1994) Phys Rev B 50:6057–6067
25. Rostovtsev VV, Green LG, Fokin VV, Sharpless KB (2002) Angew Chem Int Ed 41:2596–2599
26. Tornoe CW, Christensen C, Meldal M (2002) J Org Chem 67:3057–3064
27. Lutz JF (2007) Angew Chem Int Ed 46:1018–1025
28. Nandivada H, Jiang X, Lahann J (2007) Adv Mater 19:2197–2208
29. Collman JP, Devaraj NK, Chidsey CED (2004) Langmuir 20:1051–1053
30. Collman JP, Devaraj NK, Eberspacher TPA, Chidsey CED (2006) Langmuir 22:2457–2464
31. Devaraj NK, Dinolfo PH, Chidsey CED, Collman JP (2006) J Am Chem Soc 128:1794–1795
32. Seo TS, Bai XP, Ruparel H, Li ZM, Turro NJ, Ju JY (2004) Proc Natl Acad Sci USA 101:5488–5493
33. Joralemon MJ, O'Reilly RK, Hawker CJ, Wooley KL (2005) J Am Chem Soc 127:16892–16899
34. Agard NJ, Prescher JA, Bertozzi CR (2004) J Am Chem Soc 126:15046–15047
35. Marrani AG, Dalchiele EA, Zanoni R, Decker F, Cattaruzza F, Bonifazi D, Pratoc M (2008) Electrochim Acta 53:3903–3909
36. Devadoss A, Chidsey CED (2007) J Am Chem Soc 129:5370–5371
37. Rozkiewicz DI, Gierlich J, Burley GA, Gutsmiedl K, Carell T, Ravoo BJ, Reinhoudt DN (2007) Chem Bio Chem 8:1997–2002
38. Duan XX, Sadhu VB, Perl A, Peter M, Reinhoudt DN, Huskens J (2008) Langmuir 24:3621–3627
39. Spruell JM, Dichtel WR, Heath JR, Stoddart JF (2008) Chem Eur J 14:1468–1477
40. Urbani CN, Bell CA, Whittaker MR, Monteiro MJ (2008) Macromolecules 24:3621–3627
41. Park IS, Kwon MS, Kim Y, Lee JS, Park J (2008) Org Lett 10:497–500
42. Lipshutz BH, Taft BR (2006) Angew Chem Int Ed 45:8235–8238
43. Lee LV, Mitchell ML, Huang SJ, Fokin VV, Sharpless KB, Wong CH (2003) J Am Chem Soc 125:9588–9589

44. Wang Q, Chan TR, Hilgraf R, Fokin VV, Sharpless KB, Finn MG (2003) J Am Chem Soc 125:3192–3193
45. Diaz DD, Punna S, Holzer P, McPherson AK, Sharpless KB, Fokin VV, Finn MG (2004) J Polym Sci Part A Polym Chem 42:4392–4403
46. Rodionov VO, Fokin VV, Finn MG (2005) Angew Chem Int Ed 44:2210–2215
47. Tsoncheva T, Vankova S, Mehandjiev D (2003) Fuel 82:755–763
48. Iijima J, Lim JW, Hong SH, Suzuki S, Mimura K, Isshiki A (2006) Appl Surf Sci 253:2825–2829
49. Haber JA, Lewis NS (2002) J Phys Chem B 106:3639–3656
50. Notsu H, Kubo W, Shitanda I, Tatsuma T (2005) J Mater Chem 15:1523–1527

Chapter 5
Heterogeneous Catalysis of a Copper-Coated Atomic Force Microscopy Tip for Direct-Write Click Chemistry

5.1 Introduction

Spatial control over the chemical composition of surfaces with sub-100 nm precision has been demonstrated [1–5] with a range of scanning-probe lithographic (SPL) methods. These methods combine high resolution direct-write surface patterning with real-time imaging of patterned surfaces, offering—under certain circumstances—significant advantages over conventional top-down lithographic approaches. Nevertheless, the majority of these techniques are essentially destructive to the surface—involving the initial oxidation [6, 7], reduction [8], or mechanical displacement [9–11] of surface materials—which are often incompatible with the direct deposition of delicate soft materials, such as biomolecules.

A particularly appealing SPL method is to use catalysis to attach soft materials directly to surfaces. Catalytic scanning probe tips capable of *destructive* chemical transformations have been used to hydrogenate surface-bound organic azides [8, 12], oxidize an organic dye photocatalytically [7] and hydrolyze silyl ethers [13]. More importantly, some catalytic scanning probe tips are capable of *constructive* chemical transformations allowing the direct attachment of molecular compounds to surfaces. For example, atomic force microscopy (AFM) tips coated with palladium films and nanoparticles have been employed to couple organosilanes to alkene terminated surfaces [12], and to drive Suzuki [14, 15] and Heck [15] coupling reactions at surfaces under basic conditions. In some cases, the conditions required for such reactions may not be suitable for the coupling of

This chapter is reproduced in part with permission from: Paxton WF, Spruell JM, Stoddart JF, *J. Am. Chem. Soc.* **2009**, *131*, 6692–6694.
AuthorContributions: W.F. Paxton and J.M. Spruell conceived the project. W.F. Paxton and J.F. Stoddart prepared the original manuscript. J.M. Stoddart synthesized all compounds used in these investigations. W.F. Paxton performed the AFM experiments and characterization. J.M. Spruell performed the microcontact printing control studies.

J. M. Spruell, *The Power of Click Chemistry for Molecular Machines and Surface Patterning*, Springer Theses, DOI: 10.1007/978-1-4419-9647-3_5,

delicate molecules. Thus, developing other versatile strategies for attaching a wide range of molecules covalently to surfaces would expand the toolkit of techniques afforded by scanning probe methods.

Copper-mediated azide–alkyne 1,3-dipolar cycloaddition [16–18] (CuAAC)—"click" chemistry—is another promising candidate for coupling molecules to surfaces catalytically. This remarkable reaction proceeds in high yield under mild conditions with a demonstrated tolerance for a wide range of functional groups not exhibited by traditional coupling reactions. The procedure for carrying out these reactions homogeneously in solution has been adapted to functionalize either azide-[19] or alkyne-terminated [20] surfaces, involving relatively stable Cu(I) compounds or the in situ chemical [19] or electrochemical [21] reduction of Cu(II) to the catalytically active Cu(I) species. This reaction has also been applied towards scanning probe lithography. In a beautiful demonstration of catalytic scanning probe lithography, Frommer and Malkoch et al. [22] attached organoazides covalently to alkyne-terminated surfaces using dip-pen nanolithography (DPN) [23–29]. In their approach, AFM tips inked with an acetonitrile solution containing (i) copper(I) iodide, (ii) diisopropylethylamine, and (iii) azide-functionalized dendrons were used to *write* features (i.e., the dendrons) onto acetylide surfaces. Using this method of localized "click" chemistry, it was possible to prepare features with linewidths as small as 300 nm. In addition to the homogenous Cu(I) catalysts, heterogeneous copper metal alone is known [30–34] to catalyze this reaction in solution, a procedure that can be generalized to surfaces as well. In fact, we have recently demonstrated [35] that heterogeneous copper metal stamps for microcontact printing, when inked with a terminal alkyne, are capable of catalyzing this reaction locally—i.e., where the stamp is in contact with a suitable substrate, and on the microscale. In this case, the reaction—believed to be catalyzed by Cu(I) that exists [36] in the native copper oxide layer—proceeds without the need for in situ reduction or additional reagents. We reasoned that, in an appropriate environment, a nanoscale heterogeneous copper surface would catalyze this reaction as well as a microscale one, even as it moves across a reactive surface.

5.2 Results and Discussion

In this chapter, we report an alternative approach (Fig. 5.1) towards direct-write coupling of molecules to surfaces via CuAAC using a movable heterogeneous copper surface—in the form of a thin layer of copper deposited onto an AFM tip. This method is capable of catalyzing CuAAC on a suitable surface locally without the need for auxiliary reagents. Using this approach, we observed a significantly higher degree of spatial control than previously reported [23–25]. In contrast to DPN experiments, this work was carried out under EtOH because of its ability to solvate a variety of alkynes and its chemical compatibility with the liquid cell. For each experiment, a silicon wafer with an azide-terminated SAM was fixed into a

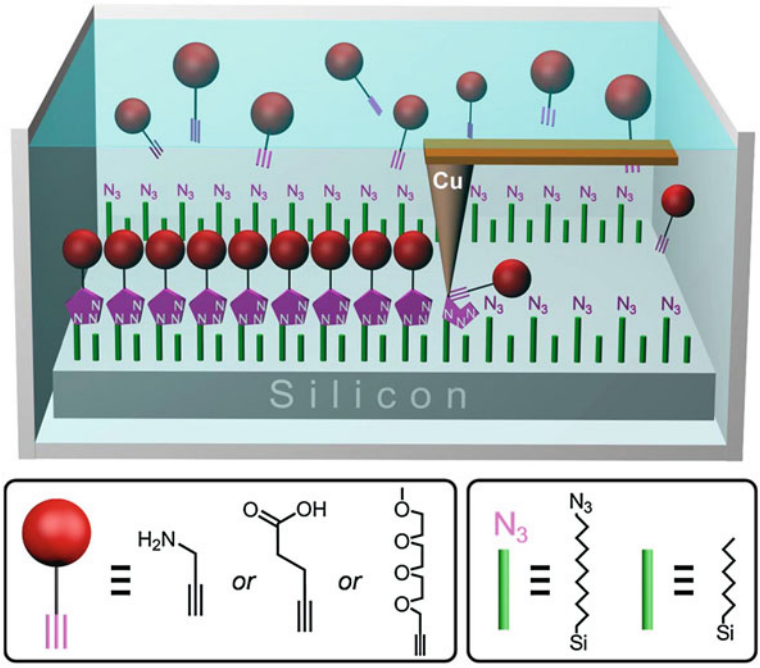

Fig. 5.1 A schematic representation of a scanning probe lithography approach to copper-catalyzed azide–alkyne cycloaddition (CuAAC) on surfaces, illustrating the three critical elements required for direct-write "click" chemistry: (1) a surface-anchored azide-terminated species that can be functionalized selectively with (2) a solvated terminal alkyne in the presence of (3) a copper catalyst. Terminal alkynes (including propargyl-amine, 4-pentynoic acid, and 2,5,8,11-tetraoxatetradec-13-yne) dissolved in EtOH are "clicked" to a reactive surface—a mixed monolayer of 11-azido-undecyltrichlorosilane and octyltrichlorosilane (1:1) on a silicon wafer—as the copper-coated AFM tip is moved across the surface with spatial resolution comparable to the tip dimensions

polystyrene Petri dish which was then filled with a 50 mM ethanolic solution of a compound bearing a terminal alkyne.

Catalytically-active tips were produced by thermal evaporation of a 4 nm adhesion layer of titanium, followed by a 10 nm layer of copper onto commercially available silicon nitride AFM tips (DNP-S from Veeco Instruments, Woodbury, NY). These copper-coated tips were then aged in air for at least 24 h to facilitate the formation of the catalytically-active oxide layer. Azide-terminated silicon wafers were prepared using an adaptation of a previously described [37] procedure. Briefly, mixed monolayers of 11-bromo-undecyltrichlorosilane and octyl-trichlorosilane (1:1) were formed on piranha-cleaned silicon wafer pieces. The terminal bromide was then displaced from the SAM-coated silicon by soaking wafers in a 0.1 M solution of NaN_3 in DMF.

Because the reaction proceeds at some finite rate and requires good contact between the reacting surface and the catalyst, we presumed that—as with other

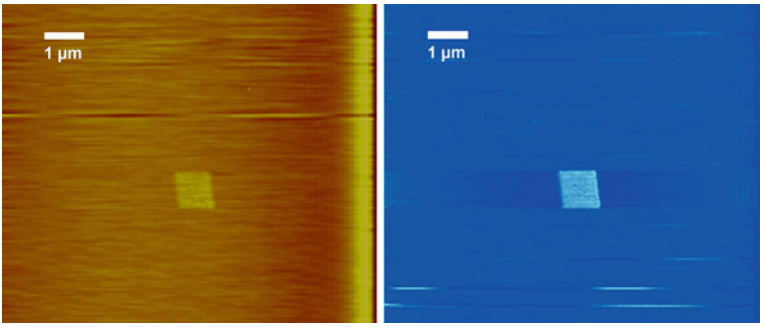

Fig. 5.2 Contact mode AFM images in an ethanolic solution of 4-pentynoic acid (50 mM) using a copper-coated AFM tip. Topography (*left*) and tip-substrate friction (*right*) of a 9 × 10 μm region at low force (30 nN) and high speed (40 μm/s) after *writing* a 1 × 1 μm square (*center*) at high force (200 nN) and low speed (1 μm/s)

AFM-based direct-write methods—it would be possible to switch between *read* and *write* modes by changing the applied force and the scanning speed of the copper AFM tip. Figure 5.2 shows the topography and friction contact mode AFM images (*reading*) of a 9 × 10 μm region acquired using a relatively low scan force (30 nN) and fast scan speed (40 μm/s) after scanning (*writing*) a 1 × 1 μm area at a higher force (300 nN) and slower scan speed (2 μm/s) in a 50 mM ethanolic solution of 4-pentynoic acid. The written feature is evident in both the topography and friction images, indicating the deposition of a material (increase in topography) that exhibits higher friction compared with the surrounding areas. These changes in topography and friction are consistent with "clicked" monolayers of 4-pentynoic acid on azide surfaces formed by microcontact printing. Writing of alkynes onto azide surfaces was also possible with propargylamine and 2,5,8,11-tetraoxatetradec-13-yne (see Experimental Section). Control experiments attempting to reproduce this same effect with an unmodified silicon–nitride AFM tip on the same surface in 50 mM 4-pentynoic acid failed, as did experiments using a copper-modified tip on an azide surface in EtOH that did not contain a terminal alkyne (see Supporting Information). In each of these cases, no pattern was evident in either the topography or the friction image at scanning forces below 400 nN. Above 400 nN, deformation of the SAM was evident, resulting in topographical depressions (rather than raised features) and regions of lower (rather than higher) friction, presumably as a result of mechanical deformation of the SAMs at high scanning forces. These control experiments indicate that copper metal and a molecule bearing a terminal alkyne group are both required to produce features.

We explored the effect (Table 5.1) of *writing* at different scan forces and at different scan speeds. In each case, the written surfaces were *read* using a scan force of 53 nN and a scan speed of 40 μm/s. Scanning at a force in excess of 200 nN was required in order to cause any changes in surface topography. Thereafter, the degree of surface modification scales to some extent with increased forces up to at least 350 nN. Despite the lack of topographical changes at forces

Table 5.1 Effect of varying *writing* scan speed and contact force on observed height and friction of 0.25 μm^2 4-pentynoic acid features written via direct-write click chemistry[a]

Speed (m/s)	Force (nN)	Height (nm)	Max. Friction (arb. units)
2	350	1.1	12
2	300	1.4	12
2	260	1.3	13
2	200	0.4	15
2	200	0	15
2	31	0	7
2	53	0	10
4	53	0	9
8	53	0	11
16	53	0	5
32	53	0	5
64	53	0	2

[a] Imaging (*reading*) in all cases was performed over a 25 μm^2 area using scan force and speed of 53 nN and 40 μm/s, respectively

below 200 nN, we observed changes in the friction image even at forces as low as 31 nN with these tips. This relatively low force is on the order of that used previously [15] in surface Suzuki and Heck couplings.

We also adjusted the scan speed and found that these changes in tip-surface friction were still evident—but to a lesser degree—at *writing* speeds as high as 64 μm/s! This surprising observation indicates that, although *reading* at scan speeds up to 64 μm/s cannot completely prevent reaction, the scan speed can be adjusted to decrease the extent of the surface functionalization. More importantly, the ability to pattern surfaces with this method using these significantly higher scan speeds amounts to an important advantage over typical DPN methods [38] and should facilitate higher throughput SPL patterning of nanoscale features.

In addition to *writing* relatively simple patterns, we have successfully produced more elaborate features as well. The outline of the letter "N"—written by a copper AFM tip on an azide-terminated surface in a 50 mM ethanolic solution of 4-pentynoic acid and shown in Fig. 5.3—demonstrates the spatial control possible with this method. The enlarged region (Fig. 5.3, *right*) shows minimum linewidths on the order of 50 nm, in contrast with the 300 nm linewidths reported previously [22]. These linewidths are comparable with the nominal unmodified AFM tip diameter (20 nm), and could presumably be reduced by using sharper AFM tips.

5.3 Conclusions

In summary, we have demonstrated an alternative approach towards the constructive patterning of surfaces using azide–alkyne cycloadditions in which the coupling reaction is catalyzed by a copper-coated AFM tip. This method builds

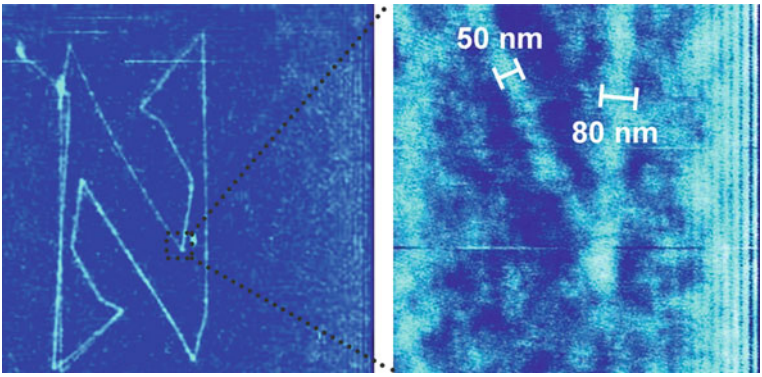

Fig. 5.3 Friction image (*left*) of a 4 μm tall "N" catalytically *written* in 4-pentynoic acid onto an azide-terminated surface using a copper-coated AFM tip, and a 0.8 × 0.8 μm close-up (*right*) of features indicating resolution of copper-catalyzed direct-write "click" chemistry

upon previous work [35] by using spatially controlled heterogeneous (rather than homogeneous) catalysis to attach molecules covalently to an appropriate surface under relatively mild conditions, without the need for additional reagents, and with dramatically improved spatial resolution. All that is required is (1) an azide surface (2) a solution of a terminal alkyne and (3) a copper-coated AFM tip. The CuAAC reaction can be carried out under liquid which becomes essentially an infinite reservoir of molecular "ink." Surprisingly, substantial patterning of alkynes onto azide surfaces is possible at *writing* speeds as high as 64 μm/s, a marked improvement over those required for patterning with conventional DPN. Because our method uses the same platform as many AFM-based methods, it is amenable to other advantageous modifications, such as massive parallelization [39]. These advantages open the door for the direct covalent attachment of a potentially limitless library of molecules that bear terminal alkyne functionality—including biomolecules—under relatively mild conditions, with sub-100 nm spatial resolution.

5.4 Experimental Section

5.4.1 Microcontact Printing of Alkyne Molecules onto Azide-Terminated Silicon Wafer Pieces

Our procedure for preparing surfaces containing microcontact printed features for comparison to features written via direct-write click chemistry (adapted from a published procedure [35]) was as follows: Polydimethylsiloxane (PDMS) stamps were prepared from a 10:1 mixture of PDMS-Sylgard Elastomer 184 and Sylgard Curing Agent 184 (Dow Corning Corp. Midland, MI), poured over a fluoro-coated patterned silicon wafer—SAM of (trideca-fluoro-1,1,2,2-tetrahydroocty)-1-

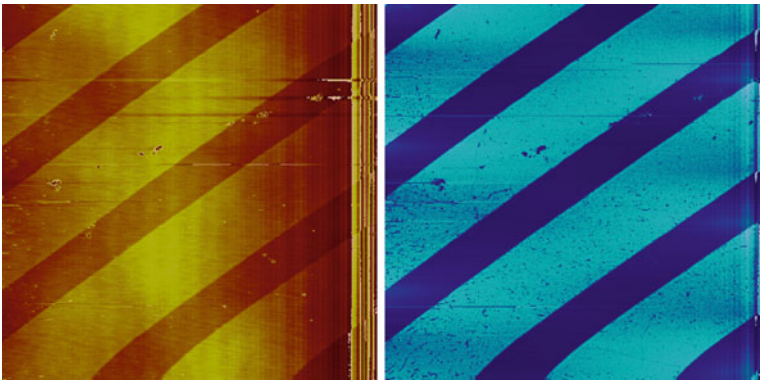

Fig. 5.4 50 × 50 Micron region contact mode atomic force microscopy topography (*left*) and friction (*right*) images in EtOH of 4-pentynoic acid monolayers stamped onto azide-terminated silicon wafers. Topography image indicates a height of 1.0(2) nm. Friction image indicates the carboxylic acid terminated regions exhibit higher friction than the unreacted (azide-terminated) regions

trichlorosilane (Gel-est, Inc., Morrisville, PA)—in a Petri dish. The mixture was allowed to stand at room temperature for 1 h before being placed into an oven at 60°C for 16 h. The cured PDMS was then peeled away from the patterned silicon wafer and cut into ~ 1 cm^2 pieces and used as stamps. These stamps were oxidized in UV/ozone plasma (200 W, 10 s) and stored in deionized H_2O until ready for use. Oxidized PDMS stamps were removed from H_2O and dried under a stream of N_2, and were then immediately inked with 1 drop of 1 mM $CuSO_4 \bullet 5H_2O$ in EtOH, 1 drop of 2 mM ascorbic acid in EtOH, and 4 drops of 5 mM terminal alkyne in EtOH. This mixture was allowed to combine on the stamp for 30 s before being removed from the stamp under a stream of N_2. The stamp was placed immediately onto an azide-terminated silicon wafer piece for at least 1 h. The stamp was then removed from the silicon wafer piece which was rinsed liberally in EtOH, followed by deionized H_2O, and then dried under a stream of N_2 and stored in a fluoroware container, protected from heat and light. Figures 5.4–5.6 show AFM images (topography and friction) of typical features prepared by microcontact printing the three compounds used in this chapter: 4-pentynoic acid, propargylamine, and 2,5,8,11-tetraoxatetradec-13-yne (TEG-alkyne). Analysis of microcontact printed films by contact mode AFM indicated that the carboxylic acid terminated regions were approximately 1 nm taller than unreacted azide-terminated regions.

5.4.2 *Direct-Write Click Chemistry of Propargyl-Amine and TEG-Alkyne*

Writing of alkynes onto azide surfaces was also possible with propargylamine and TEG-alkyne (Figs. 5.4 and 5.5) under the same conditions used to write 4-pentynoic acid.

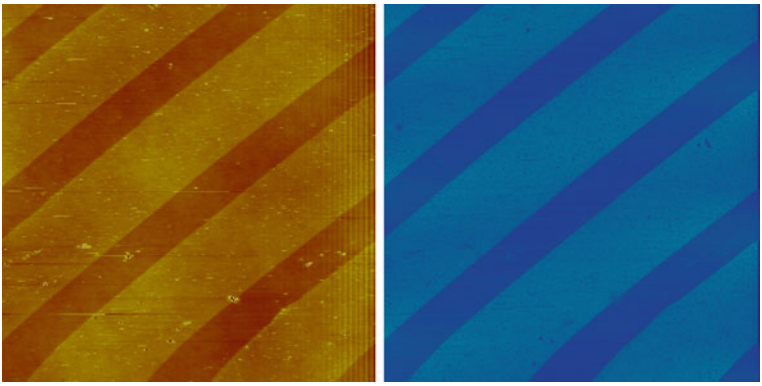

Fig. 5.5 50 × 50 Micron region contact mode atomic force microscopy topography (*left*) and friction (*right*) images in EtOH of 2,5,8,11-tetraoxatetradec-13-yne (TEG-alkyne) monolayers stamped onto azide-terminated silicon wafers. Topography image indicates a height of 1.0(1) nm. Friction image indicates the TEG-alkyne-terminated regions exhibit higher friction than the unreacted (azide-terminated) regions

5.4.3 Control Experiments

Attempts to reproduce direct-write click chemistry using SiN AFM tips on azide-terminated surfaces in 50 mM 4-pentynoic acid in EtOH failed. A constant scan rate of 2 μm/s for *writing* at forces <400 nN failed to produce any raised features of higher friction. *Writing* with a force ∼400 nN appeared to perturb the monolayer, possibly because of monolayer destruction [40]. Control experiments involving a copper AFM tip and 50 mM of ethanolic alkyne (4-pentynoic acid) on an azide-terminated surface produced similar results, confirming that both alkyne and a copper AFM tip are required to pattern an azide surface using this method. The contact mode topography and friction images shown in Fig. 5.6—taken after attempting to write TEG-alkyne onto an azide surfaces using an *unmodified* SiN AFM tip—are representative of the results of these control experiments.

5.4.4 Materials

All reagents were obtained from commercial sources and were used as received. For AFM experiments we used 100% EtOH (Chromasolv, Sigma–Aldrich) and silicon–nitride AFM tips (DNP-S; Veeco Instruments, Woodbury, NY) with nominal tip radii of 10 nm and force constants ranging from 0.5 to 1 N/m. 2,5,8,11-Tetraoxatetradec-13-yne was prepared using a previously described procedure [41].

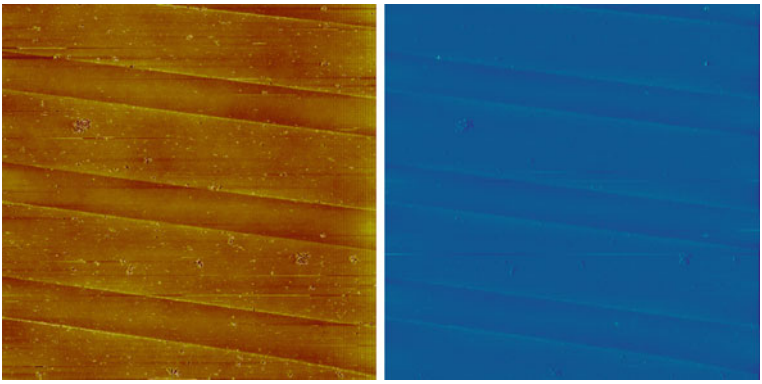

Fig. 5.6 50 × 50 Micron region contact mode atomic force microscopy topography (*left*) and friction (*right*) images in EtOH of propargylamine monolayers stamped onto azide-terminated silicon wafers

5.4.5 AFM

All AFM work was performed on a Bioscope II (Veeco Instruments, Woodbury, NY) at the NUANCE Center at Northwestern University. All AFM imaging was done in contact mode. All images were subject to standard image processing protocols, including image flattening.

References

1. Nyffenegger RM, Penner RM (1997) Chem Rev 97:1195–1230
2. Kramer S, Fuierer RR, Gorman CB (2003) Chem Rev 103:4367–4418
3. Wouters D, Schubert US (2004) Angew Chem Int Ed 43:2480–2495
4. Tang Z, Shi SQ, Zhao LM (2004) J Nanosci Nanotechnol 4:948–963
5. Garcia R, Martinez RV, Martinez J (2006) Chem Soc Rev 35:29–38
6. Maoz R, Cohen SR, Sagiv J (1999) Adv Mater 11:55–61
7. Zorbas V, Kanungo M, Bains SA, Mao YB, Hemraj-Benny T, Misewich JA, Wong SS (2005) Chem Commun 4598–4600
8. Müller WT, Klein DL, Lee T, Clarke J, mcEuen PL, Schultz PG (1995) Science 268:272–273
9. Wendel M, Kuhn S, Lorenz H, Kotthaus JP, Holland M (1994) Appl Phys Lett 65:1775–1777
10. Garnaes J, Bjornholm T, Zasadzinski JAN (1994) J Vac Sci 12:1839–1842
11. Liu GY, Xu S, Qian YL (2000) Acc Chem Res 33:457–466
12. Blackledge C, Engebretson DA, McDonald JD (2000) Langmuir 16:8317–8323
13. Péter M, Li XM, Huskens J, Reinhoudt DN (2004) J Am Chem Soc 126:11684–11690
14. Davis JJ, Coleman KS, Busuttil KL, Bagshaw CB (2005) J Am Chem Soc 127:13082–13083
15. Davis JJ, Bagshaw CB, Busittil KL, Hanyu Y, Coleman KS (2006) J Am Chem Soc 128:14135–14141
16. Rostovtsev VV, Green LG, Fokin VV, Sharpless KB (2002) Angew Chem Int Ed 41:2596–2599
17. Tornoe CW, Christensen C, Meldal M (2002) J Org Chem 67:3057–3064

18. Huisgen R (1989) Pure Appl Chem 61:613–628
19. Collman JP, Devaraj NK, Chidsey CED (2004) Langmuir 20:1051–1053
20. Ciampi S, Bocking T, Kilian KA, James M, Harper JP, Gooding JJ (2007) Langmuir 23:9320–9329
21. Devaraj NK, Dinolfo PH, Chidsey CED, Collman JP (2006) J Am Chem Soc 128:1794–1795
22. Long DA, Unal K, Prat RC, Malkoch M, Frommer J (2007) Adv Mater 19:4471–4473
23. Piner RD, Zhu J, Xu F, Hong SH, Mirkin CA (1999) Science 283:661–663
24. Ginger DS, Zhang H, Mirkin CA (2004) Angew Chem Int Ed 43:30–45
25. Salaita K, Wang YH, Mirkin CA (2007) Nat Nanotechnol 2:145–155
26. Jung H, Kulkarni R, Collier CP (2003) J Am Chem Soc 125:12096–12097
27. Auletta T, Dordi B, Mulder A, Sartori A, Onclin S, Bruinink CM, Peter M, Nijhuis CA, Beijleveld H, Schonherr H, Vancso GJ, Casnati A, Ungaro R, Ravoo BJ, Huskens J, Reinhoudt DN (2004) Angew Chem Int Ed 43:369–373
28. Salazar RB, Shovsky A, Schonherr H, Vancso GJ (2006) Small 2:1274–1282
29. Braunschweig AB, Senesi AJ, Mirkin CA (2009) J Am Chem Soc 131:922–923
30. Spruell JM, Dichtel WR, Heath JR, Stoddart JF (2008) Chem Eur J 14:1468–1477
31. Urbani CN, Bell CA, Whittaker MR, Monteiro MJ (2008) Macromolecules 24:3621–3627
32. Park IS, Kwon MS, Kim Y, Lee JS, Park J (2008) Org Lett 10:497–500
33. Lipshutz BH, Taft BR (2006) Angew Chem Int Ed 45:8235–8238
34. Himo F, Lovell T, Hilgraf R, Rostovtsev VV, Noodleman L, Sharpless KB, Fokin VV (2005) J Am Chem Soc 127:210–216
35. Spruell JM, Sheriff BA, Rozkiewicz DI, Dichtel WR, Rohde RD, Reinhoudt DN, Stoddart JF, Heath JR (2008) Angew Chem Int Ed 47:9927–9932
36. Iijima J, Lim JW, Hong SH, Suzuki S, Mimura K, Isshiki A (2006) Appl Surf Sci 253:2825–2829
37. Fryxell GE, Rieke PC, Wood LL, Engelhard mH, Williford RE, Graff GL, Campbell AA, Wiacek RJ, Lee L, Halverson A (1996) Langmuir 12:5064–5075
38. Weeks BL, Noy A, Miller AE, De Yoreo JJ (2002) Phys Rev Lett 88, 255505-1–255505-4
39. Salaita K, Wang YH, Fragala J, Vega RA, Liu C, Mirkin CA (2006) Angew Chem Int Ed 45:7220–7223
40. Onclin S, Ravoo BJ, Reinhoudt DN (2005) Angew Chem Int Ed 44:6282–6304
41. Eder E, Preishuber-Pflugl P, Stelzer F (2000) J Mol Catal A Chem 160:63–69

Chapter 6
A Push-Button Molecular Switch

6.1 Introduction

The chemistry of catenanes [1–6] has experienced a resurgence in recent years, driven in part by improved template-directed protocols [7–14] enabling their synthesis as well as technical applications made possible by virtue of their unique molecular topologies. By calling upon molecular recognition and self-assembly [1, 2, 15, 16], mechanically interlocked molecules (MIMs) are efficiently brought into being, allowing the use of these chemical compounds as the basis for constructing artificial molecular machines [17, 18] and fabricating molecular electronic devices [19–24]. The introduction of bi- and multistable MIM platforms [21, 23, 25–32] enables these applications, particularly if the basis for switching involves electrochemical processes.

Our long-standing interest in the synthesis and applications of charged MIMs—specifically those that incorporate as one ring component the π-electron poor tetracationic cyclobis(paraquat-*p*-phenylene) ($CBPQT^{4+}$) cyclophane [33–35]—have allowed the production of a variety of electrochemically switchable molecules [19–24, 36]. Traditionally, $CBPQT^{4+}$-based catenanes and rotaxanes have been synthesized by "clipping" a partially formed $CBPQT^{4+}$ ring around a π-donor unit [37, 38], such as 1,5-dioxynaphthalene (DNP) or tetrathiafulvalene (TTF), as part of a preformed macrocycle or a dumbbell compound. While this

This Chapter is reproduced in part with permission from: Spruell JM, Paxton WF, Olsen J-C, Benítez D, Tkatchouk E, Stern CL, Trabolsi A, Friedman DC, Goddard WA, Stoddart JF, *J. Am. Chem. Soc.* **2009**, *131*, 11571–11580.
Author Contributions: J.M. Spruell and W.F. Paxton conceived the project. J.M. Spruell and J.F. Stoddart prepared the original manuscript. J.M. Spruell synthesized all compounds investigated in this work. D. Benítez, E. Tkatchouk and W.A. Goddard performed DFT calculations. J.M. Spruell and D.C. Friedman performed NMR spectroscopic investigations together. J.M. Spruell and A. Trabolsi performed electrochemical analysis together.

J. M. Spruell, *The Power of Click Chemistry for Molecular Machines and Surface Patterning*, Springer Theses, DOI: 10.1007/978-1-4419-9647-3_6,

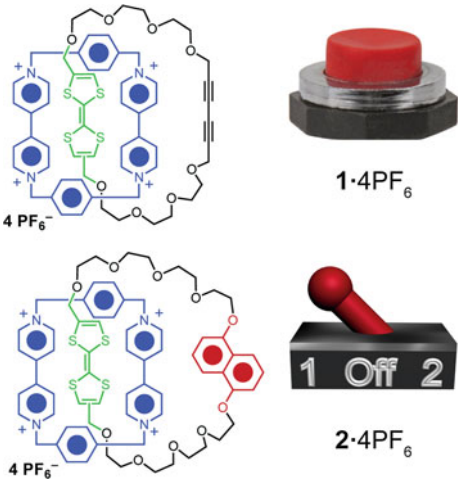

Fig. 6.1 The structural formulas of the switchable single-station [2]catenane **1**·4PF_6 (*top*) which is represented as a two-state push-button molecular switch incorporating a single tetrathiafulvalene (TTF) station and the traditional switchable bistable [2]catenane **2**·4PF_6 (*bottom*) which is represented as a three-state switch incorporating both TTF and 1,5-dioxynaphthalene (DNP) stations

approach has successfully yielded a number of useful compounds in the past, recent investigations [5, 39–43] have shown that the synthesis of MIMs from pseudorotaxanes containing fully-formed $CBPQT^{4+}$ rings can be more effective and efficient. Central to the implementation of this "threading-followed-by-clipping" approach to catenane synthesis has been the introduction of ultra-mild reactions to effect the final macrocyclization, yielding the catenane in the presence of the $CBPQT^{4+}$ ring which is sensitive to bases, nucleophiles, and reducing agents. Of particular success has been the use of Cu^{1+}- and Cu^{2+}-mediated processes in alkyne-based couplings, such as the CuAAC reaction [44] and Eglinton coupling [45].

Here, we report (i) the facile template-directed synthesis and characterization of a switchable [2]catenane through a Cu^{2+}-mediated Eglinton coupling [45] on a [2]pseudorotaxane formed between $CBPQT^{4+}$ and a bispropargyl-functionalized tetrathiafulvalene (TTF) unit, which, as a consequence of containing a single switchable binding station, (ii) exists in one translational form in its ground state that (iii) may be mechanically switched wholly to another translation form in the excited oxidized state and (iv) exhibits very fast and reversible switching between both forms. Moreover, this compound expands our understanding of the mechanics of switching within a catenated framework whereby the elimination of the weaker secondary binding station, traditionally found in bistable MIMs, results in the reduction of complexity to that of a simple push-button operated switch (Fig. 6.1). In the parlance [46] of electrical engineering, this "single-pole single-throw" (SPST) molecular switch operates between two distinct working positions through electrochemical stimuli. The simplicity of this single-station switch stands in contrast to previously constructed [19–24, 36], more complicated bi- and multi-station molecular switches analogous to "single-pole double-throw" (SPDT) switches. These observations and perspectives are supported by a solid-state structure, extensive NMR spectroscopic studies, cyclic voltammetry, and spectroelectrochemistry, as well as computational investigations.

6.2 Results and Discussion

Variants of the Eglinton coupling have been used extensively to prepare [2]- and [3]catenanes of mixed compositions through both covalent-[3, 47, 48] and template-directed [49–55] protocols. We recently applied [40, 41] this useful homocoupling to prepare hetero[2]catenanes bearing 1,5-dioxynaphthalene as a single station for a $CBPQT^{4+}$ ring in very high yields under mild reaction conditions. Inspired by the novelty of these simple and high yielding approaches to catenane synthesis, we speculated that the same protocols could be employed to create a hetero[2]catenane bearing the electrochemically switchable TTF unit and thus arrive at an electrochemically switchable catenane.

TTF and its derivatives have been used extensively [19–24, 36] to create electrochemically switchable MIMs. The π-electron rich neutral state may be oxidized reversibly either once or twice to π-electron poor radical cation and dication states, respectively. Toggling between the neutral and oxidized states, when the TTF is incorporated into a catenane or rotaxane containing $CBPQT^{4+}$, allows the ejection of the oxidized TTF^{2+} dication from inside the ring through electrostatic repulsion. Usually a secondary weaker binding station, such as DNP, is incorporated into the molecule to replace the oxidized TTF^{2+} dication within the $CBPQT^{4+}$ cavity upon its ejection, providing a discrete and long-lived switched co-conformation, even following the reinstatement of the neutral TTF unit. Breaking with tradition, we have synthesized a single-station [2]catenane, compound **1**·$4PF_6$, which operates through an electrostatic repulsive mechanism and may be switched (*vide infra*) between two discrete translational states, eliminating the need for a secondary station.

The π-electron rich TTF derivative **4** was prepared (Scheme 6.1) by propargylation of the two arms of TTF diol **3** [27]. Upon mixing **4** and CBPQT·$4PF_6$ in a 2:1 molar ratio, respectively, in MeCN, the solution became intensely emerald green as a consequence of the formation of pseudorotaxane [**4** ⊂ CBPQT]·$4PF_6$. The addition of $Cu(OAc)_2 \cdot H_2O$ (1.25 equiv per terminal alkyne) at 23 °C for 2 d effected the desired Eglinton coupling, affording the [2]catenane **1**·$4PF_6$ as a green solid in 64% yield. This exceptionally high yield in the formation of a complex mechanically interlocked topology through macrocyclization reflects the synthetic advantages of the "threading-followed-by-clipping" approach invoked in its design. A very similar [2]catenane **2**·$4PF_6$ (Fig. 6.1) containing both TTF and DNP recognition units was prepared [36] previously by the traditional "clipping" of a partially-formed $CBPQT^{4+}$ ring around one of these recognition sites in the TTF/DNP macrocycle. Although this protocol produced a very useful bistable molecular switch, the final "clipping" step afforded that catenane in only 23% yield. The current method results in a switchable catenane in much higher yield than that previously reported, while the structural replacement of a DNP binding moiety with a butadiyne unit in compound **1**·$4PF_6$ affects the switching behavior of the molecule profoundly.

Slow diffusion of $i Pr_2O$ into a MeCN solution of **1**·$4PF_6$ at room temperature produced light green, needle-like single crystals suitable for X-ray structural

Scheme 6.1 Preparation of the push-button catenane **1**·4PF$_6$

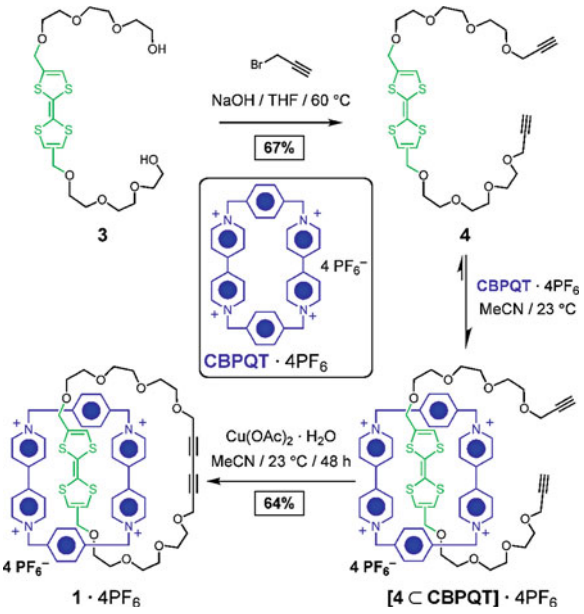

analysis. Two different views of the solid-state structure of $\mathbf{1}^{4+}$ represented as ellipsoids as well as with space-filling representation are shown in Fig. 6.2. Of the two constitutional isomers possible for disubstituted TTF, only the *trans* isomer was observed in the solid state, similar to that for the previously reported [36] TTF/DNP catenane. The CBPQT^{4+} ring encircles the TTF unit in an association that is stabilized through a combination of π–π stacking interactions and [C–H···O] interactions from α-bipyridinium hydrogen atoms to, in one instance, the second and third oxygen away from the TTF in the oligoether chain, and in another, to the second oxygen atom away from the TTF in the oligoether chain. In common with the previously [41] reported DNP-based Eglinton coupled catenanes, the butadiyne fragment is aligned approximately parallel to the external bipyridium face of the CBPQT^{4+} cyclophane with an interplanar distance of 3.34 Å, a short contact that could be a consequence of a stabilizing π–π interaction. Catenane $\mathbf{1}^{4+}$ packs in the presence of its four disordered PF_6^- counterions with the butadiyne units as the closest point of contact, and so does not form an extended donor–acceptor stacking arrangement.

^{1}H NMR Spectroscopy provides (Fig. 6.3a) additional confirmation of the interlocked nature of **1**·4PF$_6$, as well as the relative position of the CBPQT^{4+} ring encircling the TTF unit exclusively in the ground state. Most notable is the presence of two sets of signals arising from both the α- and β-bipyridium protons of the CBPQT^{4+} ring at room temperature. When encircling the TTF moiety, the local symmetry of the TTF unit is commuted to the CBPQT^{4+} ring such that the pairs of α- and β-bipyridium protons are rendered heterotopic and are thus each separated into a set of anisochronous signals [56]. Interestingly, although the *cis*

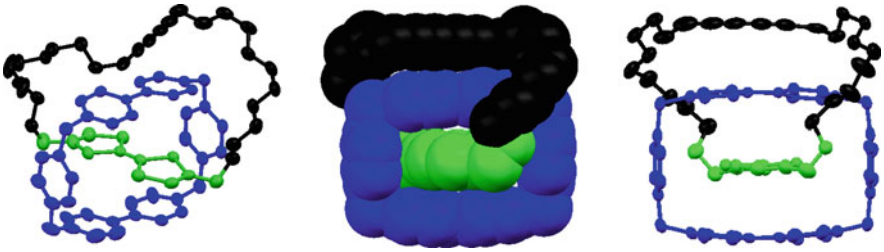

Fig. 6.2 Solid-state structure of $\mathbf{1}^{4+}$ displayed from two angles. In addition to the disordered PF_6^- counterions, hydrogen atoms and solvent molecules are omitted for clarity. The $CBPQT^{4+}$ ring is shown in blue, the TTF unit in green, and the butadiyne and glycol units shown in black

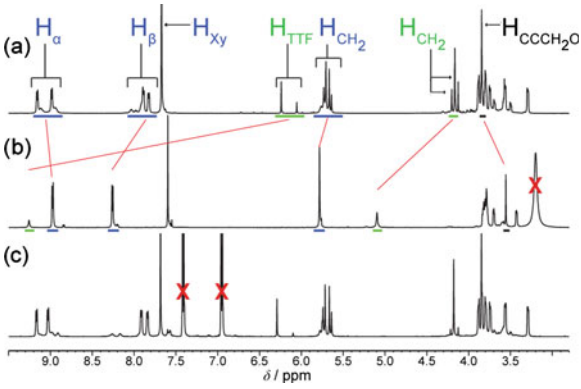

Fig. 6.3 ^{1}H NMR spectra (500 MHz, CD_3CN, 293 K) of (**a**) compound $\mathbf{1}\cdot 4PF_6$, (**b**) fully oxidized compound $\mathbf{1}^{6+}$ after the addition of 2 equiv of chemical oxidant tris(4-bromophenyl) ammoniumyl hexachloroantimonate, and (**c**) re-reduced compound $\mathbf{1}^{4+}$ after the addition of Zn dust. Resonances arising from the chemical oxidant and residual solvent are marked with an "X"

and *trans* isomers of the disubstituted TTF unit can rapidly interconvert [57] in the presence of a trace of acid, both configurational isomers appear to be present after isolation and purification of $\mathbf{1}\cdot 4PF_6$. Two clear singlets are observed in a 3:1 ratio for the protons on the TTF rings located at δ 6.24 and 6.06 ppm. This ratio is repeated throughout the entire spectrum, not only for the signals of protons neighboring the TTF and the ethylene glycol units of its own macrocycle, but also for those of the $CBPQT^{4+}$ ring. Upon chemical oxidization and re-reduction of the TTF (vide infra) effecting the translational switching of the catenane, this ratio is increased to 13:1 in favor of the major—most likely *trans*—configurational isomer. Interestingly, this same distribution is arrived at without switching the molecule after the catenane has remained in solution for at least five months, indicating that this distribution represents the equilibrated state of configurational isomers within this catenane. We believe that this equilibrium is reached so much more slowly relative to other TTF-based mechanically interlocked systems because, in this unique catenane, TTF constitutes the only station for the $CBPQT^{4+}$ ring. In bistable systems, such as $\mathbf{2}\cdot 4PF_6$, the $CBPQT^{4+}$ ring is commonly distributed between both stations within the ensemble to some degree—depending on the relative binding affinities of the constituents—such that for a single molecule, although the $CBPQT^{4+}$ ring sits around the TTF unit on average more often than

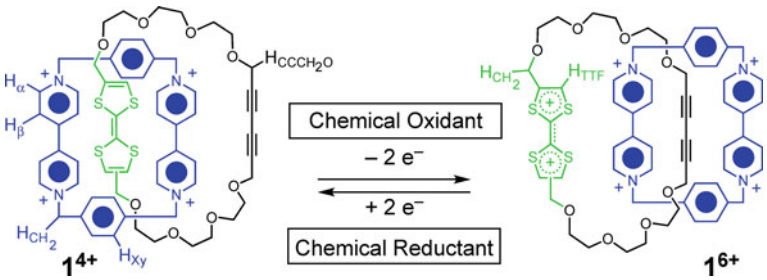

Scheme 6.2 Oxidative switching mechanism of the push-button molecular switch

the competing station, it spends a considerable amount of time well away from the TTF unit. We propose that it is only during this "off-time" that the TTF is able to interconvert between its *cis* and *trans* configurational isomers. Since there is minimal "off-time" allowed in the case of the monostation catenane $\mathbf{1}^{4+}$, the $CBPQT^{4+}$ ring kinetically traps the TTF, increasing the time necessary for it to equilibrate into its steady state distribution of configurational isomers.

Chemical oxidation of $\mathbf{1}^{4+}$ to $\mathbf{1}^{6+}$ was performed (Scheme 6.2) in CD_3CN using 2 equiv of tris(4-bromophenyl) ammoniumyl hexachloroantimonate as the chemical oxidant [58, 59] and the effects of chemical switching were probed using ^1H NMR spectroscopy. After oxidation, substantial changes were observed (Fig. 6.3b) in the ^1H NMR spectrum. Most notable were the large downfield shifts for the resonances corresponding to the TTF^{2+} protons as well as for the methylene protons neighboring the TTF^{2+} dication. Such large shifts are a consequence of building up positive charge which is shared across the TTF unit. Structurally, this oxidation forces the tetracationic $CBPQT^{4+}$ ring away from the TTF^{2+} unit, moving it to the position furthest away. The relationship of the TTF and the butadiyne units within their macrocycle dictates that the butadiyne represents the position furthest away from the TTF^{2+} unit and the most stable site for the $CBPQT^{4+}$ ring. The resonances for the methylene units neighboring the butadiyne are shifted upfield by 0.29 ppm, reflecting the movement of the $CBPQT^{4+}$ ring from being around the TTF to that of encircling the butadiyne moiety. Although ^{13}C NMR chemical shifts are inherently insensitive to ring current shielding effects, thus limiting the probe nuclei available across the all carbon butadiyne chain to ascertain the position of the $CBPQT^{4+}$ ring in the oxidized state $\mathbf{1}^{6+}$, a series of 1D NOE experiments clearly show (Fig. 6.4) through-space correlations between the resonances for the methylene protons neighboring the butadiyne units and the $CBPQT^{4+}$ ring resonances in $\mathbf{1}^{6+}$, interactions that are not present in $\mathbf{1}^{4+}$. Additionally, 1D NOE correlations, which were present between the signals for the methylene protons neighboring the TTF unit and the $CBPQT^{4+}$ ring in $\mathbf{1}^{4+}$ disappear after it is switched to $\mathbf{1}^{6+}$. The resonances of the $CBPQT^{4+}$ ring shift upon oxidation to $\mathbf{1}^{6+}$ and are also substantially simplified. Both the α- and β-bipyridium protons, as well as the methylene protons within the cyclophane become homotopic, since they are no longer under the influence of the local symmetry of the TTF unit. This increased symmetry indicates that, not

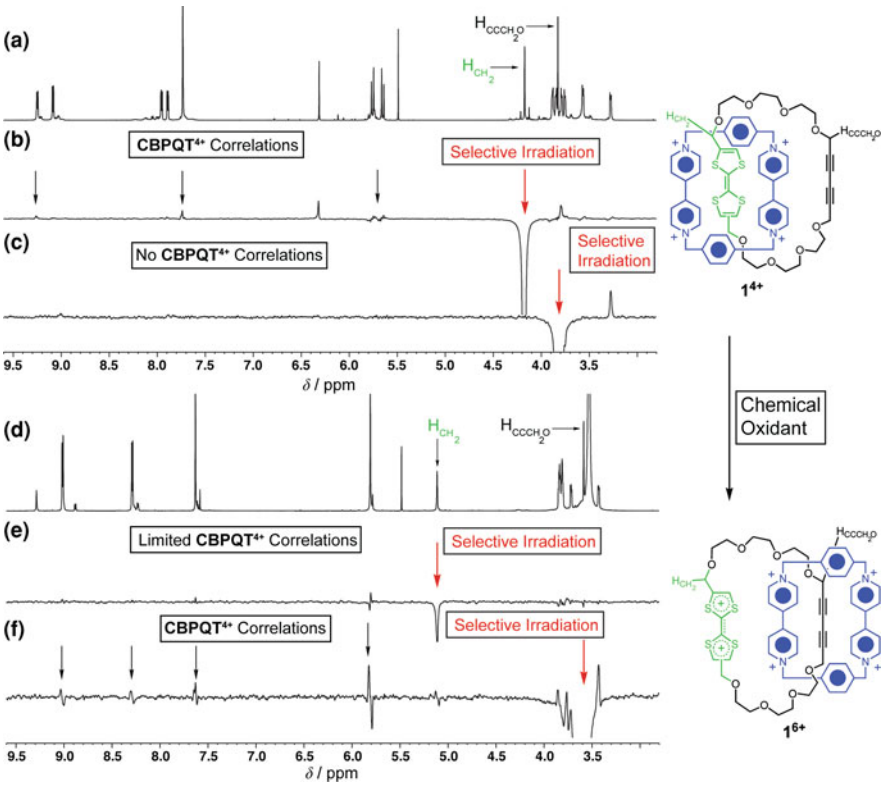

Fig. 6.4 1D NOE through-space correlations of $\mathbf{1}^{4+}$ and $\mathbf{1}^{6+}$ (600 MHz, 273 K); (**a**) ^{1}H NMR spectrum of compound $\mathbf{1}^{4+}$ which displays (**b**) through-space correlations with the CBPQT^{4+} ring after selectively pulsing the nearest the TTF moiety, but displays (**c**) no through-space correlations with the CBPQT^{4+} ring after selectively pulsing the nearest the diyne, (**d**) ^{1}H NMR spectrum of compound $\mathbf{1}^{6+}$ which displays (**e**) no through-space correlations with the CBPQT^{4+} ring after selectively pulsing the nearest the TTF moiety, but displays (**f**) through-space correlations with the CBPQT^{4+} ring after selectively pulsing the nearest the butadiyne. Additional 1D NOE correlations not highlighted with a small black arrow are attributable to close interactions with the nearest neighbor protons of the selectively irradiated resonances rather than through-space correlations between protons within each macrocycle of the catenane

surprisingly, rotation of the cyclophane around the butadiyne unit is fast on the NMR time-scale. Finally, the addition of 2 equiv of Zn dust to re-reduce $\mathbf{1}^{6+}$ restores the original spectrum (Fig. 6.3c) of $\mathbf{1}^{4+}$, indicating that the TTF unit once again resides within the CBPQT^{4+} cavity.

The switching of $\mathbf{1}\cdot 4PF_6$ was also induced electrochemically. Cyclic voltammetry (CV) experiments (Fig. 6.5) using NBu_4PF_6 as the electrolyte in MeCN were performed probing the TTF-centered oxidation processes, specifically the reversible TTF → TTF$^{\bullet+}$, and TTF$^{\bullet+}$ → TTF^{2+} one electron events. These processes are well resolved in the CV (Fig. 6.5b) of compound **3**, displaying two distinct oxidation peaks centered at +404 and +793 mV (vs. Ag/AgCl),

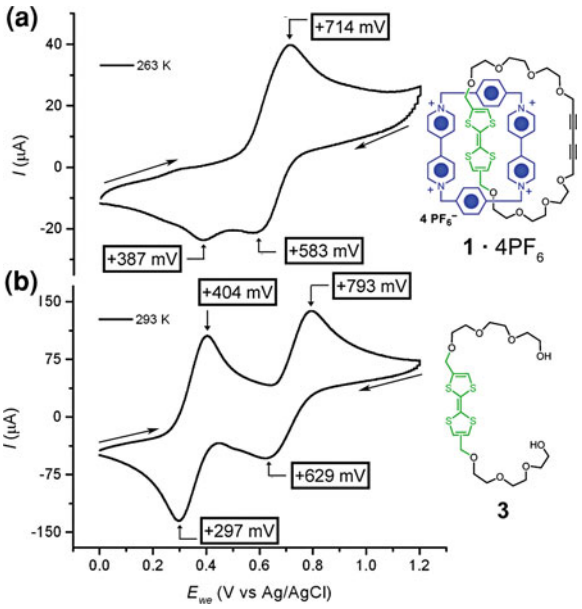

Fig. 6.5 Oxidative cyclic voltammagrams (second scans, MeCN, 100 mM NBu_4PF_6, 1,000 mV/s) of (**a**) **1**·4PF_6 displaying the overlapping first and second oxidation of the TTF moiety to TTF^{2+} (performed at 263 K) and (**b**) **3** displaying two distinct one-electron oxidation processes to the $TTF^{\bullet+}$ and TTF^{2+} (performed at 298 K). The first and successive oxidative scans of **1**·4PF_6 were identical. For clarity, only the second oxidative scan is shown

respectively. It has been well established [19–24] that, when encircled by the electron poor $CBPQT^{4+}$ ring, the first oxidation of TTF is shifted substantially to more positive potentials, usually to near the potential of the second oxidation for the unencircled TTF. Thus, the first oxidative scan of **1**·4PF_6 shows (Fig. 6.5a) only one broad peak centered at 714 mV (vs. Ag/AgCl), corresponding to both distinct one-electron processes producing TTF^{2+} via the $TTF^{\bullet+}$ from the neutral TTF unit. The translation of the $CBPQT^{4+}$ ring is intimately involved with this oxidation process and is known [19–24] to occur upon the first oxidation to the $TTF^{\bullet+}$ species, leaving the second oxidation to TTF^{2+} to occur at the same potential it would in the absence of the macrocycle. In the case of traditional multistation TTF-based catenanes or rotaxanes, such as [2]catenane **2**·4PF_6, the first oxidative scan contains signals attributed to the first TTF oxidation at lower potentials for unencircled co-conformations. Indeed, integration of the first oxidation at lower potentials relative to the other oxidative signals forms the basis of determining the ratio of metastable to ground state co-conformations within the molecular ensemble of these traditional multistation switches. No such first oxidative signal was present for **1**·4PF_6, indicating that there is only one available station for the $CBPQT^{4+}$ ring—it encircles the TTF fully in the ground state and no other translational states exist.

Performing two successive oxidative scans at various scan rates and temperatures allows the elucidation of the kinetics associated with the return of the $CBPQT^{4+}$ ring from the oxidized co-conformation to the ground state co-conformation (GSCC) [20, 26, 27, 32]. In traditional bistable MIMs, oxidation of the TTF in the first CV scan forces the $CBPQT^{4+}$ ring onto the weaker binding station. Because the $CBPQT^{4+}$ ring

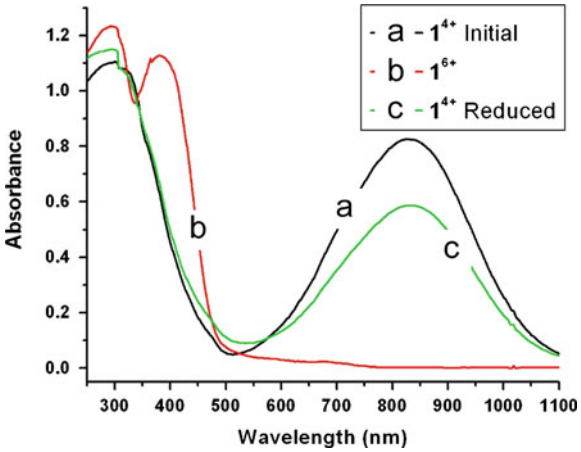

Fig. 6.6 Spectroelectrochemistry (MeCN, 100 mM NBu_4PF_6) of (**a**) $\mathbf{1}^{4+}$ displaying a strong absorption centered at 830 nm corresponding to the TTF–$CBPQT^{4+}$ CT absorption, (**b**) $\mathbf{1}^{6+}$ after sustained current flow at +1.2 V where the CT absorption is replaced by a strong absorption arising from TTF^{2+} at 400 nm, and (**c**) $\mathbf{1}^{4+}$ reformed after sustained reduction at 0 V displaying the regained CT absorption

has an affinity for the weaker binding station—sitting in a local energy minimum—reduction of the TTF unit to it neutral state does not immediately result in the return to the GSCC. This co-conformation, in which the $CBPQT^{4+}$ ring encircles the weaker binding station while the TTF is in its neutral state, is known [20] as the metastable state co-conformation (MSCC). The conversion of the MSCC to the GSCC is an activated process such that it occurs over a finite time period (between the first and second successive CV scans) and is dependent [19–24] upon both the temperature and the environment of the MIM. However, no matter how fast the scan rate or low the temperature used in the CV (1,000 mV/s and 263 K, shown in Fig. 6.5a), the presence of a MSCC, as would be indicated by the first oxidation of unencircled TTF in the second scan, was not observed for $\mathbf{1}{\cdot}4PF_6$. Standing in contrast to the case of single-station catenane $\mathbf{1}{\cdot}4PF_6$, a thorough electrochemical investigation of the MSCC to GSCC relaxation process for two-station catenane $\mathbf{2}{\cdot}4PF_6$ was possible [32] across a range of scan rates and temperatures between 263–283 K because the weaker binding DNP station slows the return of the $CBPQT^{4+}$ ring to the TTF. The lack of any observable MSCC for $\mathbf{1}{\cdot}4PF_6$ suggests that the butadiyne moiety has very little, if any, affinity for the tetracationic macrocycle, and serves as no more than a passive bystander following a convenient catenation protocol for the formation of this [2]catenane, i.e., there is no experimental evidence for an electronic interaction, be it stabilizing or destabilizing, between the butadiyne moiety and the $CBPQT^{4+}$ ring.

Substantial changes occur in the UV–Vis spectrum of $\mathbf{1}{\cdot}4PF_6$ upon electrochemical oxidation. The UV–Vis spectrum of $\mathbf{1}^{4+}$ in MeCN (with 100 mM NBu_4PF_6) contains (Fig. 6.6a) a broad charge transfer (CT) absorption centered at 830 nm, characteristic of a $CBPQT^{4+}$-encircled TTF. The catenane was fully

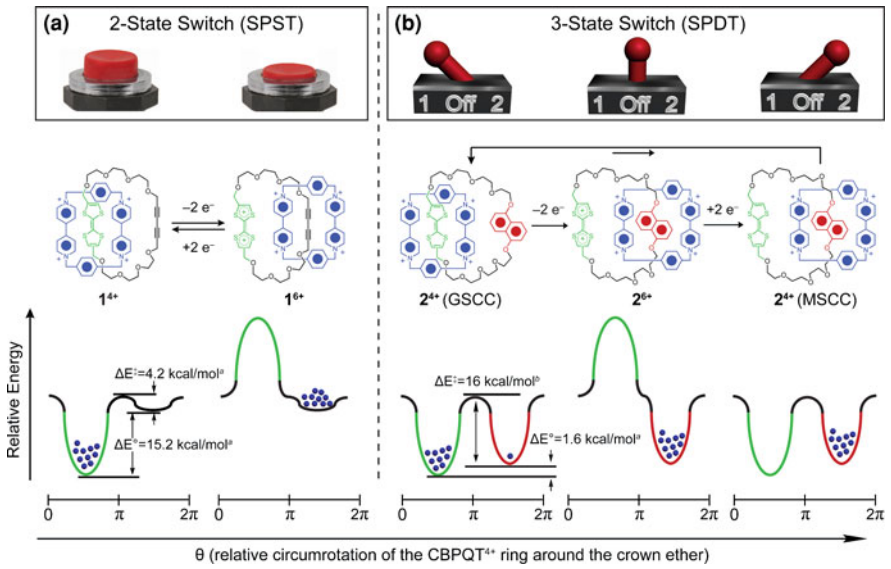

Fig. 6.7 Relative energy surface diagrams depicting the energetic consequences of electrochemically switching the TTF to TTF^{2+} in (**a**) the single-station catenane **1**·$4PF_6$ and in (**b**) the traditional double station catenane **2**·PF_6 where the $CBPQT^{4+}$ ring position is represented by blue spheres. Compound $\mathbf{1}^{4+}$ exists as a single translational state which may be switched wholly to its inverse state as described by a 180° circumrotation of the $CBPQT^{4+}$ ring around the TTF containing crown ether to arrive at $\mathbf{1}^{6+}$, where the $CBPQT^{4+}$ ring only sits in a local minimum as a consequence of its aversion to the TTF^{2+} dication. Conversely, $\mathbf{2}^{4+}$ exists as a mixture of the GSCC and MSCC in which the $CBPQT^{4+}$ ring encircles the TTF and the DNP units, respectively. Upon oxidation of the TTF unit, the $CBPQT^{4+}$ ring encircles only the DNP unit of $\mathbf{2}^{6+}$ and remains there for a finite length of time even after reduction of the TTF unit reforming $\mathbf{2}^{4+}$. [a]Values were calculated as described in the text; [b]Value was measured and originally reported [32]

switched to $\mathbf{1}^{6+}$ after passing a sustained current held at +1.2 V (vs. Ag/AgCl) for several hours in a custom built [60] spectroelectrochemical cell, as indicated by the complete loss of the CT band at 830 nm and the appearance of a band at 400 nm characteristic of the TTF^{2+} dication. Interestingly, the lack of any transition that can be attributed to an electronic interaction between the butadiyne moiety and the $CBPQT^{4+}$ ring in $\mathbf{1}^{6+}$ (Fig. 6.6b) supports the hypothesis that no affinity exists between these two components. The original spectrum of $\mathbf{1}^{4+}$ was restored (Fig. 6.6c), albeit somewhat attenuated, after re-reduction by holding the potential at 0 V (vs. Ag/AgCl) for several hours.

The experimental data illustrate a generalized view (Fig. 6.7) of the changes in the energy surface of **1**·$4PF_6$ upon electrochemical switching. In order to investigate the exact nature of this energy landscape, we turned to quantum mechanical modeling. Because only one translational state was observed for **1**·$4PF_6$ in the first scan using CV, the difference in energy between the co-conformation in which the $CBPQT^{4+}$ ring encircles the butadyine unit, as opposed to the TTF unit, could not

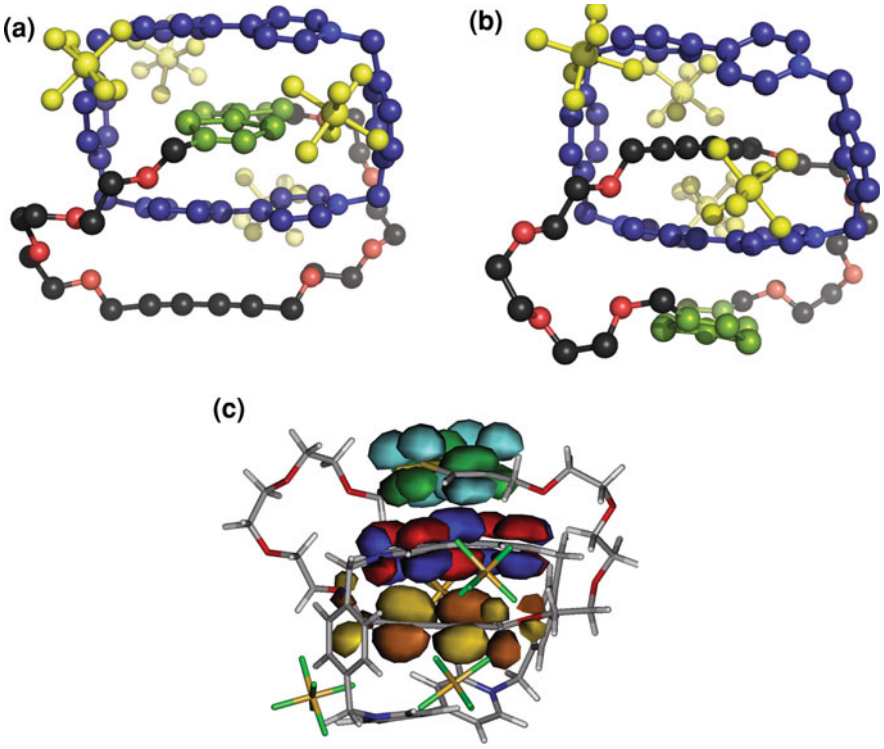

Fig. 6.8 Computed structures for $\mathbf{1}^{4+}$ in (**a**) the ground state co-conformation (GSCC) and (**b**) the metastable state co-conformation (MSCC). (**c**) The MSCC for 1^{4+} has the LUMO (depicted as the orbitals sandwiched in the structure) localized on the $CBPQT^{4+}$ ring with the HOMO (depicted as the top set of orbitals) localized on the TTF while the HOMO–1 (depicted as the lower set of orbitals) localized on the butadiyne unit

be directly measured. Equally challenging, the return rate of the $CBPQT^{4+}$ ring to the TTF unit after restoring the ground state of the oxidized catenane occurs far too quickly to measure, thus preventing the experimental calculation of the barrier to circumrotation of the $CBPQT^{4+}$ ring around the crown ether. In any event, quantum mechanical investigations provide the means to study these key processes in more detail on the extremely fast time-scales through which the molecular switch $\mathbf{1}\cdot 4PF_6$ operates.

In order to understand the energy profile and mechanism for the switching process of $\mathbf{1}^{4+}$, we turned to density functional theory (DFT) of the M06 flavor [61, 62], which we have established [63] to provide excellent accuracy for energetics of other rotaxane-based architectures. We performed geometry optimizations for the TTF-encircled (GSCC) and butadiyne-encircled (MSCC) translational isomers of $\mathbf{1}^{4+}$ at the M06/6-31G** level of theory, leading to predicted structures which are displayed in Fig. 6.8. We calculated a difference in binding energy of 15.2 kcal/mol between the GSCC and MSCC in MeCN as solvent. This predicted energy

difference between the GSCC and MSCC suggests a differential population of 10^{11}:1 (GSCC:MSCC) at 298 K.

Since we were most interested in learning about the energy profile for the switching process, we mapped the potential energy surface by performing a manually-steered scan for the rotation of the TTF-butadiyne macrocycle with respect to the electron deficient $CBPQT^{4+}$ ring. We used the less computationally expensive M06-L functional to generate structures along the path from the MSCC to the GSCC. After further optimization of the highest energy structures (using the M06 functional), we estimate that the process of resetting the MSCC to the GSCC has a barrier of $\sim$4.2 kcal/mol. These results agree with the inability to observe an MSCC under the experimental conditions [60] employed (263 K, 1,000 mV/s). Our estimated barrier of $\sim$4.2 kcal/mol for the resetting of the MSCC to GSCC corresponds to a 2×10^{-10} s ($\sim$200 ps) relaxation time at 298 K ($\sim$600 ps at 263 K). Although this small "barrier" to circumrotation may be partly due to weak binding between the butadiyne fragment and $CBPQT^{4+}$ ring—the HOMO–1 to LUMO interaction—it is most likely dominated by the alongside stabilizing interaction with the HOMO, which is located almost entirely on the neutral TTF unit. Figure 6.8c depicts the empty orbital on the $CBPQT^{4+}$ cyclophane—LUMO in red and blue—and the doubly occupied orbitals on the TTF—HOMO in green and turquoise—and on the butadiyne fragment—HOMO–1 in brown and orange. From these calculations, we estimate that the excitation energy for a possible CT transition between the $CBPQT^{4+}$ ring and the encircled butadiyne moiety for the oxidized translational state $\mathbf{1^{6+}}$. Using the experimental value for the $CBPQT^{4+}$-encircled TTF CT absorption band ($\lambda_{max} = 830$ nm, Fig. 6.6) and the calculated HOMO (−0.1957 Eh) and HOMO–1 (0.2477 Eh) energies, the LUMO is estimated to be −0.1415 Eh. Extending these energies to the oxidized catenane $\mathbf{1^{6+}}$, a CT transition between the HOMO (the HOMO–1 in $\mathbf{1^{4+}}$) localized on the butadiyne unit and the LUMO + 1 (the LUMO in $\mathbf{1^{4+}}$) would lead to an absorption centered around $\sim$425 nm—which would likely overlap and be eclipsed by the intense absorption of the TTF^{2+} dication.

Our experimental and computational results suggest strongly that the catenane $\mathbf{1}\cdot 4PF_6$ behaves as a very simple push-button molecular switch (Fig. 6.7a) in which the ground state contains two local minima but of vastly different energies, separated by 15.2 kcal/mol, such that the TTF-encircled translational state is nearly solely populated (roughly 1 out of every $\sim 10^{11}$ molecules exists in the other translational state). Oxidation of the TTF unit—pushing the button—inverts the local minimum, creating a local maximum, and thus effecting the complete circumrotation of the $CBPQT^{4+}$ ring around its companion macrocycle so that it rests securely in the local minimum on the butadiyne moiety as long as the TTF^{2+} retains its dicationic character. Inversion of the local maximum around the TTF^{2+} dication, by reduction to the neutral species—releasing the button—re-establishes the situation represented by the original energy diagram whereby the $CBPQT^{4+}$ ring quickly—during several hundred picoseconds—migrates over a very small "barrier", estimated to be

$\sim$4.2 kcal/mol, to occupy the deep well it enjoys by encircling the TTF unit. This very small $\Delta E^{\ddagger}$ value, although technically an activation barrier, hardly constitutes even what we might call a "speed bump" for the circumrotation such that the process occurs at the "diffusion" controlled rate of 5×10^9 s^{-1} at room temperature, allowing the mechanical switching from $\mathbf{1}^{6+}$ to $\mathbf{1}^{4+}$ to occur almost instantaneously.

This situation is quite different from that of the traditional, two-station [2]catenane $\mathbf{2}\cdot 4PF_6$ (Fig. 6.7b) in which a battle is waged between the TTF and the DNP units for occupancy by the $CBPQT^{4+}$ ring in the ground state, until an equilibrium is established such that, within the ensemble, the $CBPQT^{4+}$ ring occupy the TTF and DNP local energy minima in a 9:1 ratio based around the ΔG° of 1.6 kcal/mol [20]. In this case, oxidation of the TTF unit converts its position from a local minimum to a local maximum, such that the DNP unit becomes the sole local minimum and all of the $CBPQT^{4+}$ rings migrate to encircle it. Although re-reduction of the TTF^{2+} dication reestablishes the TTF unit as the global minimum, the $CBPQT^{4+}$ rings remain kinetically trapped within the DNP local energy well for some time until they transverse a relatively large barrier $\Delta G^{\ddagger}$ of 16 kcal/mol [32] in order to equilibrate once again to form the 9:1 ratio of co-conformers. While a complex interplay between local energy minima and transient excited states allows the switching within the two-station catenane $\mathbf{2}\cdot 4PF_6$, the situation is much less complicated in the case of the single-station catenane $\mathbf{1}\cdot 4PF_6$ where the simple push of a button toggles between energy surfaces each with a singly occupied minimum.

6.3 Conclusions

We have demonstrated the efficient synthesis, to all intents and purposes, of a single-station, yet switchable, hetero[2]catenane by means of the Eglinton coupling-based macrocyclization of a TTF thread around a $CBPQT^{4+}$ ring. The simplicity of the synthetic approach and molecular design belie the effectiveness of $\mathbf{1}\cdot 4PF_6$ as a perfect switch in which the ensemble is composed nearly completely of one co-conformation in both the ground and excited states. The push-button switching nature of $\mathbf{1}\cdot 4PF_6$ sheds light upon the operation of switchable mechanically interlocked molecules, tempting us to celebrate the simplicity of a single-station, yet switchable architecture, in the context of more complicated—and synthetically more challenging—molecular targets. The unique combination of two discrete translational forms, coupled with the ability to toggle completely between these two electrochemically controllable states, positions this push-button molecular switch as an ideal candidate for introduction into solid-state electronic device settings. It is towards these and other goals that we will continue to apply mechanically interlocked architectures afforded through the Eglinton coupling and other mild alkyne-based reactions.

6.4 Experimental Section

6.4.1 General Methods

All reagents were purchased from commercial suppliers (Aldrich or Fisher) and used without further purification. Cyclobis(paraquat-*p*-phenylene) hexafluorophosphate [33], 1-iodo-8-tetrahydropyranyloxy-3,6-dioxaoctane [64], and 4,4′(5′)-bis[methanol]tetrathia-fulvalene [65] were prepared according to literature procedures. Thin layer chromatography (TLC) was performed on silica gel 60 F_{254} (E. Merck). Column chromatography was performed on silica gel 60F (Merck 9385, 0.040–0.063 nm). Nuclear magnetic resonance (NMR) spectra were recorded at 25 °C (unless otherwise noted) on Bruker Avance 500 and 600 spectrometers, with working frequencies of 500 and 600 MHz for ^{1}H, and 125 and 150 MHz for ^{13}C nuclei, respectively. Chemical shifts are reported in ppm relative to the signals corresponding to the residual non-deuterated solvents [66]. All ^{13}C spectra were recorded with the simultaneous decoupling of proton nuclei. Transient ^{1}H-^{1}H NOE experiments were performed using a Double Pulsed Field Gradient Spin Echo NOE (DPFGSE-NOE) pulse sequence with a mixing time of 600 ms. Electrospray Ionization (ESI) mass spectra were obtained on a Agilent 6210 LC-TOF high resolution mass spectrometer. Cyclic voltammetry experiments were performed on a Princeton Applied Research 263 A Multipurpose instrument interfaced to a PC using a glassy carbon working electrode (0.018 cm^2, Cypress system). The electrode surface was polished routinely with 0.05 μm^2 alumina/water slurry on a felt surface immediately before use. The counter electrode was a Pt coil and the reference electrode was a AgCl coated Ag wire. The concentrations of the samples were 1 mM in 100 mM electrolyte solution (NBu_4PF_6 in MeCN). UV–Vis absorption spectra were recorded on a Varian Cary-300 spectrophotometer. The X-ray intensity data were measured on a Bruker APEX II CCD system equipped with a graphite monochromator and a CuKα ImuS microsource ($\lambda = 1.54178$ Å).

6.4.2 Computational Methods

Calculations were performed on all systems using density functional theory (DFT) with the M06-L, M06 functionals, as implemented in Jaguar 7.6. The M06 functional is a new hybrid meta-GGA exchange–correlation functional that leads to impressive accuracy for a very large validation set of systems, including van der Waals dimers, reactions, and transition metal complexes. Starting with a structure from the crystallographic data we optimized the geometry using the 6-31G** basis set with the M06 functional in the gas phase. Single point energies were calculated using the M06 functional and the 6-311 ++G** basis set. Solvent corrections were based on single point self-consistent Poisson-Boltzmann continuum solvation calculations for acetonitrile ($\varepsilon = 37.5$, $R_0 = 2.18$ Å) using the PBF module in Jaguar.

6.4.3 Preparation of *3*

4,4′(5′)-Bis[methanol]tetrathiafulvalene (1.500 g, 5.673 mmol) was added to a slurry of NaH (60% dispersion in oil, 1.743 g, 43.57 mmol) in dry THF (700 mL) and the mixture was heated under reflux in an N_2 atmosphere for 1 h. A solution of 1-iodo-8-tetrahydropyranyloxy-3,6-dioxaoctane (7.420 g, 21.56 mmol) in dry THF (75 mL) was added to the reaction mixture dropwise over 1 h. The reaction mixture was refluxed under an N_2 atmosphere for 24 h. After cooling the mixture to RT, MeOH was added, the solution was filtered through a plug of silica, and the solvents were removed *in vacuo*. The crude brown oil was partitioned between CH_2Cl_2 (300 mL) and 1 M NH_4Cl (300 mL), the organic phase washed with H_2O (1 × 100 mL) and brine (1 × 100 mL), dried ($MgSO_4$), and the solvent removed *in vacuo*. The residual brown oil was dissolved in a 1:1 mixture of CH_2Cl_2:MeOH (150 mL) and HCl (0.4 mL, 12 M) was added. The solution was stirred at RT for 1.5 h, after which 1 M NaOH (200 mL) was added. The mixture was extracted with CH_2Cl_2 (3 × 100 mL), dried ($MgSO_4$), the solvent removed *in vacuo*, and subjected to chromatography (SiO_2, 97:3 to 95:5 CH_2Cl_2:MeOH eluent) to provide a yellow oil (1.316 g, 44%). **3**: ^{1}H NMR (500 MHz, CD_2Cl_2): δ 6.27 (s, 2H, SC*H*), 4.26 (s, 4H, SCCH_2), 3.68–3.54 (m, 24H), 2.59–2.49 (m, 2H, O*H*); ^{13}C NMR (125 MHz, CD_2Cl_2): δ 135.04, 134.94, 116.87, 116.75, 110.82, 72.91, 72.89, 70.99, 70.80, 70.70, 69.78, 69.77, 68.50, 62.02; HRMS (ESI) Calcd for $C_{20}H_{32}O_8S_4$: 528.0980, Found: 529.1046 ($[M + H]^+$).

6.4.4 Preparation of *4*

A solution of propargyl bromide in PhMe (80% by weight, 0.930 mL, 10.4 mmol) was added to a mixture of **3** (920 mg, 1.74 mmol) and NaOH (696 mg, 17.4 mmol) in THF (20 mL). The mixture was heated at 60 °C under ambient atmosphere for 24 h. The mixture was partitioned between EtOAc (100 mL) and 1 M NH_4Cl (100 mL) and the aqueous phase was washed with EtOAc (2 × 75 mL). The combined organic phases were washed with 1 M NH_4Cl (75 mL) and brine (75 mL), dried ($MgSO_4$), the solvent removed *in vacuo*, and subjected to chromatography (SiO_2, 1:1 to 8:3 EtOAc : hexanes eluent) to provide a brown oil (704 mg, 67%). **4**: ^{1}H NMR (500 MHz, CD_2Cl_2): δ 6.26 (s, 2H, SC*H*), 4.27 (s, 4H, SCCH_2), 4.17 (d, ^4J (H,H) = 2.3 Hz, 4H, C ≡ CCH_2O), 3.66–3.58 (m, 24H), 2.49 (t, ^4J (H,H) = 2.3 Hz, 2H, C ≡ C*H*); ^{13}C NMR (125 MHz, CD_2Cl_2): δ 135.06, 135.00, 116.81, 116.71, 80.23, 74.65, 70.94, 70.90, 70.85, 70.70, 69.78, 69.60, 68.47, 58.63; HRMS (ESI) Calcd for $C_{26}H_{36}O_8S_4$: 604.1293, Found: 604.1310 (M^+), 622.1634 ($[M + H_2O]^+$), 627.1191 ($[M + Na]^+$).

6.4.5 Preparation of $1 \cdot 4PF_6$

$Cu(OAc)_2 \cdot H_2O$ (61.4 mg, 0.295 mmol) was added to a green solution of **4** (71.2 mg, 0.118 mmol) and $CBPQT \cdot 4PF_6$ (65.0 mg, 0.059 mmol) dissolved in MeCN (45 mL) and the solution was stirred for 48 h under ambient conditions. The solvent was removed *in vacuo* and the green residue was subjected to chromatography (SiO_2, Me_2CO to 1% NH_4PF_6 in Me_2CO eluent). The green band was collected, concentrated *in vacuo*, and treated with cold H_2O to precipitate a green solid (64.4 mg, 64%). $\mathbf{1} \cdot 4PF_6$: ^{1}H NMR (600 MHz, CD_3CN, 0 °C): δ 9.15 (d, ^3J (H,H) = 6.7 Hz, 4H, α-$CBPQT^{4+}$-H), 8.99 (d, ^3J (H,H) = 6.7 Hz, 4H, α-$CBPQT^{4+}$-H), 7.89–7.87 (m, 4H, β-$CBPQT^{4+}$-H), 7.83–7.81 (m, 4H, β-$CBPQT^{4+}$-H), 7.66 (s, 8H, *p*-Xylyl $CBPQT^{4+}$), 6.26 (s, 2H, SC*H*), 5.73–5.59 (m, 8H, CBPQT CH_2), 4.15 (s, 4H, $SCCH_2$), 3.87–3.86 (m, 4H), 3.84–3.82 (m, 4H), 3.81 (s, 4H, $C \equiv CCH_2O$), 3.78–3.76 (m, 4H), 3.75–3.73 (m, 4H), 3.57–3.54 (m, 4H), 3.28–3.26 (m, 4H); ^{13}C NMR (125 MHz, CD_3CN): δ 146.66, 145.69, 144.83, 136.94, 133.94, 131.73, 126.65, 126.23, 126.14, 120.30, 108.87, 76.93, 72.12, 71.56, 71.26, 71.21, 71.00, 70.76, 69.86, 68.83, 65.40, 59.15; HRMS (ESI) Calcd for $C_{62}H_{66}F_{24}N_4O_8P_4S_4$: 1,702.2309 ($M + 4PF_6$), 1,557.2669 ($[M + 3PF_6]^+$), 706.1514 ($[M + 2PF_6]^{2+}$), 422.4463 ($[M + PF_6]^{4+}$), 280.5937 ($M^{4+}$), Found: 1,557.2734 ($[M + 3PF_6]^+$), 706.1514 ($[M + 2PF_6]^{2+}$); mp 155–158 °C with decomposition.

References

1. Collin J-P, Heitz V, Sauvage J-P (2005) Top Curr Chem 262:29–62
2. Schalley CA, Weilandt T, Brüggemann J, Vögtle F (2004) Top Curr Chem 248:141–200
3. Godt A (2004) Eur J Org Chem, pp 1639–1654
4. Lankshear MD, Beer PD (2007) Acc Chem Res 40:657–668
5. Dichtel WR, Miljanić OŠ, Zhang W, Spruell JM, Patel K, Aprahamian I, Heath JR, Stoddart JF (2008) Acc Chem Res 41:1750–1761
6. Fujita M (1999) Acc Chem Res 32:53–61
7. Anderson S, Anderson HL, Sanders JKM (1993) Acc Chem Res 26:469–475
8. Cacciapaglia R, Mandolini L (1993) Chem Soc Rev 22:221–231
9. Schneider JP, Kelly JW (1995) Chem Rev 95:2169–2187
10. Stoddart JF, Tseng H-R (2002) Proc Natl Acad Sci USA 99:4797–4800
11. Aricó F, Badjić JD, Cantrill SJ, Flood AH, Leung KC-F, Liu Y, Stoddart JF (2005) Top Curr Chem 249:203–259
12. Williams AR, Northrop BH, Chang T, Stoddart JF, White AJP, Williams DJ (2006) Angew Chem Int Ed 45:6665–6669
13. Northrop BH, Aricó F, Tangchiavang N, Badjić JD, Stoddart JF (2006) Org Lett 8:3899–3902
14. Cantrill SJ, Poulin-Kerstein KG, Grubbs RH, Lanari D, Leung KC-F, Nelson A, Smidt SP, Stoddart JF, Tirrell DA (2005) Org Lett 7:4213–4216
15. Philp D, Stoddart JF (1991) Synlett 445–458
16. Philp D, Stoddart JF (1996) Angew Chem Int Ed 35:1155–1196
17. Kay ER, Leigh DA, Zerbetto F (2007) Angew Chem Int Ed 46:72–191
18. Saha S, Stoddart JF (2007) Chem Soc Rev 36:77–92

19. Green JE, Choi JW, Boukai A, Bunimovich Y, Johnston-Halpering E, DeIonno E, Luo Y, Sheriff BA, Xu K, Shin YS, Tseng H-R, Stoddart JF, Heath JR (2007) Nature 445:414–417
20. Tseng H-R, Wu DM, Fang NXL, Zhang X, Stoddart JF (2004) Chem Phys Chem 5:111–116
21. Luo Y, Collier CP, Jeppesen JO, Nielsen KA, DeIonno E, Ho G, Perkins J, Tseng H-R, Yamamoto T, Stoddart JF, Heath JR (2002) Chem Phys Chem 3:519–525
22. Dichtel WR, Heath JR, Stoddart JF (2007) Philos Trans R Soc London Ser A 365:1607–1625
23. Flood AH, Stoddart JF, Steuerman DW, Heath JR (2004) Science 306:2055–2056
24. Viterisi A, Orsini A, Weibel JM, Pale P (2006) Tetrahedron Lett 47:2779–2781
25. Liu Y, Flood AH, Bonvallett PA, Vignon SA, Northrop BH, Tseng H-R, Jeppesen JO, Huang TJ, Brough B, Baller M, Magonov S, Solares SD, Goddard WA, Ho CM, Stoddart JF (2005) J Am Chem Soc 127:9745–9759
26. Steuerman DW, Tseng H-R, Peters AJ, Flood AH, Jeppesen JO, Nielsen KA, Stoddart JF, Heath JR (2004) Angew Chem Int Ed 43:6486–6491
27. Tseng H-R, Vignon SA, Celestre PC, Perkins J, Jeppesen JO, Di Fabio A, Ballardini R, Gandolfi MT, Venturi M, Balzani V, Stoddart JF (2004) Chem Eur J 10:155–172
28. Leigh DA, Wong JKY, Dehez F, Zerbetto F (2003) Nature 424:174–179
29. Balzani V, Credi A, Ferrer B, Silvi S, Venturi M (2005) Top Curr Chem 262:1–27
30. Mandl CP, König B (2004) Angew Chem Int Ed 43:1622–1624
31. Hernández JV, Kay ER, Leigh DA (2004) Science 306:1532–1537
32. Flood AH, Peters AJ, Vignon SA, Steuerman DW, Tseng H-R, Kang S, Heath JR, Stoddart JF (2004) Chem Eur J 10:6558–6564
33. Asakawa M, Dehaen W, L'abbé G, Menzer S, Nouwen J, Raymo FM, Stoddart JF, Williams DJ (1996) J Org Chem 61:9591–9595
34. Doddi G, Ercolani G, Mencarelli P, Piermattei A (2005) J Org Chem 70:3761–3764
35. Odell B, Reddington MV, Slawin AMZ, Spencer N, Stoddart JF, Williams DJ (1988) Angew Chem Int Ed Engl 27:1547–1550
36. Asakawa M, Ashton PR, Balzani V, Credi A, Hamers C, Matterstig G, Montalti M, Shipway AN, Spencer N, Stoddart JF, Tolley MS, Venturi M, White AJP, Williams DJ (1998) Angew Chem Int Ed 37:333–337
37. Ashton PR, Goodnow TT, Kaifer AE, Reddington MV, Slawin AMZ, Spencer N, Stoddart JF, Vicent C, Williams DJ (1989) Angew Chem Int Ed Engl 28:1396–1399
38. Anelli P-L, Spencer N, Stoddart JF (1991) J Am Chem Soc 113:5131–5133
39. Dichtel WR, Miljanić OŠ, Spruell JM, Heath JR, Stoddart JF (2006) J Am Chem Soc 128:10388–10390
40. Miljanić OŠ, Dichtel WR, Mortezaei S, Stoddart JF (2006) Org Lett 8:4835–4838
41. Miljanić OŠ, Dichtel WR, Khan SI, Mortezaei S, Heath JR, Stoddart JF (2007) J Am Chem Soc 129:8236–8246
42. Spruell JM, Dichtel WR, Heath JR, Stoddart JF (2008) Chem Eur J 14:1468–1477
43. Braunschweig AB, Dichtel WR, Miljanić OŠ, Olson MA, Spruell JM, Khan SI, Heath JR, Stoddart JF (2007) Chem Asian J 2:634–647
44. Rostovtsev VV, Green LG, Fokin VV, Sharpless KB (2002) Angew Chem Int Ed 41:2596–2599
45. Siemsen P, Livingston RC, Diederich F (2000) Angew Chem Int Ed 39:2633–2657
46. Kim HC, Chun K (2007) IEEJ Trans 2:249–261
47. Duda S, Godt A (2003) Eur J Org Chem, pp 3412–3420
48. Ünsal Ö, Godt A (1999) Chem Eur J 5:1728–1733
49. Hamilton DG, Sanders JKM, Davies JE, Clégg W, Teat SJ (1997) Chem Commun pp 897–898
50. Hamilton DG, Feeder N, Prodi L, Teat SJ, Clegg W, Sanders JKM (1998) J Am Chem Soc 120:1096–1097
51. Hamilton DG, Prodi L, Feeder N, Sanders JKM (1999) J Chem Soc Perkin Trans 1:1057–1065
52. Dietrich-Buchecker CO, Hemmert C, Khémiss A-K, Sauvage J-P (1990) J Am Chem Soc 112:8002–8008

53. Dietrich-Buchecker CO, Khémiss A, Sauvage J-P (1986) J Chem Soc Chem Commun 1376–1378
54. Gunter MJ, Farquhar SM (2003) Org Biomol Chem 1:3450–3457
55. Sato Y, Yamasaki R, Saito S (2009) Angew Chem Int Ed 48:504–507
56. Vignon SA, Stoddart JF (2005) Collect Czech Chem Commun 70:1493–1576
57. Souizi A, Robert A (1987) J Org Chem 52:1610–1611
58. Tseng H-R, Vignon SA, Stoddart JF (2003) Angew Chem Int Ed 42:1491–1495
59. Connelly NG, Geiger WE (1996) Chem Rev 96:877–910
60. Babaei A, Connor PA, McQuillan AJ, Umapathy S (1997) J Chem Educ 74:1200–1204
61. Zhao Y, Truhlar DG (2008) Theo Chem Acc 120:215–241
62. Zhao Y, Truhlar DG (2008) Acc Chem Res 41:157–167
63. Benítez D, Tkatchouk E, Yoon I, Stoddart JF, Goddard WA III (2008) J Am Chem Soc 130:14928–14929
64. Fuchter MJ, Beall LS, Baum SM, Montalban AG, Sakellariou EG, Mani NS, Miller T, Vesper BJ, White AJP, Williams DJ, Barrett AGM, Hoffman BM (2005) Tetrahedron 46:6115–6130
65. Andreu R, Garín J, Orduna J, Savirón M, Cousseau J, Gorgues A, Morisson V, Nozdryn T, Becher J, Clausen RP, Bryce MR, Skabara PJ, Dehaen W (1994) Tetrahedron Lett 35:9243–9246
66. Gottlieb HG, Kotlyar V, Nudelman A (1997) J Org Chem 62:7512–7515

Chapter 7
Highly Stable TTF Radical Dimers in a Five-State [3]Catenane

7.1 Introduction

The observation of π–π radical-cation dimers upon the redox stimulation of electron rich or poor heterocycles is long precedented [1]. However, investigations on such systems have been hindered by the inherent sensitivity of even the simplest radical-cation dimers, such that they have only been observed at low temperatures or in the solid state [2–6], an attribute which has relegated them to be considered as mere novelties, rather than the fundamental cornerstone of functional devices [7]. Specifically, methyl viologen (MV^{2+}), the predominant member of a class of organic salts [8], valued previously for their herbicidal activity and endemic to many disciplines and industries, was observed [9–15] long ago to form diamagnetic radical cation dimers following the one-electron reduction of the dication, but which were only stable at low temperatures and high concentrations in strictly air-free environments. Similar π–π radical-cation and mixed-valence dimers of tetrathiafulvalene [16] (TTF) are known to form upon the one-electron oxidation of the neutral compound to its stable radical-cation. As the simple parent

---

This chapter is reproduced in part with permission from: Spruell JM, Coskun A, Friedman DC, Forgan RS, Sarjeant AA, Trabolsi A, Fahrenbach AC, Barin G, Paxton WF, Dey SK, Olson MA, Benítez D, Tkatchouk E, Colvin MT, Carmielli R, Caldwell ST, Rosair GM, Hewage SG, Duclairoir F, Seymour JL, Slawin AMZ, Goddard WA, Wasielewski MR, Cooke G, Stoddart JF, *Nature Chemistry*, **2010**, *2*, 870–879.

Author Contributions: J.M. Spruell and A. Coskun conceived the project. J.M. Spruell and J.F. Stoddart prepared the original manuscript. J.M. Spruell prepared all compounds investigated in this work. W.F. Paxton provided valuable insights into the switching mechanism. D. Benítez, E. Tkatchouk and W.A. Goddard performed DFT calculations. J.M. Spruell and D.C. Friedman performed NMR spectroscopic studies. J.M. Spruell and A. Trabolsi performed electrochemical analysis together. J.M. Spruell, M.T. Colvin, R. Carmielli, and M.R. Wasielewski performed EPR investigations together. J.L.S. performed mass spectroscopic analysis. A.M.Z. Slawin, R.S. Forgan, A.A. Sarjeant, G.M. Rosair, S.G. Hewage and G. Cooke performed X-ray structural analysis.

J. M. Spruell, *The Power of Click Chemistry for Molecular Machines and Surface Patterning*, Springer Theses, DOI: 10.1007/978-1-4419-9647-3_7,

compound, however, the dimeric complex is once again only stable at low temperatures and in the solid state [4, 7].

In recent years, a renaissance [17–26] in the radical cation dimer chemistry of both MV^{2+} and TTF has been spurred on by the discovery that inclusion complexes of each species exhibit exceptionally high stabilities in solution at room temperature. Kim and co-workers [18, 19] observed that cucurbit[8]uril [27] enhances the stability of both $(MV^{\bullet+})_2$ and $(TTF^{\bullet+})_2$ radical-cation dimers by encapsulating the desired species such that they could be studied in solution at room temperature. Subsequently, Fujita observed [20] mixed-valence dimer $(TTF)_2^{\bullet+}$ stabilized within self-assembled cages. When held in place covalently as members of crown ethers [21], molecular clips [22], or appended to calixarenes [23], TTF units also form stable radical-cation dimers. Of particular interest for radical-dimerized species is the fact that the redox activation used in their production represents an affinity *umpolung*—a concept borrowed from classical [28, 29] reactivity *umpolung*—whereby an inversion in supramolecular affinity [30], rather than polarity, is brought about through redox events. This affinity reversal has been used to drive the switching in carefully designed molecular machinery [17, 24–26] whereby the ground states of both MV^{2+} and TTF form stable complexes with electron rich or poor species, respectively, while the high affinity for their dimerized states upon redox stimulation forces the adoption of a switched molecular (co)conformation [17, 24]. Here, we elucidate further the concept of affinity *umpolung* through the exploration of a series of tetrathiafulvalene dimer pairs formed and stabilized across two oxidation states under ambient conditions, held together by virtue of mechanical bonds in a five-state [3]catenane molecular framework demonstrating electronic and translational switching.

7.2 Results and Discussion

Over the past several years we have applied ultramild Cu^{+}- and Cu^{2+}-catalyzed alkyne-based covalent couplings [31–35] for the efficient formation of mechanical bonds in a suite of donor–acceptor rotaxanes and catenanes incorporating as one ring component the π-electron poor cyclophane [36, 37], cyclobis(paraquat-*p*-phenylene) ($CBPQT^{4+}$), which acts as the template for the production of these mechanically interlocked molecules. These methods rely on the stoppering or macrocyclization of a component threaded through the fully-formed $CBPQT^{4+}$ ring, a situation that takes advantage of the full binding energy of the two components and enables the formation of higher-order rotaxanes and catenanes as a result of templation. One such method, the Eglinton Cu^{2+}-based oxidative alkyne homocoupling [38], a reaction well-established [32, 33, 39–48] for the efficient synthesis of catenanes, was recently used to macrocyclize a bispropargyl-functionalized TTF derivative around the $CBPQT^{4+}$ ring [49], forming a single-station switchable [2]catenane where the newly bonded butadiyne unit serves largely a structural role which allowed the operation of an exceptionally simple switching

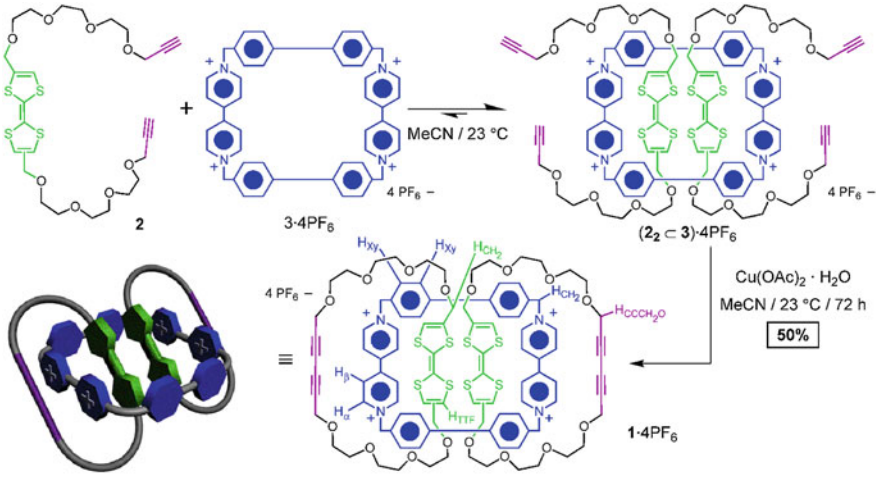

Scheme 7.1 [3]Catenane synthesis. Template-directed synthesis of the [3]catenane **1**·4PF$_6$ consisting of two TTF units threaded through a cyclobis(paraquat-4,4́-biphenylene) ring and mechanically interlocked by the formation of structural butadiyne linkers

motif. Building upon this initial research, we applied the same synthetic approach in order to form (Scheme 7.1) the switchable [3]catenane **1**·4PF$_6$ incorporating the expanded cyclobis(paraquat-4,4′-biphenylene) as the templating π-electron poor macrocycle [50, 51] in which now two π-electron rich components are known [52–54] to coexist comfortably.

Upon mixing the π-electron rich bispropargylated TTF derivative **2** with cyclobis(paraquat-4,4′-biphenylene) (**3**·4PF$_6$) in a 5:1 molar ratio in MeCN, the solution became an intense emerald green color, indicating the formation of the [3]pseudorotaxane (**2**$_2$ ⊂ **3**)·4PF$_6$. Reaction with Cu(OAc)$_2$·H$_2$O (1.0 equiv per terminal alkyne) at room temperature for 3 days effected the desired oxidative homocoupling, affording the [3]catenane **1**·4PF$_6$ as a green solid in 50% overall yield (Scheme 7.1). Remarkably, no [2]catenane or the ring-in-ring complex byproducts were isolated—a finding which indicates the strong templation effected through the wrapping of the ethylene glycol chains around the bipyridinium faces of **3**·4PF$_6$ in [C–H···O] type interactions [55].

The mechanically interlocked molecular structure was confirmed by X-ray crystal structural analysis performed on green needlelike crystals obtained by slow diffusion of *i*Pr$_2$O into a MeCN solution of **1**·4PF$_6$ at 0 °C. Three different views of the molecular structure are displayed in Fig. 7.1, using both ball-and-stick and space-filling representations. Both TTF units (shown in green) exist in their *trans* configurations and are housed within the cyclobis(paraquat-4,4′-biphenylene) cavity (shown in blue) and stabilized by means of a combination of weak interactions. These stabilizing elements consist of π–π stacking contacts with close distances (3.58 Å) between the bipyridinium faces and the included TTF units, as well as [C–H···O] close contacts [55], observed with the second and third oxygen

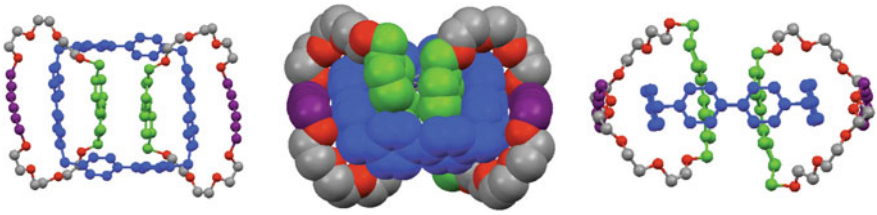

Fig. 7.1 Solid-state structural investigations. The solid-state structure of [3]catenane $\mathbf{1}^{4+}$ displayed (*left*) as a top-down view in a ball-and-stick representation, (*center*) as a perspective view in a space-filling representation, and (*right*) as a side-on view in a ball-and-stick representation. The inclusion of the TTF units within the tetracationic cyclophane places them in the ideal arrangement to form stable dimers in higher oxidation states. The disordered PF_6^- counterions, hydrogen atoms, and MeCN solvent molecules have been omitted for clarity

atoms (2.67 Å (116.6°) and 2.23 Å (171.6°), respectively) on one arm of each TTF containing crown ether and the α-bypyridinium hydrogen. In keeping with previously reported Eglinton-derived catenanes [33, 49], the butadiyne fragments (shown in purple) align themselves approximately parallel to the external bipyridinium faces with close interplanar distances of 3.64 Å. Of considerable interest within the interlocked framework of $\mathbf{1}{\cdot}4PF_6$ is the relationship forged between the two TTF units which are held side-by-side with each other by virtue of the two mechanical bonds. When both TTF units are neutral—as in $\mathbf{1}^{4+}$—they are expected to experience very little electronic interaction one with the other. The crystal structure of $\mathbf{1}^{4+}$ supports this notion since the TTF units experience a slipped-stacked arrangement within the tetracationic cyclophane, their average planes being separated by 3.63 Å. It is this close internal contact and the resulting high relative concentration that provide $\mathbf{1}{\cdot}4PF_6$ with the possibility of forming strongly coupled TTF dimers throughout its various oxidation states.

Cyclic voltammetry (CV) performed at room temperature was used to investigate the electrochemical switching mechanism of $\mathbf{1}{\cdot}4PF_6$. The entire potential scanning range for the [3]catenane, recorded (Fig. 7.2) at 200 mV/s, reveals four separate one-electron oxidation events present in the [3]catenane: they occur at 405, 655, 1,320, and 1,470 mV versus Ag/AgCl. A large potential gap exists between the first two (I and II) and final two (III and IV) oxidation events of $\mathbf{1}{\cdot}4PF_6$, amounting to shifts in excess of 530 mV for the second oxidation of the TTF units when compared with the control compound **2**. Such large shifts in oxidation potential indicate the formation of a highly stabilized species upon the second oxidation event. In order to describe these oxidation events, we propose a switching mechanism (Scheme 7.2) whereby the TTF units of $\mathbf{1}{\cdot}4PF_6$ are oxidized individually in four separate steps, forming two stable dimers of tetrathiafulvalene as the mixed-valence state, $(TTF)_2^{\bullet+}$ labeled $\mathbf{1}^{5+}$, and the radical-cation dimer, $(TTF^{\bullet+})_2$ labeled $\mathbf{1}^{6+}$, as well as a novel radical-cation/butadiyne dimer, labeled $\mathbf{1}^{7+}$. The formation of $\mathbf{1}^{7+}$ occurs after the stepwise ejection the TTF^{2+} dication

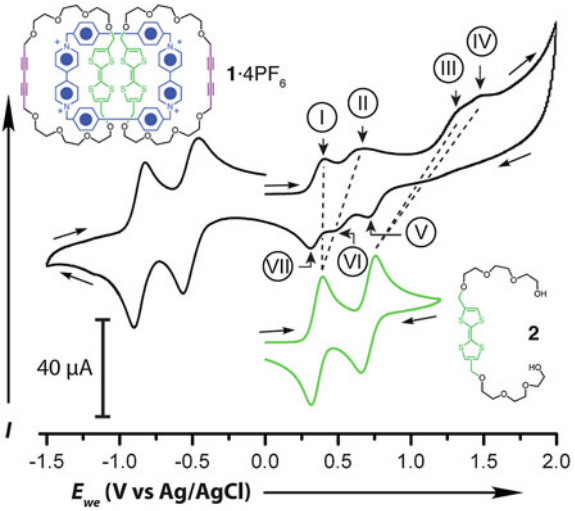

Fig. 7.2 Cyclic voltammetry (CV). Full range CVs (1 mM in MeCN, 100 mM NBu_4PF_6, 200 mV/s) of **1**·$4PF_6$ and **2** performed at room temperature. Four distinct one-electron oxidation processes are observed for **1**·$4PF_6$—(I) 405 mV, (II) 655 mV, (III) 1.32 V, and (IV) 1.47 V. The subsequent re-reductions occur in three steps—(V) a two-electron process centered on 709 mV, (VI) a one-electron process centered on 476 mV, and (VII) a one-electron process centered on 311 mV. Each of these process occur at potentials significantly shifted from the analogous redox processes for **2**, centered on 404 (*ox*), 793 (*ox*), 629 (*red*), and 297 (*red*) mV. These shifted oxidation potentials indicate the formation of stabilized mixed-valence $(TTF)_2^{\bullet+}$ and radical-cation $(TTF^{\bullet+})_2$ dimer states, as well as a $TTF^{\bullet+}$-butadiyne interaction

from inside the tetracationic cyclophane—an act which causes the circumrotation of one of the crown ethers such that its butadiyne unit now occupies the cavity of the cyclophane—leaving a $TTF^{\bullet+}$ radical-cation associated with the other crown ether and the newly presented butadiyne to constitute a stabilizing interaction inside the cyclophane. The final oxidation of the $\mathbf{1}^{7+}$ species results in the ejection of the second TTF^{2+} dication from inside the tetracationic cyclophane in $\mathbf{1}^{8+}$, forming the translational state where both the dications occupy alongside positions with respect to the bipyridinium units on the cyclophane. Further proof of the translational change involved in the formation of $\mathbf{1}^{8+}$ is brought into focus again when we consider the re-reduction of this highly charged structure. The first re-reduction occurs as a two-electron process, reforming the highly stabilized radical-cation $(TTF^{\bullet+})_2$ dimer in $\mathbf{1}^{6+}$. This re-reduction occurs very near the potential for the first re-reduction of the control compound **2**, an indication that the TTF^{2+} dications, once removed from the cavity of the tetracationic cyclophane, are re-reduced to radical-cations while outside of the cyclophane. It is worthy of note that the re-formation of the $(TTF^{\bullet+})_2$ dimer in $\mathbf{1}^{6+}$ strongly favors the insertion of two cationic units—constituting the radical-cation dimer—inside the tetracationic cyclophane. Further reduction of the molecule occurs as two distinct one-electron events with the mixed-valence $(TTF)_2^{\bullet+}$ dimer $\mathbf{1}^{5+}$ formed after the first

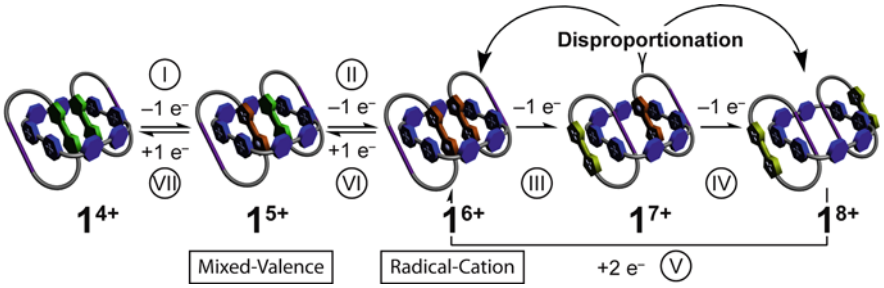

Scheme 7.2 Step-wise oxidative dimerization mechanism. The proposed oxidative switching mechanism exhibited by the [3]catenane **1**·4PF_6 proceeds in four distinct oxidation events (labelled I through IV), forming stable intermediaries $\mathbf{1}^{5+}$, $\mathbf{1}^{6+}$, and $\mathbf{1}^{8+}$. States $\mathbf{1}^{5+}$ and $\mathbf{1}^{6+}$ are composed of stabilized mixed-valence $(TTF)_2^{\bullet+}$ and radical-cation $(TTF^{\bullet+})_2$ dimers housed within the 'molecular flask' created by the [3]catenane's mechanically interlocked architecture. Two molecules of intermediate $\mathbf{1}^{7+}$ are believed to disproportionate to give the more stable $\mathbf{1}^{6+}$ and $\mathbf{1}^{8+}$ combination. The re-reduction of $\mathbf{1}^{8+}$ to $\mathbf{1}^{4+}$ proceeds in three distinct events labelled V through VII, reforming the stable intermediates $\mathbf{1}^{6+}$ and $\mathbf{1}^{5+}$ along the path to the ground state $\mathbf{1}^{4+}$

and the return to the ground state $\mathbf{1}^{4+}$ after the second. The application of still further reduction potentials results in two two-electron reversible processes for the redox events of both bipyridinium moieties to the radical-cation and neutral states. Both bipyridinium units are equivalent in the symmetrical [3]catenane and hence the reduction and re-oxidation of these moieties occur simultaneously with respect to each redox event.

In order to probe the proposed switching mechanism (Scheme 7.2) from yet another angle, we conducted a series of spectro-photometric investigations on each of the oxidation states of **1**·4PF_6. The different oxidation states in bulk solution were generated by titrating the appropriate amount of an oxidant into MeCN solutions containing **1**·4PF_6 under ambient atmosphere at room temperature. The UV–Vis-NIR spectra of a solution of the [3]catenane after the stepwise addition of 0–4 equiv of $Fe(ClO_4)_3$ are displayed in Fig. 7.3. The initial spectrum of $\mathbf{1}^{4+}$ displays a broad absorption band associated with the TTF-bipyridinium charge-transfer (CT) interaction centered on 893 nm (labeled a). The addition of 1.0 equiv of oxidant resulted in the formation of a very broad NIR absorption band centered on 2040 nm, along with a new peak at 613 nm (labeled b): both absorbances are known [2, 20, 22, 23] to correspond to $(TTF)_2^{\bullet+}$ mixed-valence dimers as expected for $\mathbf{1}^{5+}$. Interestingly, the growth of these two peaks occurs with the attenuation and blue-shifting of the original TTF-bipyridinium CT absorption band to roughly half of its original intensity—an observation that is easily explained since one-half of the TTF units, originally participating in the CT interaction, are effectively removed upon their oxidation with the addition of 1.0 equiv of the oxidant. The further addition of 1.0 more equiv of the oxidant removes completely the CT absorption band as well as the NIR absorption band, and replaces them with two strong absorption bands centered on 806 and 555 nm (labeled c)—that are absorbances characteristic [2, 19, 22, 23] of $(TTF^{\bullet+})_2$ radical-cation dimers.

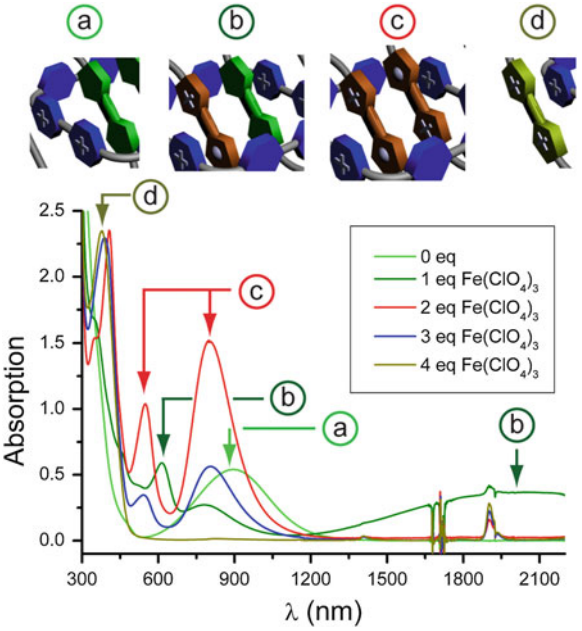

Fig. 7.3 Spectrophotometry. UV–VIS-NIR spectra of **1** (0.3 mM in MeCN, pathlength 1.0 cm, room temperature) following the titration with $Fe(ClO_4)_3$ (solution in MeCN). Absorbances arising from the TTF-bipyridinium CT, mixed-valence $(TTF)_2^{\bullet+}$ dimer, radical-cation $(TTF^{\bullet+})_2$ dimer, and TTF^{2+} dications are observed (and illustrated above) upon the addition of 0, 1.0, 2.0, and 4.0 eq. of $Fe(ClO_4)_3$ oxidant. The addition of 3.0 eq. of oxidant presents mixtures of absorbances attributed to the $\mathbf{1}^{6+}$ and $\mathbf{1}^{8+}$ states

The addition of a total of 3.0 equiv of oxidant resulted merely in the attenuation of these two absorbances by one-half, without the growth of any new peaks which could be attributed to $\mathbf{1}^{7+}$—a finding that was initially puzzling, but became clear later, following EPR investigations, as the product of the disproportionation of two molecules of $\mathbf{1}^{7+}$ to form one of $\mathbf{1}^{6+}$ and another of $\mathbf{1}^{8+}$. The addition of yet another 1.0 equiv of oxidant to give a total of 4.0 equiv removed all the absorbances except for a sharp peak centered on 375 nm (labeled d) characteristic of TTF^{2+} dications.

Chemical oxidation of $\mathbf{1}^{4+}$ to both $\mathbf{1}^{6+}$ and $\mathbf{1}^{8+}$ was also performed in CD_3CN using 2.0 and 4.0 equiv, respectively, of tris(4-bromophenyl)ammoniumyl hexachloro-antimonate [56] as the chemical oxidant so that the effects of oxidation on the TTF units could be probed by ^1H NMR spectroscopy. The ground state spectrum (Fig. 7.4a) of $\mathbf{1}^{4+}$ is complicated by the presence of both interconverting [57] *cis* and *trans* configurational isomers for each TTF unit within the cavity—each conferring their respective local symmetries throughout the [3]catenane. Nonetheless, the resonances attributed to all of the important functions in the molecule were easily assigned using 2D NMR techniques and they are annotated on the spectrum in Fig. 7.4a. Upon the addition of 2.0 equiv of the chemical oxidant, both TTF resonances disappeared along with broadening of all the other resonances in the spectrum—both of these observations being expected following the formation of the radical-cation $(TTF^{\bullet+})_2$ dimeric species $\mathbf{1}^{6+}$. The presence of clearly defined signals (Fig. 7.4b) for the oxidized species supports the stability and electronically coupled nature of the radical-cation $(TTF^{\bullet+})_2$ dimer within $\mathbf{1}^{6+}$. Similar behavior has been reported by Kim and co-workers [19] who also recorded an ^1H NMR spectrum of the encapsulated $(TTF^{\bullet+})_2$ radical cation-dimer, in their

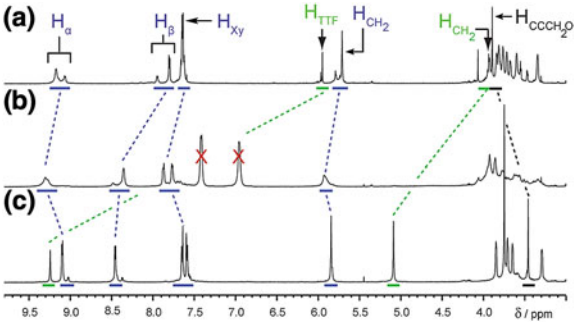

Fig. 7.4 NMR investigations. ^{1}H NMR Spectra (600 MHz, CD_3CN, 293 K) of (**a**) $\mathbf{1}^{4+}$, (**b**) $\mathbf{1}^{6+}$, and (**c**) $\mathbf{1}^{8+}$ formed through the addition of 0, 2.0, and 4.0 eq. of tris(4-bromophenyl)ammoniumyl hexachloroantimonate oxidant. The presence of well-defined signals in the spectrum of $\mathbf{1}^{6+}$ supports the notion that the $(TTF^{\bullet+})_2$ radical-cation dimer is diamagnetic

case as a supramolecular entity in cucurbit[8]uril. Finally, complete oxidation, following the addition of an excess of oxidant to form $\mathbf{1}^{8+}$, resulted in the reappearance of signals (Fig. 7.4c) for the TTF protons in a well resolved spectrum. Close inspection of the resonances for the tetracationic cyclophane during the oxidation steps reveal initial downfield migrations of all the resonances following the formation of $\mathbf{1}^{6+}$—resulting from the shielding effects of the closely associated/included $(TTF^{\bullet+})_2$ dicationic species. Upfield movements of the same cyclophane resonances occurs upon the formation of $\mathbf{1}^{8+}$, as would be expected following the ejection of the TTF^{2+} dications.

We have also performed continuous wave (CW) EPR spectroscopy over all of the oxidation states generated by titrating the $Fe(ClO_4)_3$ oxidant at 295 K into an MeCN solution of $\mathbf{1}{\cdot}4PF_6$ in unsealed quartz tubes. During the slow addition of the oxidant, a signal for the radical emerged, which reached a maximum after the addition of 1.0 equiv—producing the $(TTF)_2^{\bullet+}$ mixed-valence state of $\mathbf{1}^{5+}$—as shown in Fig. 7.5a. The radical signal of $\mathbf{1}^{5+}$ is broad, lacking hyperfine splitting, because the two neighboring protons on the TTF units do not effectively couple with the spin system. A broad signal, also lacking hyperfine splitting, was observed for the model compound **2** upon oxidation with 1.0 equiv of $Fe(ClO_4)_3$. The continued addition of the oxidant resulted in the attenuation of the radical envelope, following the addition of 2.0 total equiv—a result which was surprising at first, considering that another radical species is formed, at least formally, during the continued oxidation to $\mathbf{1}^{6+}$. The attenuation in the signal can be attributed to the strongly paired (singlet) nature of the two interacting formal radical species constituting the $(TTF^{\bullet+})_2$ radical-cation dimer. The presence of a very small radical signal can be attributed to a finite population of TTF unencircled co-conformations in $\mathbf{1}^{6+}$ wherein the free $TTF^{\bullet+}$ units behave as normal triplet state species. During the addition of another equiv of oxidant to give a total of 3.0 equiv, the expected emergence of the radical signal did not occurr—a result that can best be explained by the disproportionation of the transient $\mathbf{1}^{7+}$ species to form

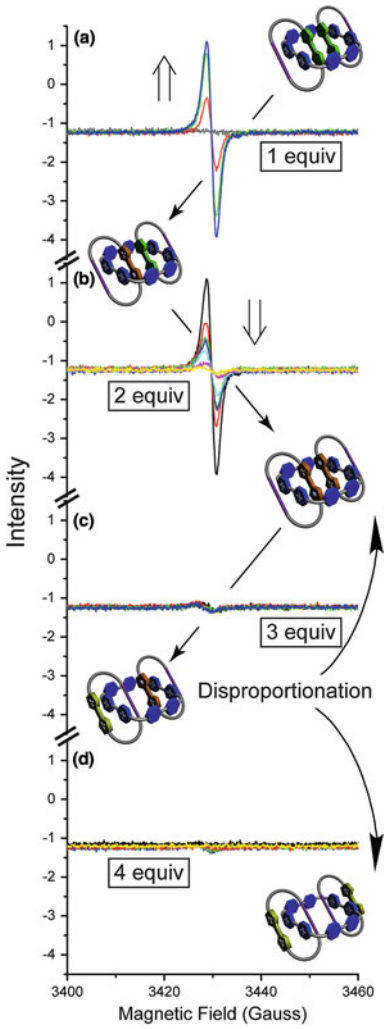

Fig. 7.5 Steady-state CW EPR spectroscopy. CW EPR spectra of the [3]catenane **1**·4PF_6 upon stepwise titration with $Fe(ClO_4)_3$ where (**a**) displays the titration from 0 to 1.0 equiv, (**b**) from 1.0 to 2.0 equiv, (**c**) from 2.0 to 3.0 equiv, and (**d**) from 3.0 to 4.0 equiv of oxidant. The growth of radical signal in response to the formation of $\mathbf{1}^{5+}$, as well as its attenuation on the formation of $\mathbf{1}^{6+}$, indicate the paramagnetic character of the former and diamagnetic of the latter. The lack of radical character upon the addition of 3.0 equiv of oxidant supports the notion of the disproportionation of $\mathbf{1}^{7+}$

the stable $\mathbf{1}^{6+}$ and $\mathbf{1}^{8+}$ which are both EPR silent species. Finally, the addition of 4.0 total equiv of the oxidant causes the complete oxidation to $\mathbf{1}^{8+}$ which bears no radical character and is completely EPR silent.

The experimental data is commensurate with a compound exhibiting stable TTF dimeric states as the mixed-valence $(TTF)_2^{\bullet+}$ and radical-cation $(TTF^{\bullet+})_2$ forms in $\mathbf{1}^{5+}$ and $\mathbf{1}^{6+}$, respectively, while also being suggestive of a novel $TTF^{\bullet+}$-butadiyne interaction in $\mathbf{1}^{7+}$. In order to investigate the exact nature and stability of these dimeric species found in the different oxidation states of **1**·4PF_6, we have resorted to quantum–mechanical modeling. Density functional theory (DFT) using the M06-suite of functionals [58], a combination that we have shown [59] previously to provide accurate structural and energetic descriptions of mechanically

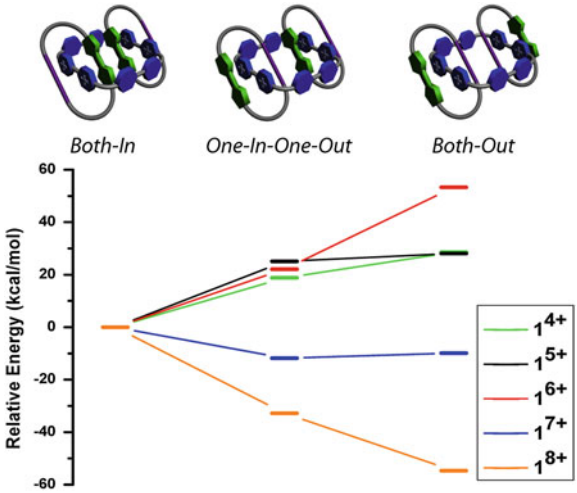

Fig. 7.6 Calculated energy landscape. DFT calculated relative energies for the five oxidation states $\mathbf{1}^{4+}$–$\mathbf{1}^{8+}$ of the three co-conformations shown. For each oxidation state the *both-in* co-conformation was arbitrarily set at 0 kcal/mol. While the absolute energies between each oxidation state are not directly comparable, the relative energetic differences between co-conformations are comparable. The data indicate stable dimeric structures, $(TTF)_2^{\bullet+}$ and $(TTF^{\bullet+})_2$, in $\mathbf{1}^{5+}$ and $\mathbf{1}^{6+}$, respectively, as well as a stabilized $TTF^{\bullet+}$-butadiyne interaction in $\mathbf{1}^{7+}$

interlocked molecules—including the recent description [49] of the related single-station TTF-based [2]catenane—was employed to shed light on the relative energetic landscape of the [3]catenane $\mathbf{1}^{4+}$ across its five different oxidation states. We performed geometry optimizations on the *both-in*, *one-in-one-out*, and *both-out* co-conformations (this convention for naming denotes the relative position of the TTF units) for each of the oxidation states, $\mathbf{1}^{4+}$–$\mathbf{1}^{8+}$, at the M06-L/6-31G** level of theory in the gas phase. Energies were calculated using the M06-2× functional, including a continuum solvation correction for MeCN.

A detailed careful analysis (Fig. 7.6) of the calculated relative energies suggests that for the $\mathbf{1}^{4+}$, $\mathbf{1}^{5+}$, and $\mathbf{1}^{6+}$ oxidation states, the *both-in* co-conformation is favored by ~20 kcal/mol, and that in fact, this co-conformation is more strongly favored in the higher oxidized states—by 6 more kcal/mol in $\mathbf{1}^{5+}$ and 3 more kcal/mol in $\mathbf{1}^{6+}$—despite the inclusion of more charged species within the tetracationic cyclophane. We attribute this increased stability to the formation of $(TTF)_2^{\bullet+}$ mixed-valence and $(TTF^{\bullet+})_2$ radical-cation dimerized states in these oxidized species. It is important to note that, because the TTF-containing crown ethers do not contain secondary π-electron rich recognition sites, bearing as they do only glycols and the butadiyne unit, no competition exists for occupancy within the cyclophane. This lack of competition between different recognition motifs allows even weakly stabilized co-conformations to be observed and indeed occupied almost quantitatively in this single-station [3]catenane [49]. An example of such a weakly stabilized co-conformation is the novel $TTF^{\bullet+}$-butadiyne interaction which

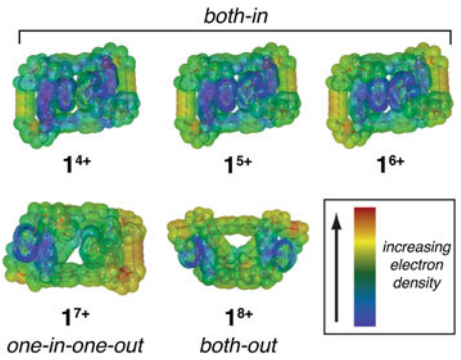

Fig. 7.7 Calculated electrostatic potential surfaces. The DFT calculated structures overlaid with the electrostatic potential maps describing the electronic interactions present across the most stable co-conformations of the [3]catenane in each of its five oxidation states

exists in the *one-in-one-out* co-conformation of $\mathbf{1}^{7+}$. It was found by calculation to be slightly more stable ($\sim$2 kcal/mol) than the *both-out* co-conformation of the same oxidation state. The observation of this stabilized interaction is consistent with the CV data in which a third sequential oxidation state exists (Fig. 7.2, marked III), accounting for the formation of $\mathbf{1}^{7+}$. This interaction is once again verified by the much larger energetic penalty (25 kcal/mol) for converting the *one-in-one-out* co-conformation to the *both-out* co-conformation of $\mathbf{1}^{6+}$—a process that would break the stabilizing $TTF^{\bullet+}$-butadiyne interaction—as compared to the same process in $\mathbf{1}^{5+}$.

The electrostatic potential surfaces calculated for the most stable co-conformations for the [3]catenane at all five oxidation states are displayed in Fig. 7.7. The ground state, structure $\mathbf{1}^{4+}$, exhibits symmetric CT interactions between the TTF units and the bipyridinium faces as indicated by the shared electropositivity localized between their adjoining faces. Throughout the oxidation sequence transforming $\mathbf{1}^{4+}$ into $\mathbf{1}^{6+}$, the electropositive regions become more and more concentrated between the encircled TTF units—an expected result since the TTF units form increasingly strong interactions in the mixed-valence $(TTF)_2^{\bullet+}$ and radical-cation $(TTF^{\bullet+})_2$ dimer states in the interior of the 'molecular flask.' Within the $\mathbf{1}^{7+}$ state, the bulk of the electropositivity rests on the ejected TTF^{2+} dication while, to a lesser extent, positive regions are also shared across the $TTF^{\bullet+}$-butadiyne interaction in the interior of the cyclophane in this unsymmetrical structure. The final oxidation to $\mathbf{1}^{8+}$ returns symmetry to the catenane, placing the highly electropositive regions squarely on the TTF^{2+} dications outside of the tetracationic cyclophane.

Finally, in order to appreciate more fully the interactions of the species incorporated within the tetracationic cyclophane of the the [3]catenane across its five oxidation states, we conducted a simple computational binding study between the encircled species in the most stable co-conformations for $\mathbf{1}^{4+}$, $\mathbf{1}^{5+}$, $\mathbf{1}^{6+}$, and $\mathbf{1}^{7+}$ in which the tetracationic cyclophane and unencircled components were excluded. By omitting the cyclophane in the theoretical model, the interactions between the included species can be investigated free of the energetic perturbations arising from charge-charge repulsion from the encircling cyclophane. The solvated interaction energy between two neutral TTF moieties—found in $\mathbf{1}^{4+}$—was calculated to be –9.5 kcal/mol, while the interaction energy between a neutral TTF

unit and a butadiyne fragment was calculated to be –5.3 kcal/mol; these values serves as a baseline for the van der Waals (vdW) interaction energy caused by bringing two π-electron surfaces into close proximity. The single-electron oxidative formation of the $(TTF)_2^{\bullet+}$ dimer—present in $\mathbf{1}^{5+}$—results in –10.5 kcal/mol in total stabilization energy—1 kcal/mol higher than for the neutral species—while the two-electron oxidation dimeric product $(TTF^{\bullet+})_2$—present in $\mathbf{1}^{6+}$— is stabilized at –12.9 kcal/mol −2.4 kcal/mol higher than the neutral species. Interestingly, the $TTF^{\bullet+}$-butadiyne dimer present in the *one-in-one-out* co-conformation of $\mathbf{1}^{7+}$ experiences –7.0 kcal/mol in stabilization energy—that is, 1.7 kcal/mol higher than the in the neutral case, most likely as a consequence of electrostatic attractive interactions. These theoretical investigations indicate very clearly the presence of moderately strong affinities, not only between the two TTF units, collectively singly and doubly oxidized, but also between $TTF^{\bullet+}$ radical cations and other π-electron accessible moieties.

7.3 Conclusions

We have demonstrated the efficient formation and enhanced stability of $(TTF)_2^{\bullet+}$ mixed-valence and $(TTF^{\bullet+})_2$ radical-cation dimers as well as an unprecedented $TTF^{\bullet+}$-butadiyne dimer within the 'molecular flask' composed of a mechanically interlocked [3]catenane. The unique nature of the mechanical bond endows the high stability of these electrochemically accessible dimeric states through both ideal geometric arrangements and high apparent concentrations, while also enabling structural and translational switching to be brought about through their formation. This affinity *umpolung* drives the dimerization and step-wise circumrotation upon the successive oxidation of the TTF units such that finite structural control emerges through electronic stimulation. The ability to generate and study in detail both the discrete mixed-valence and radical-cation tetrathiafulvalene dimers under ambient conditions within the mechanically interlocked framework marks a departure from the current state-of-the-art and positions this and similar molecules as attractive candidates for electronic and spintronic device applications while also serving as valuable synthetic models of natural analogues [60].

7.4 Experimental Section

7.4.1 General Methods

All reagents were purchased from commercial suppliers (Aldrich or Fisher) and used without further purification. Cyclobis(paraquat-4,4′-biphenylene) tetrakis-hexafluoro-phosphate [51] ($\mathbf{3}\cdot 4PF_6$) and 4,4′(5′)-bis[2-(2-{2-(propargyl)eth-oxy}eth-oxy)ethoxy]tetrathia-fulvalene [49] (**2**) were prepared according to

literature procedures. Thin layer chromatography (TLC) was performed on silica gel 60 F_{254} (E. Merck). Column chromatography was performed on silica gel 60F (Merck 9385, 0.040–0.063 nm). Nuclear magnetic resonance (NMR) spectra were recorded at 25 °C (unless otherwise noted) on Bruker Avance 500 and 600 spectrometers, with working frequencies of 500 and 600 MHz for ^{1}H, and 125 and 150 MHz for ^{13}C nuclei, respectively. Chemical shifts are reported in ppm relative to the signals corresponding to the residual non-deuterated solvents [61]. All ^{13}C spectra were recorded with the simultaneous decoupling of proton nuclei. EPR Measurements at X-band (9.5 GHz) were made using a Bruker Elexsys E580. The EPR spectrometer was outfitted with a variable Q dielectric resonator (ER-4118X-MD5-W1). Steady-state CW EPR spectra were measured using 0.2–2 mW microwave power and 0.01–0.05 mT field modulation at 100 kHz, with a time constant of 5.12 ms and a conversion time of 40.96 ms. Electrospray Ionization (ESI) mass spectra were obtained on a Agilent 6210 LC-TOF high resolution mass spectrometer. Nanoelectrospray HRMS spectra were collected on a ThermoElectron LTQ-FT-MS. Cyclic voltammetry experiments were performed on a Princeton Applied Research 263 A Multipurpose instrument interfaced to a PC using a glassy carbon working electrode (0.018 cm^2, Cypress system). The electrode surface was polished routinely with 0.05 μm^2 alumina/water slurry on a felt surface immediately before use. The counter electrode was a Pt coil and the reference electrode was a AgCl coated Ag wire. The concentrations of the samples were 1 mM in 100 mM electrolyte solution (NBu_4PF_6 in MeCN). UV–Vis-NIR Absorption spectra were recorded on a Varian Cary–500 spectrophotometer.

7.4.2 Computational Methods

Calculations were performed on all systems using density functional theory (DFT) with the M06-L and M06-2× functionals, as implemented in Jaguar 7.6r110. Starting with a structure from the crystallographic data, we optimized the geometry using the 6-31G** basis set with the M06-L functional in the gas phase. Single-point energies were calculated using the M06-2× functional and the 6-31G** basis set. Solvent corrections were based on single point self-consistent Poisson-Boltzmann continuum solvation calculations for acetonitrile ($\Sigma = 37.5$, $R_0 = 2.18$ Å) using the PBF module in Jaguar.

7.4.3 Preparation of 1·4PF$_6$

$Cu(OAc)_2{\cdot}H_2O$ (40.0 mg, 0.200 mmol) was added to a green solution of **2** (121 mg, 0.200 mmol) and **3**·4PF_6 (50.0 mg, 0.040 mmol) dissolved in MeCN (30 mL) and the solution was stirred for 72 h under ambient conditions. The solvent was removed *in vacuo* and the green residue was subjected to

chromatography (SiO_2, MeOH:2M NH_4Cl:$MeNO_2$ (7:2:1) eluent). The green band was collected, concentrated *in vacuo*, and treated with cold H_2O to precipitate a green solid (49.2 mg, 50%). **1**·4PF_6: ^{1}H NMR (600 MHz, CD_3CN, 293 K): δ 9.21–9.04 (m, 8H, α-bipy$^+$-H), 7.95–7.79 (m, 8H, β-biby$^+$-H), 7.66–7.60 (m, 16H, phenylene-H), 5.95 (s, 4H, SC*H*), 5.79–5.70 (m, 8H, macrocyclic CH_2), 3.96–3.91 (m, 8H, SCCH_2), 3.89 (s, 8H, C≡CCH_2O), 3.85–3.83 (m, 8H), 3.82–3.79 (m, 8H), 3.77–3.75 (m, 8H), 3.73–3.70 (m, 8H), 3.69–3.66 (m, 8H), 3.61–3.58 (m, 8H), 3.36–3.33 (m, 8H); ^{13}C NMR (125 MHz, CD_3CN, 293 K): δ 145.78, 145.31, 142.04, 133.67, 133.57, 131.00, 129.00, 126.73, 125.73, 119.74, 110.55, 77.28, 76.85, 72.17, 71.85, 71.36, 71.23, 71.10, 71.01, 71.00, 70.89, 70.51, 70.10, 69.84, 68.71, 68.34, 65.52, 59.26, 59.17; HRMS (ESI) Calcd for $C_{100}H_{108}F_{24}N_4O_{16}P_4S_8$: 2,311.4402 ($[M + 3PF_6]^+$), 1,083.2405 ($[M + 2PF_6]^{2+}$), 673.8389 ($[M + PF_6]^{3+}$), 469.1382 ($M^{4+}$), Found: 2,311.4394 ($[M + 3PF_6]^+$), 1,083.2416 ($[M + 2PF_6]^{2+}$), 673.8392 ($[M + PF_6]^{3+}$), 469.1385 ($M^{4+}$); mp 152–156 °C with decomposition.

7.4.4 Oxidation Studies

UV–Vis-NIR Spectra were recorded from a solution of **1**·4PF_6 (3 mL, 0.3 mM, MeCN) through a 1.0 cm path-length cuvette throughout the successive addition of a solution of $Fe(ClO_4)_3$ (2 μL aliquots, 100 mM, MeCN). EPR Spectra were recorded from a solution of **1**·4PF_6 (854 μL, 0.5 mM, MeCN) in an unsealed quartz tube (1.4 mm I.D.) tube throughout the successive addition and mixing of a solution of $Fe(ClO_4)_3$ (4 μL aliquots, 50 mM, MeCN; the solution in the tube was removed and mixed with the parent solution and added oxidant between the recording of each spectrum). Nanoelectrospray HRMS spectra were performed on solutions of $\mathbf{1^{4+}}$, $\mathbf{1^{5+}}$, $\mathbf{1^{6+}}$, and $\mathbf{1^{8+}}$ (3 μM, MeCN) prepared from the titration of $Fe(ClO_4)_3$ (50 mM, MeCN). ^{1}H NMR spectra were recorded from a solution of **1**·4PF_6 (122 μL, 2.0 μM, CD_3CN) following the successive addition of tris(4-bromophenyl)ammoniumyl hexachloroantimonate (0.4 mg aliquots).

References

1. Lewis IC, Singer L (1965) J Chem Phys 43:2712–2727
2. Torrance JB, Scott BA, Welber B, Kaufman FB, Seiden PE (1979) Phys Rev B 19:730–741
3. Bozio R, Zanon I, Girlando A, Pecile C (1979) J Chem Phys 71:2282–2293
4. Rosokha SV, Kochi JK (2007) J Am Chem Soc 129:828–838
5. Tanaka K, Kunita T, Ishiguro F, Naka K, Chujo Y (2009) Langmuir 25:6929–6933
6. Porter WW, Vaid TP (2005) J Org Chem 70:5028–5035
7. Khodorkovsky V, Shapiro L, Krief P, Shames A, Mabon G, Gorgues A, Giffard M (2001) Chem Commun 2736–2737
8. Sliwa W, Bachowska B, Zelichowicz N (1991) Heterocycles 32:2241–2273
9. Kosower EM, Cotter JL (1964) J Am Chem Soc 86:5524–5527

10. Gueder W, Hünig S, Suchy A (1986) Tetrahedron 42:1665–1677
11. Evans AG, Evans JC, Baker MW (1975) J Chem Soc Perkin Trans 2:1310–1311
12. Evans AG, Evans JC, Baker MW (1977) J Am Chem Soc 99:5882–5884
13. Claude-Montigny B, Merlin A, Tondre C (1992) J Phys Chem 96:4432–4437
14. Meisel D, Mulac WA, Metheson MS (1981) J Phys Chem 85:179–187
15. Furue M, Nozakura S (1980) Chem Lett 9:821–824
16. Bendikov M, Wudl F, Perepichka DF (2004) Chem Rev 104:4891–4945
17. Aprahamian I, Olsen J-C, Trabolsi A, Stoddart JF (2008) Chem Eur J 14:3889–3895
18. Jeon WS, Kim H-J, Lee C, Kim K (2002) Chem Commun 1828–1829
19. Ziganshina AY, Ko YH, Jeon WS, Kim K (2004) Chem Commun 806–807
20. Yoshizawa M, Kumazawa K, Fujita M (2005) J Am Chem Soc 127:13456–13457
21. Spanggaard H, Prehn J, Nielsen MB, Levillain E, Allain M, Becher J (2000) J Am Chem Soc 122:9486–9494
22. Chiang P-T, Chen N-C, Lai C-C, Chiu S-H (2008) Chem Eur J 14:6546–6552
23. Lyskawa J, Sallé M, Balandier J-Y, Le Derf F, Levillian E, Allain M, Viel P, Palacin S (2006) Chem Commun 2233–2235
24. Trabolsi A, Hmadeh M, Khashab NM, Friedman DC, Belowich ME, Humbert N, Elhabiri M, Khatib HA, Albrecht-Gary AM, Stoddart JF (2009) New J Chem 33:254–263
25. Lee JW, Hwang I, Jeon WS, Ko YH, Sakamoto S, Yamaguchi K, Kim K (2008) Chem Asian J 3:1277–1283
26. Hwang I, Siganshina AY, Ko YH, Yun G, Kim K (2009) Chem Commun 416–418
27. Kim K, Selvapalam N, Koy YH, Park KM, Kim D, Kim J (2007) Chem Soc Rev 36:267–279
28. Grobel BT, Seebach D (1977) Synthesis 6:357–402
29. Seebach D (1979) Angew Chem Int Ed Engl 18:239–258
30. Sessler JL, Karnas E, Kim SK, Ou K, Zhang M, Kadish KM, Ohkubo K, Fukuzumi S (2008) J Am Chem Soc 130:15256–15257
31. Dichtel WR, Miljanić OŠ, Spruell JM, Heath JR, Stoddart JF (2006) J Am Chem Soc 128:10388–10390
32. Miljanić OŠ, Dichtel WR, Mortezaei S, Stoddart JF (2006) Org Lett 8:4835–4838
33. Miljanić OŠ, Dichtel WR, Khan SI, Mortezaei S, Heath JR, Stoddart JF (2007) J Am Chem Soc 129:8236–8246
34. Spruell JM, Dichtel WR, Heath JR, Stoddart JF (2008) Chem Eur J 14:1468–1477
35. Dichtel WR, Miljanić OŠ, Zhang W, Spruell JM, Patel K, Aprahamian I, Heath JR, Stoddart JF (2008) Acc Chem Res 41:1750–1761
36. Asakawa M, Dehaen W, L'abbé G, Menzer S, Nouwen J, Raymo FM, Stoddart JF, Williams DJ (1996) J Org Chem 61:9591–9595
37. Odell B, Reddington MV, Slawin AMZ, Spencer N, Stoddart JF, Williams DJ (1988) Angew Chem Int Ed Engl 27:1547–1550
38. Siemsen P, Livingston RC, Diederich F (2000) Angew Chem Int Ed 39:2633–2657
39. Godt A (2004) Eur J Org Chem 1639–1654
40. Duda S, Godt A (2003) Eur J Org Chem 3412–3420
41. Ünsal Ö, Godt A (1999) Chem Eur J 5:1728–1733
42. Hamilton DG, Sanders JKM, Davies JE, Clégg W, Teat SJ (1997) Chem Commun 897–898
43. Hamilton DG, Feeder N, Prodi L, Teat SJ, Clegg W, Sanders JKM (1998) J Am Chem Soc 120:1096–1097
44. Hamilton DG, Prodi L, Feeder N, Sanders JKM (1999) J Chem Soc Perkin Trans 1:1057–1065
45. Dietrich-Buchecker CO, Hemmert C, Khémiss A-K, Sauvage J-P (1990) J Am Chem Soc 112:8002–8008
46. Dietrich-Buchecker CO, Khémiss A, Sauvage J-P (1986) J Chem Soc Chem Commun 1376–1378
47. Gunter MJ, Farquhar SM (2003) Org Biomol Chem 1:3450–3457
48. Sato Y, Yamasaki R, Saito S (2009) Angew Chem Int Ed 48:504–507

49. Spruell JM, Paxton WF, Olsen JC, Benítez D, Tkatchouk E, Stern CL, Trabolsi A, Friedman DC, Goddard WA, Stoddart JF (2009) J Am Chem Soc 131:11571–11580
50. Asakawa M, Ashton PR, Menzer S, Raymo FM, Stoddart JF, White AJP, Williams DJ (1996) Chem Eur J 2:877–893
51. Ashton PR, Menzer S, Raymo FM, Shimizu GKH, Stoddart JF, Williams DJ (1996) Chem Commun 487–490
52. Amabilino DB, Stoddart JF (1995) Chem Rev 95:2725–2828
53. Amabilino DB, Ashton PR, Reder AS, Spencer N, Stoddart JF (1994) Angew Chem Int Ed Engl 33:1286–1290
54. Amabilino DB, Ashton PR, Balzani V, Boyd SE, Credi A, Lee JY, Menzer S, Stoddart JF, Venturi M, Williams DJ (1998) J Am Chem Soc 120:4295–4307
55. Raymo FM, Bartberger MD, Houk KN, Stoddart JF (2001) J Am Chem Soc 123:9264–9267
56. Connelly NG, Geiger WE (1996) Chem Rev 96:877–910
57. Souizi A, Robert A (1987) J Org Chem 52:1610–1611
58. Zhao Y, Truhlar DG (2008) Acc Chem Res 41:157–167
59. Benítez D, Tkatchouk E, Yoon I, Stoddart JF, Goddard WA III (2008) J Am Chem Soc 130:14928–14929
60. Vácha M, Půžová T, Kvíčalová M (2009) J Exp Biol 212:3473–3477
61. Gottlieb HG, Kotlyar V, Nudelman A (1997) J Org Chem 62:7512–7515

About the Author

Jason Michael Spruell was born in Nashville, Tennessee on July 18, 1983. Although he moved from place to place throughout his childhood, he was primarily raised and educated in Chattanooga, Tennessee. Jason earned a B.S. Degree in Chemistry from the University of Alabama, graduating *Summa Cume Laude* in 2005. He and his wife, Joy, then moved to Los Angeles, California for him to work with Fraser Stoddart at the University of California at Los Angeles for his graduate degree supported by a National Science Foundation Graduate Research Fellowship as well as the Chancellor's Fellowship from UCLA. Jason earned a M.S. degree in Chemistry from UCLA in 2007 before moving with Sir Fraser to Northwestern University, where he was awarded the Presidential Fellowship. Jason is a member of Northwestern University's Society of Fellows and has been generously supported throughout the years by the Barry M. Goldwater National Scholarship, USA Today Academic All-American Team, the Presidential Scholarship from the University of Alabama, as well as the National Merit Scholarship. He and Joy are the proud parents of two sons—Nathan and London. They will all be moving shortly to the University of California at Santa Barbara for Jason to begin post-doctoral research as an Elings Fellow in Experimental Science through which he will research closely with Craig Hawker.

Index